University of Zagreb

FACULTY OF SCIENCE
DEPARTMENT OF BIOLOGY

Tea Vasiljević

THE ROLE OF TLR3 PROTEIN AND ENDOGENOUS LIGANDS IN THE MAINTENANCE AND THERAPY OF CANCER STEM CELLS

DOCTORAL THESIS

Zagreb, 2025

University of Zagreb

FACULTY OF SCIENCE
DEPARTMENT OF BIOLOGY

Tea Vasiljević

THE ROLE OF TLR3 PROTEIN AND ENDOGENOUS LIGANDS IN THE MAINTENANCE AND THERAPY OF CANCER STEM CELLS

DOCTORAL THESIS

Supervisor:
Tanja Matijević Glavan, PhD

Zagreb, 2025

Sveučilište u Zagrebu

PRIRODOSLOVNO-MATEMATIČKI FAKULTET
BIOLOŠKI ODSJEK

Tea Vasiljević

ULOGA PROTEINA TLR3 I ENDOGENIH LIGANADA U ODRŽAVANJU I TERAPIJI MATIČNIH STANICA TUMORA

DOKTORSKI RAD

Mentor:
Dr. sc. Tanja Matijević Glavan

Zagreb, 2025

This doctoral dissertation was prepared in the Laboratory for Personalized Medicine of the Division of Molecular Medicine, Ruđer Bošković Institute in Zagreb, under the supervision of Tanja Matijević Glavan, PhD, within the University Postgraduate Doctoral Study of Biology at the Department of Biology, Faculty of Science, University of Zagreb.

The dissertation was prepared within and funded by the project of the Croatian Science Foundation entitled “TollTreatTum - Toll-like receptor 3 in the development and treatment of human head and neck cancer: the role of endogenous ligands” (IP-2020-02-4225).

This research was also funded by the Croatian Science Foundation's project, “Young Researchers’ Career Development Project” (DOK-2021-02).

SUPERVISOR BIOGRAPHY

Tanja Matijevic Glavan, PhD, earned her bachelor's degree, master's degree, and PhD from the Faculty of Science at the University of Zagreb. She also graduated from the Business School „Baltazar Adam Krcelic" in Zapresic, Croatia, in project management. She currently works as a scientific advisor at the Laboratory for Personalized Medicine at the Ruđer Bošković Institute in Zagreb. Her main research interests include Toll-like receptors and their role in tumor progression, as well as cancer stem cells. She has published 31 scientific papers, mostly related to these topics, and has an h-index of 15. She served as the principal investigator on projects funded by the Croatian Science Foundation and a French-Croatian bilateral project. She has organized several scientific conferences and delivered several invited lectures. In 2017, she was appointed an assistant professor and has been involved in graduate and postgraduate education. To date, she has supervised one doctoral and four master's theses. Tanja Matijevic Glavan has received two annual awards from the Ruđer Bošković Institute and once received the Best Young Investigators' Oral Presentation Award at the Croatian Conference on Human Genetics. She actively promotes science, reviews for several journals, and has co-authored multiple book chapters. She has participated in short-term visits to various international institutions and has been involved in two interdisciplinary scientific projects.

Acknowledgments

Želim izraziti iskrenu zahvalnost svima koji su me na bilo koji način pratili i podržavali tijekom mog doktorskog puta.

Prije svega, neizmjerno zahvaljujem svojoj mentorici, dr. sc. Tanji Matijević Glavan na stručnom vodstvu, strpljenju, podršci i povjerenju koje mi je ukazivala tijekom svih faza istraživanja. Hvala što si mi dala slobodu da se razvijam kao znanstvenica, ali i sigurnost da se uvijek imam kome obratiti kad zapnem.

Veliko hvala i voditeljici laboratorija dr. sc. Sanji Kapitanović, dr. med. koja je odlučila odgovoriti na moj e-mail s otvorenom zamolbom za posao i pružila mi priliku. Taj trenutak otvorio je vrata koja su mi promijenila profesionalni život. Na tome ću Vam uvijek biti zahvalna!

Hvala Hrvatskoj zakladi za znanost na pruženoj potpori i financiranju mog doktorskog istraživanja.

Hvala članovima komisije na vrijednim ispravcima i korisnim savjetima za unaprjeđenje disertacije.

Zahvaljujem kolegicama i kolegama iz laboratorija i s instituta na svim lijepim trenutcima – osobito onima koji su mi na ovom putu postali prijateljice i prijatelji.

Neizmjerno sam zahvalna svojoj obitelji na bezuvjetnoj ljubavi i podršci. Posebno mami što je vjerovala u mene kada nitko drugi nije. I što mi je slala sarme u Zagreb.

Veliko hvala mojim prijateljicama i prijateljima na razgovorima, smijehu, i što su slušali priče o tumorima, proteinima i stanicama iako o tome nisu znali puno.

Posebne zahvale mojim suputnicima tijekom godina bez kojih gubljenje po Aziji (i ostatku svijeta) ne bi bilo isto.

Zahvaljujem mom Alenu, što je uz mene i što pokazuje puno razumijevanja, što je znao kad me treba motivirati i pogurati dalje, i najvažnije - što pazi da na mom licu uvijek bude osmijeh.

Hvala Čarliju što je najbolji i što je savršena emocionalna potpora za svaku priliku i ne priliku.

Na kraju, zahvaljujem i sebi - što nisam odustala kad je bilo teško. Što sam nastavila dalje, i kad nisam znala kamo. Što sam vjerovala, barem malo, da je sve ovo vrijedilo truda.

University of Zagreb
Faculty of Science
Department of Biology

Doctoral thesis

THE ROLE OF TLR3 PROTEIN AND ENDOGENOUS LIGANDS IN THE MAINTENANCE AND THERAPY OF CANCER STEM CELLS

Tea Vasiljević

Ruđer Bošković Institute

Toll-like receptors (TLRs) play a crucial role in the innate immune response, recognizing specific molecular patterns originating from pathogens or endogenous molecules. TLR3 recognizes dsRNA, and its synthetic analogs poly(I:C), and poly(A:U). Recent research reveals dual role of TLR3 in tumors, demonstrating that its activation may stimulate apoptosis and immune system activation, as well as tumor progression. This study investigated how TLR3 activation and increased expression of endogenous ligands, also called damage-associated molecular patterns (DAMPs), affect the cancer stem cells (CSCs) and whether CSCs release factors into the microenvironment that can influence the migration and invasion of surrounding tumor cells. We have also studied the effect of two irradiation therapies (γ-rays and protons) in combination with DAMP inhibitors and poly(I:C) as an apoptosis inducer on CSCs. We found that TLR3 stimulation enhances tumor sphere formation in all tested cell lines, but it was more pronounced in the Detroit 562 cell line. TLR3 activation induced expression and release of DAMP, which promoted migration of adherent tumor cells. Combination of pharmacological DAMP inhibitors, particularly aspirin and metformin, with poly(I:C) and proton irradiation can reduce the survival and stemness properties of head and neck CSCs. Lastly, we have also determined potential novel biomarkers for HNSCC CSC and further evaluated UFM1-specific peptidase 2 (UFSP2) and kynurenine aminotransferase 3 (KYAT3) that were overexpressed in tumor spheres compared to the adherent cells, but their expression was reduced after TLR3 activation. In conclusion, TLR3 activation stimulates CSC properties, but the novel therapy, which combines poly(I:C), DAMP inhibitors, and proton therapy, effectively eradicates CSCs.

The PhD thesis contains 138 pages, 49 figures, 7 tables, 230 references, original thesis is in English

Key words: cancer stem cells (CSC), Toll-like receptor 3 (TLR3), endogenous ligands, damage-associated molecular patterns (DAMPs), γ-radiation, proton therapy, migration, head and neck squamous cell carcinoma (HNSCC)

Supervisor: Scientific Advisor Tanja Matijević Glavan, PhD

Reviewers:

1. Senior Research Associate Maja Sabol, PhD
2. Research Associate Anđela Horvat, PhD
3. Professor Maja Matulić, PhD

Replacement: Professor Inga Urlić, PhD

Sveučilište u Zagrebu
Prirodoslovno-matematički fakultet
Biološki odsjek

Doktorski rad

ULOGA PROTEINA TLR3 I ENDOGENIH LIGANADA U ODRŽAVANJU I TERAPIJI MATIČNIH STANICA TUMORA

Tea Vasiljević

Institut Ruđer Bošković

Toll-like receptori (TLR) igraju ključnu ulogu u urođenom imunološkom odgovoru, prepoznajući specifične molekularne sljedove podrijetlom od vanjskih patogena ili one endogenog podrijetla. TLR3 prepoznaje dsRNA i njezine sintetske analoge poly(I:C) i poly(A:U). Nedavna istraživanja otkrivaju dvojaku ulogu TLR3 u tumorima, sugerirajući da njegova stimulacija može potaknuti aktivaciju apoptoze i imunološkog sustava, ali i progresiju tumora. U ovom istraživanju ispitivali smo kako aktivacija TLR3 i povećana ekspresija endogenih liganada (DAMP) utječe na karakteristike matičnih stanica tumora (CSC) te otpuštaju li CSC u mikrookoliš čimbenike koji mogu utjecati na migraciju i invaziju okolnih tumorskih stanica. Također smo proučavali učinak dviju terapija ozračivanjem (γ-zrake i protoni) u kombinaciji s inhibitorima DAMP i poly(I:C) kao aktivatora apoptoze u CSC. Otkrili smo da stimulacija TLR3 pojačava stvaranje tumorskih sfera u svim ispitanim staničnim linijama, a pogotovo u staničnoj liniji Detroit 562, te inducira ekspresiju i otpuštanje DAMP što potiče migraciju okolnih tumorskih stanica. Utvrdili smo da se kombinacijom tretmana farmakološkim inhibitorima DAMP (pogotovo aspirina i metformina) s poly(I:C) i protonskim zračenjem smanjuje preživljenje i svojstva matičnosti CSC glave i vrata. Također smo odredili potencijalne nove biomarkere CSC glave i vrata. Dodatno smo validirali UFM1-specifičnu peptidazu 2 (UFSP2) i kinurenin aminotransferazu 3 (KYAT3), koji su bili prekomjerno izraženi u tumorskim sferama u usporedbi s adherentnim stanicama, dok je njihova ekspresija bila smanjena nakon aktivacije TLR3. Zaključujemo da aktivacija TLR3 povećava svojstva matičnosti CSC, ali da kombinirana terapija s poly(I:C), DAMP inhibitorima i protonskim zračenjem uspješno eliminira CSC.

Doktorski rad sadrži: 138 stranica, 49 slika, 7 tablica, 230 literaturna navoda, jezik izvornika je engleski

Ključne riječi: matične stanice tumora (CSC), Toll-like receptor 3 (TLR3), endogeni ligandi (damage-associated molecular patterns, DAMPs), γ-zračenje, protonska terapija, migracija, karcinom pločastih stanica glave i vrata (HNSCC)

Mentor: dr. sc. Tanja Matijević Glavan, znanstvena savjetnica

Povjerenstvo:

1. dr. sc. Maja Sabol, viša znanstvena suradnica
2. dr. sc. Anđela Horvat, znanstvena suradnica
3. prof. dr. sc. Maja Matulić

Zamjena: prof. dr. sc. Inga Urlić

TABLE OF CONTENTS

1. INTRODUCTION

Toll-like receptors (TLRs) are crucial receptors in the innate immune response. They are expressed in cells of different origins, primarily immune cells such as dendritic cells and macrophages, but also fibroblasts, endothelial cells, epithelial cells, and tumor cells (Kawasaki & Kawai, 2014; Zhou et al., 2009). TLRs belong to a family of receptors known as pattern recognition receptors (PRRs). Their main role is to recognize specific molecular patterns originating from pathogens (bacteria, viruses, parasites, and fungi), termed pathogen-associated molecular patterns (PAMPs) or endogenous molecules originating from injured tissue or necrotic cells, known as damage-associated molecular patterns (DAMPs) (Vijay, 2018; Piccinini & Midwood, 2010). Both PAMPs and DAMPs can activate TLR signaling pathways. Stimulation of TLRs by their ligands triggers the activation of specific signaling pathways, resulting in the secretion of various inflammatory factors, including pro-inflammatory cytokines IL-1β, IL-18, TNF-α, and interferon type I. This leads to the activation of proliferative signaling pathways, immune system activation, or apoptosis (Hanke & Kielian, 2011).

Toll-like receptor 3 (TLR3) is an endosomal receptor that recognizes double-stranded RNA (dsRNA), usually derived from viruses. Due to its localization in the endosome rather than the cytosol, TLR3 cannot directly recognize a viral infection but can identify viruses that have undergone endocytosis and those infecting neighboring cells, subsequently subjected to phagocytosis (Karikó et al., 2004; Nishiya et al., 2005). Activation of TLR3 by viral dsRNA leads to the direct activation of innate and adaptive immune responses, such as maturation of dendritic cells and activation of specific T-cell responses (Chattopadhyay & Sen, 2014; Kumar et al., 2008).

The discovery that TLRs are expressed on tumor cells has sparked significant interest in this direction, revealing the dual role of TLR3 in tumors. Some studies have demonstrated that TLR3 activation induces apoptosis in tumors (Salaun et al., 2006), while others indicate that TLR3 activation stimulates tumor progression. TLR3 contributes to the proliferation of head and neck squamous cell carcinomas by activating NF-κB and c-Myc (Pries et al., 2008). Matijevic & Pavelic, (2011) have shown that TLR3 might be important in the process of tumor metastasis. They determined significant differences when it comes to TLR3 expression and functioning in primary and metastatic carcinoma cell lines. Matijevic Glavan et al. (2017)

discovered that TLR3 can trigger metabolic reprogramming of pharyngeal cancer cell lines by inducing aerobic glycolysis.

It has been demonstrated that TLR3 can be activated by DAMPs, such as variants of cellular RNA originating from necrotic cells (Karikó et al., 2004). This implies that the activation of TLR3 in tumor cells or their microenvironment does not necessarily require an external factor, such as a viral infection. Rather, its activation can be mediated solely by internal factors (Cavassani et al., 2008; Vasiljevic et al., 2023). DAMPs are often overexpressed in tumors or released by tumors due to the stressful conditions in the tumor microenvironment (Zapletal et al., 2023). It has already been confirmed that TLR3 is an important factor in the progression of head and neck tumors (Pries et al., 2008).

Head and neck squamous cell carcinoma (HNSCC) accounts for 90% of all head and neck cancers. It is the sixth most prevalent cancer globally and is distinguished by its recurrence tendency post-treatment. Cancers in the oral cavity and larynx are commonly linked to the use of tobacco, excessive alcohol consumption, or a combination of both. In terms of infectious agents, persistent infection with human papillomavirus (HPV) and Epstein–Barr virus (EBV), are risk factor for HNSCC arising from the oropharynx and nasopharynx (Johnson et al., 2020). Patients with HPV-related HNSCC generally exhibit better response to therapy and have better survival compared to HPV-negative patients (Ang et al., 2010).

Regardless of existing therapy, a considerable number of patients show suboptimal responses to treatment, leading to disease recurrence. It is known that a persistent factor for failure of conventional therapy in HNSCC is the frequent incidence of local recurrence and distant metastasis, which can be attributed to cancer stem cells (CSCs).

Our approach to studying the role of TLR3 in the carcinogenesis of HNSCC focuses on the investigation of CSCs. Jia et al. (2015) showed that TLR3 has a role in the formation and maintenance of tumor spheres in breast cancer, and that is the only study published on this topic. CSCs are a subset of cancer cells characterized by their self-renewal potential, the ability to differentiate into various cell types, and the capacity to initiate tumor growth. CSCs can also stimulate cell cycle arrest, entering a quiescent state that enhances their resistance to chemotherapy and radiotherapy (Phi et al., 2018).

CSCs may exhibit resistance to cell death induced by DNA damage through various mechanisms, such as protection against oxidative DNA damage by increasing reactive oxygen

species (ROS) scavenging, enhancing DNA repair capabilities via ATM and CHK1/CHK2 phosphorylation, or activating anti-apoptotic signaling pathways, including PI3K/Akt, Wnt/β-catenin, and Notch signaling pathways (Peitzsch et al., 2013).

Therefore, it is crucial to understand the mechanisms through which CSCs maintain stemness and acquire resistance to therapeutic agents and how to increase their sensitivity to cancer therapy.

The **objective** of this doctoral thesis was to determine the role of Toll-like receptor 3 (TLR3) in the progression of head and neck tumors by focusing on its role in cancer stem cells (CSCs).

The **hypotheses** of this research were as follows:

1. Activation of TLR3 stimulates the formation of tumor spheres and the maintenance of stemness.
2. CSCs may release endogenous ligands (DAMPs) or other factors into the microenvironment, which can increase migration and invasion of the surrounding tumor cells.
3. To develop potential antitumor therapy, we will determine whether the treatment with inhibitors of endogenous ligands in combination with irradiation and poly(I:C) has a cytotoxic effect on CSC and can reduce stemness markers.
4. Exploring novel CSC biomarkers will deepen our understanding of how CSCs work and help in developing more effective new therapies for HNSCC.

The research was conducted using HNSCC cell lines. The experimental methods used in this study included the tumor sphere formation assay, transient transfection, gel electrophoresis, western blot, γ- and proton irradiation, migration and invasion assay, MTT assay, cell viability assay (Via Light), and real-time qPCR.

Based on the results of this research, we suggest that:

1. TLR3 activation helps in tumor sphere formation and maintenance by showing that TLR3 activation induced the formation of an increased number of bigger tumor spheres.
2. TLR3 stimulation in CSC induces DAMP release, such as S100A9, HMGB1, or HSP70 into the tumor microenvironment. They further interact with receptors like TLR4 or RAGE on neighboring cells, setting off paracrine signals that promote the migration of surrounding tumor cells, but not tumor cell invasion. This effect can be abolished with the addition of DAMP inhibitors (especially aspirin and metformin).
3. Aspirin, especially with poly(I:C) as a TLR3 activator, holds promise as a potential anticancer drug targeting CSCs. Aspirin's main advantages are its low cost and proven safety profile. Combined treatment with γ-radiation effectively targets adherent tumor cells, and combined treatment with proton irradiation successfully targets CSCs.
4. Recognizing potential novel CSC biomarkers contributes to a deeper understanding of CSC, with potential for the development of novel therapy targeting specifically CSCs.

2. LITERATURE REVIEW

2.1. Toll-like receptors

Toll-like receptors (TLRs) belong to the class I transmembrane receptor family, which are important for innate immune response. They were first discovered in *Drosophila melanogaster* (Hashimoto et al., 1988). In 1996, Lemaitre et al. identified their association with immunity. TLRs are expressed in cells of different origins, primarily immune cells, including dendritic cells and macrophages, fibroblasts, endothelial cells, epithelial cells, and tumor cells (Kawasaki & Kawai, 2014; Zhou et al., 2009). TLRs belong to a family of receptors known as pattern recognition receptors (PRRs). Their main role is to recognize specific molecular motifs originating from pathogens (bacteria, viruses, parasites, and fungi), termed pathogen-associated molecular patterns (PAMPs) or endogenous molecules originating from injured tissue or necrotic cells, known as damage-associated molecular patterns (DAMPs) (Vijay, 2018; Piccinini & Midwood, 2010). Both PAMPs and DAMPs can activate TLR signaling pathways. When the ligand binds to TLRs, they form homodimers or heterodimers. Stimulation of TLRs by their ligands triggers the activation of specific signaling pathways and activation of transcription factors (TFs), activator protein-1 (AP-1), nuclear factor-kappa B (NF-κB), and interferon regulatory factors (IRFs). This results in the release of various inflammatory factors, including pro-inflammatory cytokines IL-18, IL-1β, TNF-α, and interferon type I, leading to different outcomes, including the activation of proliferative signaling pathways, immune system activation or apoptosis (Medzhitov et al., 1997; O'Neill & Bowie, 2007; Uematsu & Akira, 2007; Li et al., 2010). A total of 10 TLRs have been identified in humans. TLR1, TLR2, TLR4, TLR5, and TLR6 are located on the cell membrane. They mainly bind molecules originating from the membranes of various microbes, such as bacterial lipopeptides (TLR1/2 and TLR2/6), peptidoglycans (TLR2), flagellins (TLR5), lipopolysaccharides (LPS – TLR4), and lipoteichoic acid (TLR2). TLR3, TLR7, TLR8, and TLR9 are found on the endosomal membrane and initially on the membrane of the endoplasmic reticulum before trafficking to endosomes (Kawasaki & Kawai, 2014). They recognize nucleic acids of pathogen origin, such as single- (TLR 7/8) or double-stranded RNA (TLR3), and unmethylated CpG sequences on single- and double-stranded DNA (TLR9) (Barton & Medzhitov, 2002) (Figure 2.1). TLRs consist of three key structural domains: extracellular, transmembrane, and intracellular. The extracellular domain is the N-terminal of the receptor, which contains the leucine-rich repeats

(LRR). This domain plays a role in ligand binding. The transmembrane domain (TD) consists of one helix that connects the LLR domain and the intracellular toll/interleukin-1 receptor (TIR) domain, the inner C-terminal domain responsible for signal transduction (Bell et al., 2003; Botos et al., 2011). The function of TLR10 is still not defined; it is expressed on the cell membrane, but its ligands have not been confirmed.

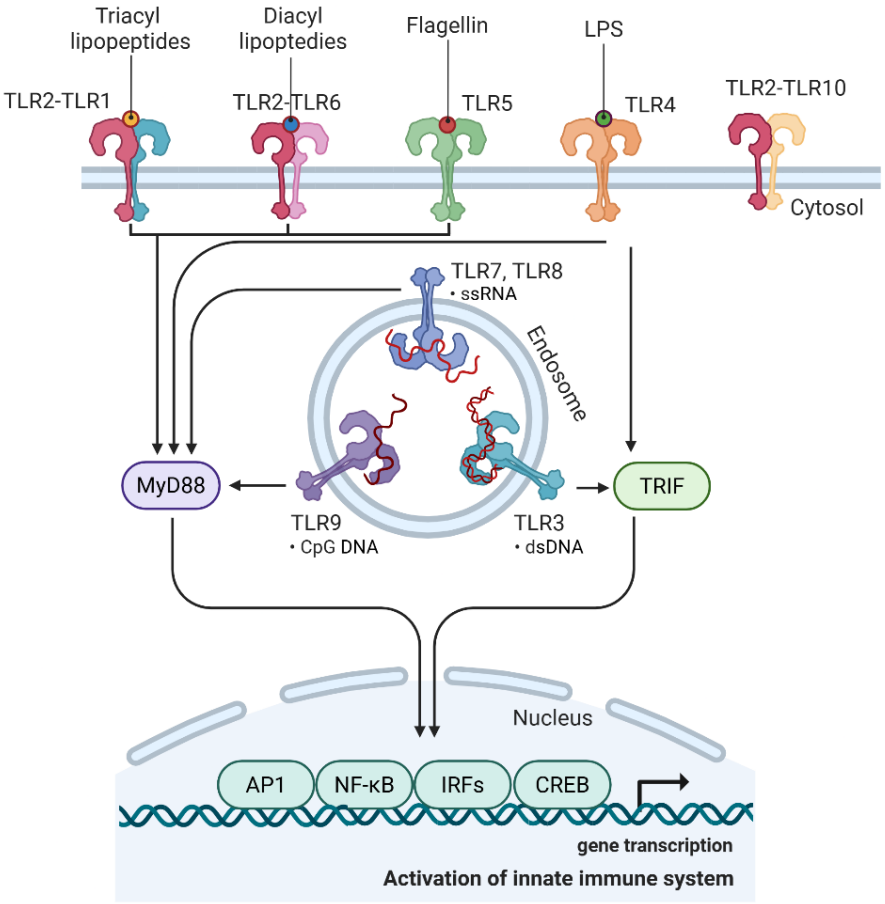

Figure 2.1. Human Toll-like receptors' localization and their ligands. TLRs recognize different molecular motifs and are therefore localized differently in the cell. TLR1, TLR2, TLR4, TLR5, TLR6, and TLR10 are localized on the cell membrane. They mainly bind molecules originating from the membranes of various microbes, such as bacterial lipopeptides (TLR1/2 and TLR2/6), peptidoglycans (TLR2), flagellins (TLR5), lipopolysaccharides (LPS – TLR4), and lipoteichoic acid (TLR2). TLR3, TLR7, TLR8, and TLR9 are localized on the membranes of endosomes. They recognize nucleic acids of pathogen origin, such as single- (TLR 7/8) or double-stranded RNA (TLR3), and unmethylated CpG sequences on single-stranded DNA (TLR9). The image was created with biorender.com.

2.2. Toll-like receptor 3

Toll-like receptor 3 (TLR3), also known as cluster of differentiation 283 (CD283), is an endosomal receptor that recognizes double-stranded RNA (dsRNA), usually derived from viruses. It was first identified in 1998 in *D. melanogaster* (Rock et al., 1998). TLR3 also recognizes synthetic analogs of dsRNA, polyinosinic:polycytidylic acid (poly(I:C)) and polyadenylic:polyuridylic acid (poly(A:U)). Poly(A:U) is a more selective TLR3 ligand compared to poly(I:C) because it does not activate other dsRNA receptors, retinoic acid-inducible gene I (RIG-I), and melanoma differentiation-associated protein 5 (MDA5) (Perrot et al., 2010).

TLR3 is found on the membrane of the endosome of dendritic cells, macrophages, and intestinal epithelial cells, but can also be found in the cell membrane of fibroblasts and some cancer cells (Helmy et al., 2009; Matsumoto et al., 2002; Fukata et al., 2008; Pries et al., 2008; Goto et al., 2008). Due to its localization, TLR3 cannot directly recognize a viral infection but can identify viruses that have undergone endocytosis and those infecting neighboring cells, subsequently subjected to phagocytosis (Alexopoulou et al., 2001; Karikó et al., 2004; Nishiya et al., 2005; Lim et al., 2022). Viral dsRNA binding to TLR3 leads to the maturation of dendritic cells, which stimulates the antigen-specific T-cell response (Kumar et al., 2008; Chattopadhyay & Sen, 2014).

TLR3 contains three main domains. The first one is an ectodomain with a horseshoe shape and consists of 23 LRRs, situated in the lumen of the endosome and serves as a ligand-binding platform. Each of the LRRs contains 20-30 amino acids. The second domain is the cytoplasmic domain, called the TIR domain, which activates signal transduction. Between the LRR and TIR domains is the transmembrane domain, which is responsible for signal transmission across the membrane but can also contribute to the position of TLR3 within the cell (Funami, 2004; Sen & Sarkar, 2005; Manavalan et al., 2011; Chattopadhyay & Sen, 2014). TLR3 receptors interact with another transmembrane protein called unc-93 homolog B1 (UNC93B1). UNC93B1 is an endoplasmic protein that has a role in the translocation of TLRs from the endoplasmic reticulum to the endosome (Kim et al., 2008; Chaturvedi & Pierce, 2009; Brinkmann et al., 2007).

2.2.1. TLR3 activation and signaling pathways

TLR3 activation begins following the homodimer formation, which happens after recognizing dsRNA or poly(I:C)/ poly(A:U). Homodimer is formed when the extracellular domain of TLR3 binds to the 45-bp segment of the dsRNA, which is a minimum length required for binding (Botos et al., 2011). The membrane protein UNC93B1 is necessary for the proteolytic processing of TLR3 and is an important cofactor for nucleic acid-sensing TLRs on endosomes (Pohar et al., 2013). Huang et al. (2021) demonstrated that human C-type lectin member 18A (CLEC18A) has an affinity for TLR3 and directly interacts with poly(I:C). This indicates that CLEC18A serves as a co-receptor alongside TLR3 within the endosome.

Upon ligand binding, TLR3 forms an active homodimer, recruiting TIR-domain-containing adapter-inducing interferon-β (TRIF) adapter proteins to bind to the TIR domain of the receptor. This interaction initiates two major downstream pathways. Unlike other TLRs, the TLR3 signaling pathway follows the myeloid differentiation primary response 88 (MyD88)-independent pathway (Figure 2.1). The TLR3 signaling pathway takes place entirely through the TRIF adapter protein (Yamamoto et al., 2003). In the first downstream pathway, TRIF interacts with TNF receptor-associated factor 6 (TRAF6) (Häcker et al., 2006). TRAF6 recruits the kinase receptor-interacting protein kinase 1 (RIP1), which then activates TGFβ-activated kinase (TAK1) and TAK1-binding protein 2 & 3 (TAB2/3) with NF-kappa-B essential modulator (NEMO). The activation of downstream molecules begins with the IkappaB kinase (IKK) complex (IKK-α, IKK-β). TAK1 phosphorylates IKK, which then phosphorylates IκBα leading to IκBα degradation by proteasomes. NF-κB is then released into the nucleus and activated, where it acts as a transcription factor and starts the transcription of genes that produce pro-inflammatory cytokines and chemokines (Kawai & Akira, 2006; Prickett et al., 2008; Tak & Firestein, 2001; Krishnan et al., 2007). It can also activate the mitogen-activated protein kinase (MAPK) cascade. TAK1 initiates the signaling cascade by activating MAPKs (p38, JNK, ERK1/2). c-Jun N-terminal kinase (JNK) phosphorylates and activates AP-1 transcription factor. AP-1 moves into the nucleus where it starts the transcription of pro-inflammatory cytokines and chemokines (Wang et al., 2001; Brown et al., 2011).

In the second downstream pathway of the TLR3 signaling, TRIF engages TRAF3, which promotes the formation of the IKK kinases TANK-binding kinase 1 (TBK1) and inhibitor of κB kinase-related kinase-ε (IKK-ε) complex, to phosphorylate the IRF3 transcription factor. Phosphorylated and activated IRF3 is a dimer, and as such, it moves from the cytoplasm to the

nucleus and initiates transcription of the type I interferon (IFN) genes (Kawasaki & Kawai, 2014). This leads to the release of type I interferons (IFNα and IFNβ), which play a crucial role in the antiviral immune response (Liu et al., 2012) (Figure 2.2).

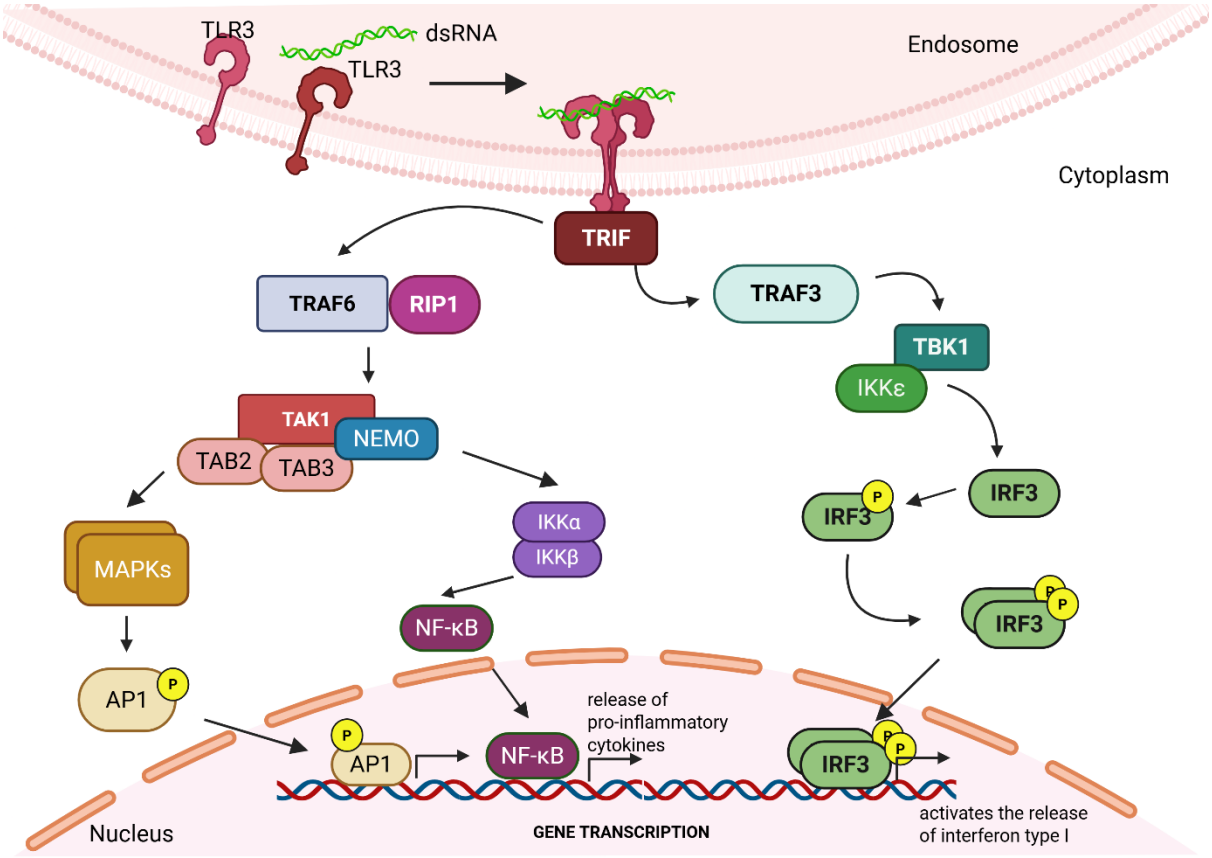

Figure 2.2. TLR3 signaling pathway. Upon ligand binding, TLR3 forms an active homodimer, recruiting the adapter molecule TRIF to bind to the TIR domain of the receptor. This interaction initiates two major downstream pathways. In one branch, TRIF recruits the protein complex containing TRAF6 and RIP1, which leads to the activation and assembly of a complex involving TAK1, TAB2/3, and the IKK complex. This complex can activate either the MAPK cascade, leading to activation of AP1, or the IKKα/IKKβ complexes, which result in NF-κB activation. In the other branch, TRIF engages TRAF3, promoting the formation of the TBK1 and IKK-ε complex. This result is the phosphorylation and activation of the IRF3, and it ultimately leads to the synthesis of interferons. The image was created with biorender.com.

2.2.2. Dual Role of TLR3 in Cancer

In addition to immune and normal epithelial cells, the expression of TLRs has been found in tumors, where TLRs seem to have two very different roles. Almost all TLRs have a dual role in cancer (TLR2, TLR3, TLR4, TLR7/8, and TLR9), one being anticancer and the other pro-tumorigenic. TLR3 was also studied in these two directions. First studies have demonstrated that TLR3 activation induces apoptosis in tumors (Salaun et al., 2006), while the following research established that TLR3 activation can also stimulate tumor progression. Pries et al. (2008) showed that TLR3 contributes to the proliferation of head and neck squamous cell carcinomas by activating NF-κB and c-Myc proto-oncogene. These authors have also shown that TLR3 is expressed in HNSCC tumor tissue but not in the normal adjacent tissue. Matijevic & Pavelic (2011) have shown that TLR3 might be important in the process of tumor metastasis. They determined significant differences when it comes to TLR3 expression and function in primary and metastatic carcinoma cell lines. Due to the tendency of cancer cells for uncontrolled proliferation and the need for a higher supply of oxygen and nutrients, they undergo metabolic reprogramming. In cancer cells, metabolic reprogramming often affects resistance to therapy and tumor invasion. Matijevic Glavan et al. (2017) have shown first that TLR3, once activated, can induce metabolic reprogramming, which leads to increased aerobic glycolysis in pharyngeal cancer cells and the Warburg effect (Warburg, 1956). Paone et al. (2010) showed that in prostate cancer, TLR3 activation leads to two very different processes. It increases expression of hypoxia-inducible factors (HIF-1), leading to reduced apoptosis, and it releases vascular endothelial growth factors (VEGF), promoting angiogenesis. TLR3 activation in tumors can also result in tumor promotion. TLR3 overexpression is associated with poor outcomes in oral cancer, gastric cancer, and prostate cancer (Muresan et al., 2020). It was revealed that in breast cancer, TLR3 can upregulate markers associated with cancer stem cells and activate the Wnt/β-catenin signaling pathway when stimulated with poly(I:C) (Jia et al., 2015). TLR3 activation leads to the production of chemokines in intestinal epithelial cancer cells (Bugge et al., 2017) and in lung cancer (Liu et al., 2016) that recruit neutrophils, which leads to tumor invasion and metastasis.

On the other hand, Muresan et al. (2020) showed that TLR3 is overexpressed in most cancers and that the overexpression in many cancers is associated with a positive prognosis and anti-tumorigenic properties. This includes melanoma, renal cancer, lung adenocarcinoma, and hepatocellular cancer. Salaun et al. (2006) showed in breast cancer that TLR3, when activated with dsRNA ligands, can start the signaling through TRIF-mediated expression of NF-κB and

type I interferons (IFN-β), which ends in the apoptosis induction. The extrinsic apoptotic pathway is related to TLR3 activation. In lung cancer cells, it has been discovered that TRIF recruits caspase 8 and RIP1 to induce apoptosis (Estornes et al., 2012). In HNSCC, decreased expression of survivin was associated with poly(I:C) dose-responsive induced apoptosis (Nomi et al., 2010). In addition, TLR3 anti-tumorigenic effects also result in the activation of the immune response (Toussi & Massari, 2014) (Figure 2.3).

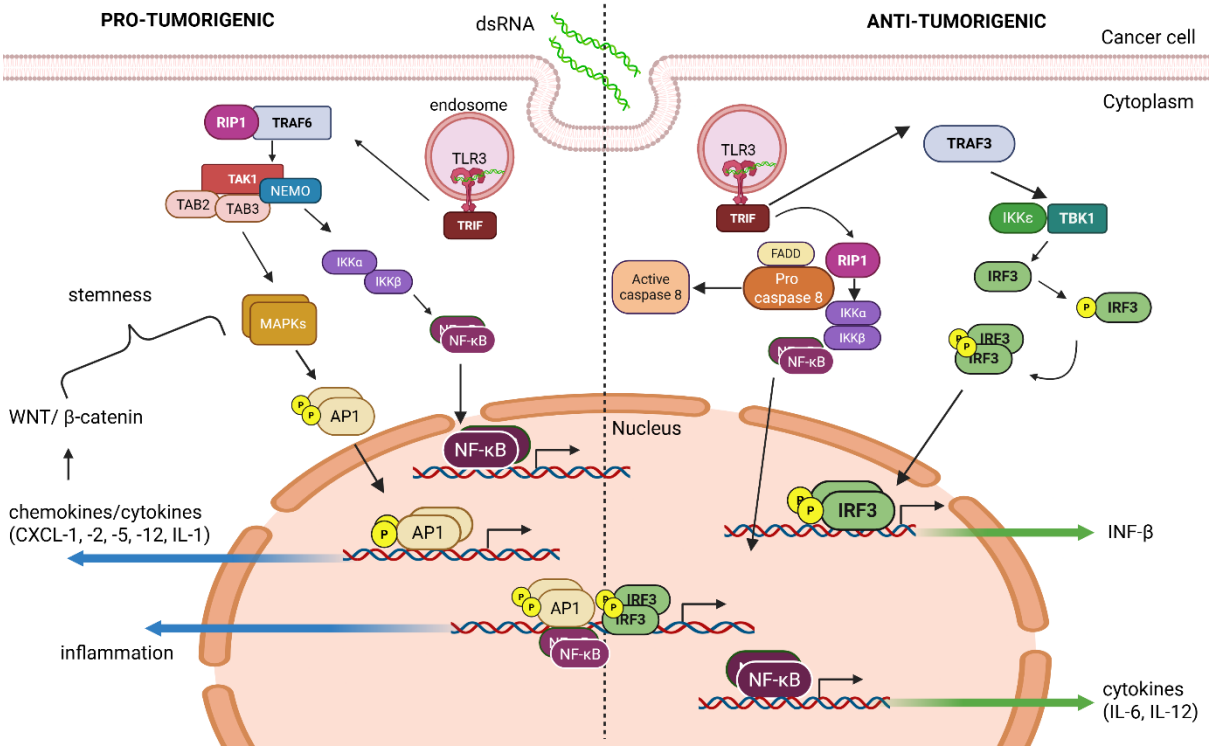

Figure 2.3. Dual role of TLR3 in cancer cells. TLR3 in tumor cells has been shown to play two very different roles. Depending on the part of the signaling cascade that is activated, it can lead to either a pro-tumorigenic outcome or an anti-tumorigenic response. The image is adapted from (Muresan et al., 2020) and created with biorender.com.

2.3. Cancer stem cells (CSCs)

Cancer stem cells (CSCs) are a small population of tumor cells that have properties of normal stem cells that include the ability to self-renew, but also the properties of the tumor cell, which include the ability to continuously proliferate. Combined characteristics result in CSCs' ability to exhibit resistance to therapy, including chemotherapy and radiotherapy, which enables tumor growth and metastasis (Yu et al., 2012). These mechanisms can include increased expression of drug efflux pumps, enhanced DNA repair capabilities, and a slower rate of cell division or even cell cycle arrest (quiescence), making them less susceptible to drugs targeting rapidly dividing cells.

The first theories on the origin of tumor cells and the existence of CSC appeared in 1855. Almost a century later, in 1937, Furth et al. showed that a single cancer cell could induce tumors; however, CSCs were identified for the first time in the 1990s. Bonnet & Dick (1997) described them in acute myeloid leukemia (AML) as a separate subgroup of leukemia cells that had stem-like properties. They observed that these cancer cells could drive tumorigenesis, they had proliferative capacities, and they were able to induce leukemia when transplanted into immunodeficient mice.

CSCs can undergo asymmetrical division. A single CSC can produce one progenitor cell and one pluripotent cell, which ensures the retention of cancer stem cell properties to ensure the maintenance of the CSC population (Mukherjee et al., 2015). Because of their great plasticity, cancer stem cells can switch from stem-like cells to more differentiated cells, depending on the microenvironment conditions (growth factors, cytokines, hypoxia (low oxygen levels), and interactions with other cell types). CSCs could be one of the main causes for unsuccessful cancer treatment, so understanding the CSCs' function could be the main lead for targeting cancer treatment.

The development of the CSC niche microenvironment, the localized region within the tumor microenvironment (TME) that maintains and regulates CSCs, is crucial for the formation and maintenance of CSCs. TME is a special ecosystem that allows the tumor cell to grow and thrive. It is created when the tumor cells start to invade the surrounding tissue. This system maintains a lower oxygen (O_2) concentration, high nitric oxide (NO), acidic pH, angiogenesis, and changed metabolites. TME consists of cancer cells, stromal cells (fibroblasts and endothelial

cells), immune cells, and anti-inflammatory cytokines. Cytokines and chemokines sustain the stem-like properties of CSCs (Hanahan & Coussens, 2012; Chu et al., 2024) (Figure 2.4).

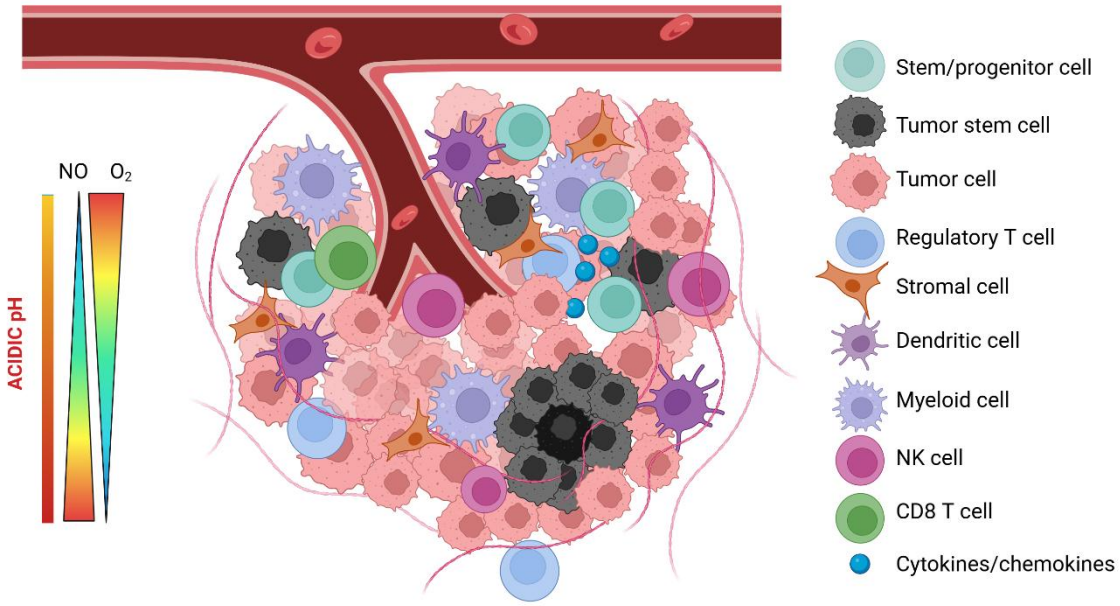

Figure 2.4. Tumor microenvironment (TME). The CSC niche is a special region within the TME that supports the survival and self-renewal of cancer stem cells. TME is characterized by low oxygen (O_2), high nitric oxide (NO), acidic pH, and active angiogenesis, etc. It consists of cancer cells, immune cells, stromal cells, cytokines/chemokines, and other molecules that preserve the stem-like properties of CSC. The image was created with biorender.com.

2.3.1. Evolution models of CSC

The concept of CSC has significantly reshaped the understanding of cancer biology. Over the past few decades, several models of CSC origin and evolution have been proposed.

Currently, there are three proposed evolution models for the development of CSC. The first hierarchical model was proposed in 1997. by Bonnet & Dick. This theory supports that the CSCs are at the top of the hierarchy and drive the development of new cancer cells and the spread of the tumor. The diversity within the tumors stems from the CSCs differentiating into various non-stem cancer cells, but generally from a single (or a few initiating) CSC. The hierarchical model would explain the resistance to therapy of some cancer cells and the ability

for recurrence of the disease. However, this model assumes a relatively fixed fate of cancer cells, which may oversimplify the complex behaviors of tumors (Batlle & Clevers, 2017).

On the other hand, in the stochastic (clonal) model, it is proposed that all the tumor cells can become CSCs within the tumor, and they can act as CSCs and metastasize when they have the right environmental conditions or intrinsic stimuli. According to this model, the tumor cell heterogeneity is a result of genetic and epigenetic variations, and all the mutations are a product of the errors accumulated during hyperproliferation. Any tumor cell can acquire mutations to gain stem-like properties (Greaves & Maley, 2012). The stochastic evolutionary model is relevant in explaining therapy-induced selection and CSC targeting in treatment, especially in cases when the non-CSC population survives the treatment and later gains CSC properties (Creighton et al., 2009).

The third model of CSC evolution is the cellular plasticity model. It connects the two, making the hybrid view of stochastic and hierarchical models, but also highlights the importance of both CSCs and TME. It is proposed that cancer cells can acquire or lose stemness and switch between a stem-like and non-stem-like state. This response depends on changes in the microenvironment, which include hypoxia, inflammatory signals, or therapy, allowing them to (de)differentiate as needed. This model indicates a dynamic CSC phenotype, a behavior that has been observed in colorectal and breast cancer. These finding highlights the importance of targeting not only CSC but the entire TME (Chaffer et al., 2013; Rich, 2016).

2.3.2. CSC markers in HNSCC

CSCs express markers that are absent in normal somatic cells, and those markers depend on the type of cancer (Zhao et al., 2017). Aldehyde dehydrogenase (ALDH) (intracellular enzyme) (Chen et al., 2009), CD133 (transmembrane glycoprotein) (Wu & Wu, 2009), and CD44 (cell-surface glycoprotein) (Prince et al., 2007) have effectively served as markers for identifying highly tumorigenic cancer stem cells in head and neck squamous cell carcinoma (HNSCC).

CD133 (prominin-1), a cell surface glycoprotein involved primarily in membrane organization, is a biomarker for stem cells. It is also involved in cell metabolism, renewal, differentiation, apoptosis, and regeneration (Li, 2013). It was found to be increased in oral cancers, which were linked to higher tumorigenicity and metastasis (Chiou et al., 2008). CD133 suppression reduces

stemness properties and promotes apoptosis of CSCs in HNSCC (Chen et al., 2011). ALDHs are enzymes that convert aldehydes into carboxylic acids using NAD(P)+. They play a role in detoxification, defend against oxidative stress, and regulate cellular functions (Shortall et al., 2021), thus helping CSCs in DNA protection and chemoresistance. CD44, a hyaluronic acid receptor, is a type I transmembrane glycoprotein receptor that has a function in cell adhesion, proliferation, migration, and angiogenesis (Hassn Mesrati et al., 2021). Some findings indicate that CD44 has a role in tumor metastasis and growth of HNSCC (Wang et al., 2009). The determination of stem-like markers allows CSC identification and the development of cancer therapy by targeting CSC specifically (Chen et al., 2016).

Octamer-binding transcription factor 4 (OCT4) is associated with stemness properties of CSC, including self-renewal and maintenance of pluripotency. OCT4 plays a role in the maintenance of stem cells. It is overexpressed in pluripotent cells, and its transcription regulates the fate of embryonic stem cells. OCT4 becomes downregulated as the cells undergo differentiation (Shi & Jin, 2010). OCT4 is often found to be upregulated in HNSCC. It promotes radioresistance in HNSCC through DNA damage response regulation and sustaining the stem-like phenotype. Its expression correlates with increased tumor aggressiveness and poor prognosis, including resistance to therapy. OCT4 is an interesting target in CSC therapy due to its important regulatory function in stem cells and CSCs (Chiou et al., 2008; Nathansen et al., 2021). ATP binding cassette subfamily G member 2 (ABCG2) is a membrane transporter protein. It plays a role in drug efflux and drug resistance. Increased expression of ABCG2 has been detected in CSCs, where it contributes to drug resistance, resulting in the enhanced survival of CSCs under therapeutic stress (El-Ashmawy et al., 2025) (Figure 2.5).

Besides CSC markers, CSC factors are crucial for the maintenance of CSC and tumor progression. CSC factors include transcription factors and other proteins involved in the signaling pathways that are a part of the regulation of the stemness properties. Different stem cell factors that play a role in supporting the CSC properties in HNSCC include transcription factors Octamer-binding transcription factors (Oct3/4), SRY (Sex-determining Region Y)-Box (Sox2), Nanog, B cell-specific Moloney murine leukemia virus integration site 1 (Bmi-1), Twist, and Snail. Other factors include nuclear factor erythroid 2-related factor (Nrf2) and interleukin-4 (IL-4) (Vukovic Đerfi et al., 2023).

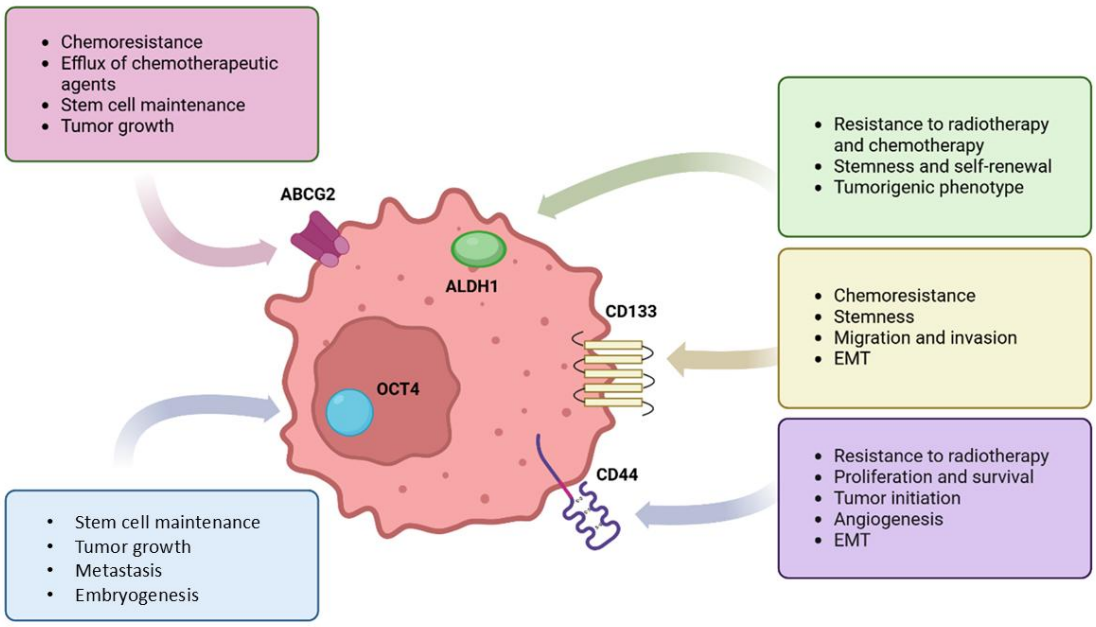

Figure 2.5. CSC markers in HNSCC and their functions in CSCs. ALDH, CD133, and CD44 have effectively served as markers for identifying CSCs in HNSCC. OCT4 is also a stemness marker that can contribute to tumor growth and metastasis, while ABCG2 is a drug resistance marker involved in chemoresistance. The image is adapted from (Vukovic Đerfi et al., 2023) and created with biorender.com.

2.3.3. Signaling pathways in HNSCC CSCs

To maintain CSC properties (therapy resistance, self-renewal, and proliferation), CSCs activate certain signaling pathways, such as Wnt, Hedgehog-GLI (HH-GLI), Notch, Hippo, and JAK-STAT (Figure 2.6).

During embryonic development, the Wnt signaling pathway plays a role in cell differentiation, proliferation, and migration. In β-catenin-dependent Wnt signaling, in the absence of Wnt, β-catenin is targeted for degradation by the so-called destruction complex, which consists of axin, APC (adenomatous polyposis coli), and two kinases: casein kinase 1 (CK1) and glycogen synthase kinase 3 (GSK3). This complex phosphorylates β-catenin in the absence of a ligand. Once phosphorylated, the β-catenin is then ubiquitinated for proteasomal breakdown. This prevents accumulation in the nucleus. When Wnt ligand binds to Frizzled receptor, it forms a complex with the co-receptor low-density lipoprotein receptor (LRP), which recruits cytoplasmic protein Dishevelled (Willert & Jones, 2006). The destruction complex gets

inactivated and β-catenin is no longer phosphorylated or affected by ubiquitins, which allows it to accumulate in the cytosol and is transported to the nucleus, where it joins T-cell factor/lymphoid enhancer-binding factor (TCF/LEF) to start gene transcription, which promotes cell proliferation and cell survival (Liu et al., 2022).

The Hedgehog-GLI (HH-GLI) signaling pathway plays a role in angiogenesis, proliferation, and tissue homeostasis. Cells secrete a ligand called Sonic-Hedgehog (SHH). This ligand binds to the Patched (PTCH1) receptor on the nearby cells. Once attached, PTCH1 no longer inhibits Smoothened (SMO) protein, and activated SMO initiates an intracellular signaling cascade. This results in the inhibition of the phosphorylation and proteolytic processing of GLI proteins, their translocation and accumulation in the nucleus where they act as transcriptional activators, binding to specific DNA sequences and promoting the expression of HH-GLI target genes (Carballo et al., 2018).

The Notch signaling pathway controls proliferation, differentiation, and apoptosis, but is also crucial for angiogenesis. It is involved in direct contact between two cells, the sending cell (which contains the ligand) and the receiving cell (which contains the receptor). The NOTCH receptor is a dimer that attaches itself to nearby cells' signaling transmembrane proteins. There are 4 neurogenic locus notch homolog (NOTCH 1-4) receptors in humans. Ligands of the NOTCH receptors are divided into two groups. First are the Jagged protein family (JAG1 and JAG2). The other group is Delta-like proteins (DLL1, DLL3, and DLL4). When the dimerization occurs, the Notch protein undergoes proteolytic cleavage in the canonical pathway initially, which is caused by A disintegrin and metalloprotease (ADAM) protease and subsequently by intracellular secretase-γ, which releases the notch intracellular domain (NICD) into the cytoplasm. It then translocates into the nucleus where it binds to a DNA-binding protein, CSL (CBF-1, Suppressor of hairless, Lag-1). This binding converts CSL from a transcriptional repressor to an activator, leading to the transcription of Notch target genes (Zhou et al., 2022).

The Hippo signaling pathway plays a key role in immune response, wound healing, regeneration, and tissue homeostasis. It is particularly interesting because it can integrate different physiological and environmental information by reacting to a broad variety of stimuli. In humans, the three kinases, mitogen-activated protein 4 kinase (MAP4K), the hippo homolog mammalian STE20-like kinase 1/2 (MST1/2), large tumor suppressor kinase 1/2 (LATS1/2), and Salvador homolog 1 (Sav1), are part of the cascade of the Hippo signaling pathway. When

the complex is formed, the yes-associated protein 1/tafazzin (YAP/TAZ) is phosphorylated by activated LATS1/2. This prevents nuclear translocation and leads to degradation. When YAP/TAZ is unphosphorylated, it translocates to the nucleus, binds to TEA domain transcription factor (TEAD 1-4), and activates transcription of genes that regulate cell proliferation, stem cell renewal, and cell death (Fu et al., 2024; Faraji et al., 2022).

The JAK-STAT pathway gets activated with the binding of different ligands that include cytokines, growth factors, or hormones, to their receptors. It plays crucial roles in inflammation and apoptosis. Receptor dimerization or conformational changes upon ligand binding bring the associated JAKs into proximity, which allows the JAKs to transphosphorylate each other. JAK phosphorylates the tyrosine residues of the receptor, which act as a docking point for STAT proteins. STATs are phosphorylated by the JAKs and dissociated from the receptor and form homo- or heterodimers via their SH2 domains. Next, they enter the nucleus and bind to specific promoter domains, activating transcription of target genes (Hu et al., 2021).

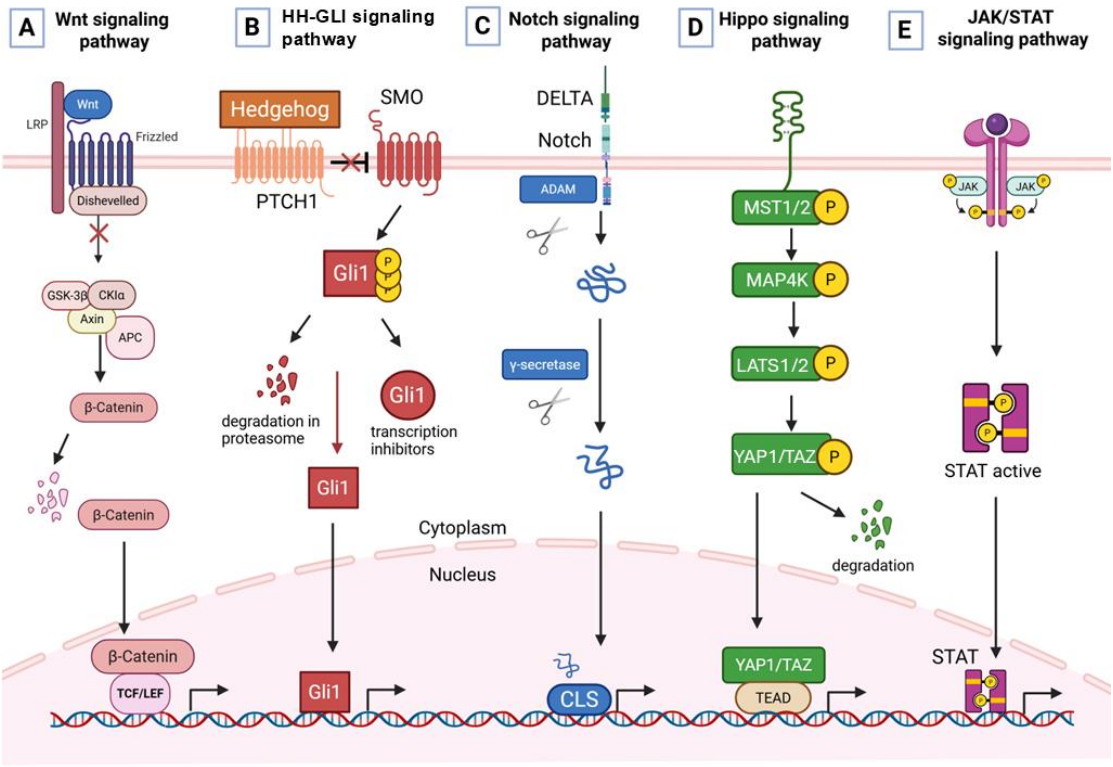

Figure 2.6. CSC signaling pathways in HNSCC: Wnt, HH-GLI, Notch, Hippo, JAK/STAT. (A) Wnt ligand binding to the Frizzled receptor complex and LRP co-receptor leads to recruitment of the Dishevelled protein. This suppresses the β-catenin destruction complex, allowing β-catenin to accumulate, translocate into the nucleus, and induce gene transcription. **(B)** Hedgehog ligand binding to the PTCH1 receptor removes its inhibition of the SMO protein. This prevents degradation of GLI, which enters the nucleus and transactivates Hh target genes. **(C)** Notch receptor ligand binding leads to sequential cleavage by ADAM protease and γ-secretase. The released intracellular domain travels to the nucleus, binds to CLS, and activates transcription. **(D)** Different stimuli initiate the MST1/2-MAP4K-LATS1/2 signaling cascade, which leads to phosphorylation of the coactivator YAP1/TAZ. This prevents nuclear translocation. When YAP/TAZ is unphosphorylated, it translocates to the nucleus, binds to TEAD, and activates transcription**. (E)** Ligand-activated non-receptor JAK kinases phosphorylate STAT protein. The dimerized, phosphorylated STATs travel to the nucleus and function as TFs. The image is adapted from (Ang et al., 2023) and created with biorender.com.

2.3.4. CSC and resistance to therapy

Resistance to conventional anti-cancer therapy is one of the main characteristics of CSCs. This includes chemotherapy, radiotherapy, and targeted treatments. CSCs can also prompt cell cycle arrest, entering a quiescent state that enhances their resistance to chemotherapy and radiotherapy (Phi et al., 2018; Chikamatsu et al., 2012). Traditional cancer therapy is based on DNA damage induction. CSCs may exhibit resistance to cell death induced by DNA damage through various mechanisms, such as protection against oxidative DNA damage by increasing reactive oxygen species (ROS) scavenging, enhancing DNA repair capabilities via Ataxia-Telangiectasia Mutated (ATM) a protein kinase that plays an important role in DNA damage response; and checkpoint kinase 1 and 2 (CHK1/CHK2) phosphorylation, or activating anti-apoptotic signaling pathways, including PI3K/Akt, Wnt/β-catenin, and Notch signaling pathways (Peitzsch et al., 2013). CSCs may also have genetic mutations or epigenetic alterations that could affect multidrug transporters, ATP-binding cassettes (ABCs), and changes in drug metabolism and drug resistance. CSCs have higher expression levels of ABCs, which leads to faster elimination of anti-cancer drugs and drug resistance, but also alters the enzymatic activity, such as ALDH activity (Dean et al., 2005). CSCs exhibit lower mitotic activity than standard cancer cells and therefore may not be affected by the chemotherapeutics that target fast-dividing cells (Chen et al., 2016).

2.3.4.1. CSC and resistance to therapy in HNSCC

The high recurrence of HNSCC cancer could be a result of CSC mechanisms for therapy resistance. Traditional chemotherapy is effective in reducing the bulk of the tumor mass, but CSCs are not eliminated, and over time, they can renew the tumor in the same tissue or metastasize. Increased stemness markers such as ALDH, CD133, Sox2, Bmi-1, Nanog, but also fibroblast growth factor receptor (FGFR) signaling, may lead to higher resistance to cisplatin (Lu et al., 2016; McDermott et al., 2018). CD44 marker has been studied in association with radiotherapy resistance in HNSCC (Dubey et al., 2022). Therefore, it is crucial to understand the characteristics and mechanisms by which CSCs manifest resistance to therapeutic agents and how to enhance their sensitivity to cancer therapy. Consequently, targeting and eliminating these tumor-initiating cells could disrupt tumor regrowth and prevent metastasis (Krishnamurthy & Nör, 2012).

2.3.5. Tumor spheres

Our approach to studying the role of TLR3 in the carcinogenesis of HNSCC focuses on the study of CSCs. Jia et al. showed in 2015 that TLR3 has a role in the formation and maintenance of tumor spheres in breast cancer. However, no other publications on other types of cancer have been published since. CSCs represent a small subgroup of the tumor population, making them more challenging to research. Methods for culturing, analyzing, and isolation of CSCs are still being developed.

The isolation of CD44+ cells using fluorescence-activated cell sorting (FACS) and the isolation based on other CSC markers are some of the methods used for CSC detection (Masciale et al., 2019; Chen & Wang, 2019). The differentiation characteristics and self-renewal of cells can be tested using gel-embedding, the models that include embedding cells onto gels similar to the extracellular matrix, such as Matrigel or collagen (Han et al., 2014). CSC can also be isolated based on their side population, which includes variable efflux dye capacity (Chen & Wang, 2019). Petrić & Sabol (2023) also described some other common methods for spheroid cultivation in prostate cancer. These include the suspension cell cultures, hanging drops, prefabricated scaffolds, and organ-on-a-chip technology. Organ-on-a-chip technology uses microfluid devices to precisely imitate the *in vivo* tumor microenvironment in *in vitro* conditions. Prefabricated scaffolds have structures similar to *in vivo* conditions and are used as a replacement for the extracellular matrix model. Tumor cells can form spheres or spheroids through self-aggregation. Aggregation depends on cell-cell adhesion molecules (e.g., E-cadherin, integrins) and extracellular matrix components. The method of sphere formation includes culturing tumor cells under specific conditions in low-attachment plates. This allows them to detach from their natural environment, survive, and aggregate into 3D structures. Another method of tumor sphere creation is hanging drop cultures, where tumor cells are seeded in a droplet of medium and allowed to hang in a petri dish. This method allows the formation of a smaller number of tumor spheres.

When cancer cells form spheres, they retain stem cell properties over multiple generations. Their ability to reform spheroid shape and structure, and form another generation of tumor spheres, even after the dissociation of the previous generation, acts as evidence of their ability to self-renew. In addition, the determination of phenotypic markers enables their identification (Vukovic Đerfi et al., 2023).

Tumor spheres can vary in size, typically ranging from 50 to 500 micrometers in diameter. Their shape and size depend on cell type and culture conditions. Tumor spheroids exhibit heterogeneous cellular organization. They consist of the outer layer, which consists of proliferating cells that are exposed to nutrients and oxygen. The middle layer contains non-dividing live cells due to limited sources of oxygen and nutrients. The third layer is the core that contains the necrotic zone, which contains dead cells because of hypoxic conditions and nutrient deprivation. Usually, larger tumor spheroids will form necrotic cores after developing oxygen and nutrient gradients. This formation is similar to solid tumors in the body, which makes tumor spheres a better model for cancer research compared to 2D monolayers (Gunti et al., 2021). Until now, the tumor spheres were studied in various types of cancer, including breast cancer spheres (mammospheres), neural (neurospheres), prostate, but also HNSCC (orospheres) (Pastrana et al., 2011; Krishnamurthy et al., 2010). Krishnamurthy & Nör (2012) indicate that sphere formation ability of HNSCC seems to be a suitable method for studying the mechanism of CSCs in HNSCC and might further impact the treatment development. Tumor spheres provide insights into tumor growth, resistance to therapy, and metastasis. Some tumor spheres show invasive abilities mimicking cancer metastasis. The morphology of invasive tumor spheres can indicate the metastatic potential of the cancer cells (Hamilton & Rath, 2019).

2.4. Endogenous ligands/damage-associated molecular patterns (DAMPs)

Numerous intracellular molecules known as endogenous ligands or damage-derived molecular patterns are generated during cell damage. DAMPs are often released from necrotic cells after being exposed to stressors. Necrotic cell death can happen due to chemical or physical effects, including radiation, chemotherapy, toxins, mechanical injury, burn-induced damage, or cryonecrosis (Zhang et al., 2014) (Figure 2.7).

DAMPs can be cellular proteins, lipids, metabolites, extracellular matrix molecules, and nucleic acids that are being released during cell injury or tissue damage. DAMPs are an important part of the immune system signaling. When DAMPs bind to their corresponding receptors, they will induce an immune response and activate the immune system (Piccinini & Midwood, 2010). The list of DAMPs and their receptors can be found in Table 2.1. Some of the DAMP receptors are TLRs, receptors for advanced glycation end products (RAGE), RIG-I-like receptors (RLRs), NOD1-like receptors (NLRs), and AIM2-like receptors (Huang et al., 2015).

RAGE is a transmembrane pattern recognition receptor that is expressed on the endothelial, immune, and tumor cells. RAGE recognizes endogenous molecules that are released from damaged tissues, playing a role as a receptor in many inflammatory disorders (Cross et al., 2024). RAGE receptors bind advanced glycation end products (AGEs) but also DAMP molecules, HMGB1, HSPs, and S100 proteins. RAGE is an important player in chronic inflammation and cancer progression (Fritz, 2011; Daffu et al., 2013; Riehl et al., 2009).

High mobility group box 1 (HMGB1) is a highly conserved nuclear protein. , which plays an important role in DNA-associated processes that include transcription, replication, and DNA repair. It acts as a DNA chaperone, facilitating DNA bending and unwinding, which is crucial for processes like gene transcription, DNA replication, and DNA repair mechanisms. Intracellularly, HMGB1 loss will lead to increased DNA damage, cell death, and consequently, its release from the cells. Extracellularly, it acts as a pro-inflammatory mediator and tumorigenic factor, which binds to TLR2, TLR4, and RAGE. Ligand binding further activates signaling pathways involved in cancer progression and tumor sphere formation. In addition, HMGB1 contributes to invasion, stimulates autophagy, acts as an immune suppressor, and plays a role in resistance to anti-cancer therapy (Zapletal et al., 2023).

S100 is a family of intracellular proteins that act as regulatory proteins for calcium binding. They also regulate cell growth and differentiation, apoptosis, cell migration, and invasion (Donato et al., 2012). Some of them also act as DAMP ligands in cancer. In the TME, they are associated with immune activation, migration, invasion, and tumor progression in the majority of tumors. The exception is S100A2, which acts as a tumor suppressor in oral cancer (Tsai et al., 2006) but as a tumor promoter in others (Bresnick et al., 2015).

Heat shock proteins (HSPs) are a group of ubiquitously expressed stress proteins. They are upregulated in certain cellular stress conditions that include toxin exposure, hypoxia, and hyperthermia. They are primarily molecular chaperones, and their function is to preserve protein structure and proper folding, as well as protein signaling activation, and prevent cell death. They play a crucial role in maintaining cellular homeostasis (Singh et al., 2024). Due to stressors like hypoxia and nutrient deficiency in TME, HSPs are often elevated in tumors. This can lead to cancer cell survival by blocking apoptosis, but also by contributing to therapy resistance and enhancing metastatic traits like EMT (Zapletal et al., 2023).

It has been demonstrated that TLR3 can be activated by DAMPs, such as variants of cellular RNA originating from necrotic cells (Figure 2.7), including mRNA from necrotic cells, which has been described as the first endogenous ligand for TLR3 (Karikó et al., 2004). This implies that the activation of TLR3 in tumor cells or their microenvironment does not necessarily require an external factor, such as a viral infection. Their activation could be induced by internal factors only (Cavassani et al., 2008; Vasiljevic et al., 2023). DAMPs are often overexpressed in tumors or released by tumors due to the stressful conditions in the TME (Zapletal et al., 2023), where they activate TLR signaling pathways or RAGE. TLR activation by DAMPs induces the activation of the immune response (Piccinini & Midwood, 2010).

Table 2.1. List of DAMPs and their receptors. Table taken from Zapletal et al., 2023.

Type of DAMP	DAMPs	Receptors
Proteins	HMGB1	TLR2, TLR4, RAGE
	Histone	TLR2, TLR4
	S100	TLR2, TLR4, RAGE
	HSPs	TLR2, TLR4, CD91, RAGE
	Annexin A1	FPR1
	Versican	TLR2, TLR6, CD14
	Fibronectin (EDA domain)	TLR4
	Fibrinogen	TLR4
	Tenascin C	TLR4
	F-actin	DNGR-1
	Cyclophilin A	CD147
	Aβ	TLR2, NLRP1, NLRP3, CD36,
	IL1α/IL33	IL-1R/ST2
	Formyl peptide	FPR1
	Calreticulin	CD91
	Defensins	TLR4
	Cathelicidin (LL37)	P2X7, FPR2
	Granulysin	TLR4
Lipids and carbohydrates	LMW hyaluronan	TLR2, TLR4, NLRP3
	SAA	TLR2, TLR4
	Heparan sulfate	TLR4
Metabolite-related DAMPs	ATP	P2X7, P2Y2
	Uric acid	NLRP3, P2X7
Nucleic acids	DNA	TLR9, AIM2
	RNA	TLR3, TLR7/8, RIG-I, MDA5
	mtDNA	TLR9

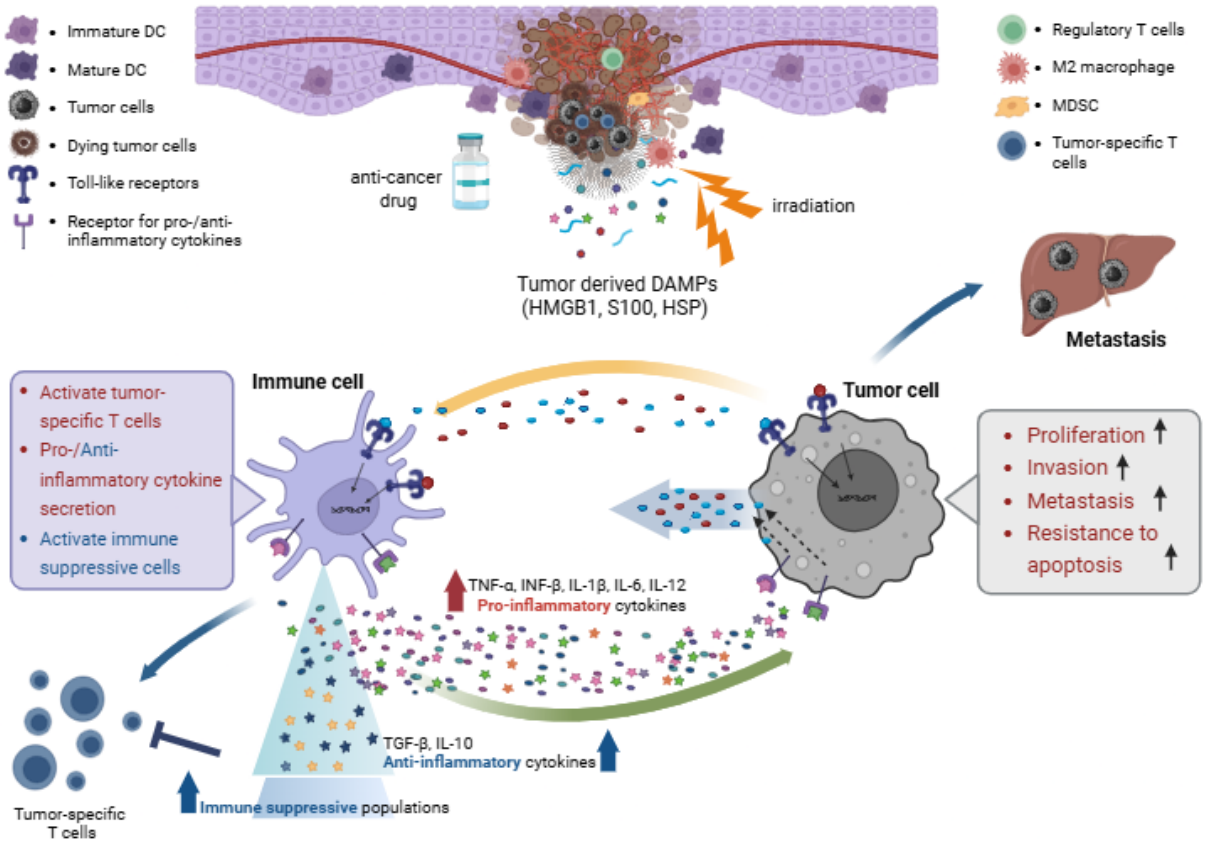

Figure 2.7. DAMPs released from necrotic tumor tissue activate TLRs on either immune cells or on tumor cells in the tumor microenvironment. DAMPs can be released after tissue damage due to chemotherapy, radiotherapy, or other factors. They can stimulate different responses after binding to TLRs on tumor cells or immune cells. Immune cells may activate an immune response or induce immune suppressive cells, and tumor cells may induce cell proliferation, metastasis, invasion, and resistance to apoptosis. The image is adapted from (Jang et al., 2020) and created with biorender.com.

2.5. Head and neck squamous cell carcinoma (HNSCC)

Head and neck cancers include different tumors of the aerodigestive tract. Tumors can develop in the oral cavity, mucosal membrane, pharynx, larynx, nasal cavity, muscles, or nerves of the head and neck area (Argiris et al., 2008) (Figure 2.8). Each of these regions is lined with squamous epithelium cells. Most head and neck tumors are diagnosed as squamous cell carcinomas. Mucosal epithelium is where the cancer stems from. It starts with the hyperplasia of the epithelial cells, succeeded by dysplasia and carcinoma in situ, which ends with an invasive malignant tumor (Johnson et al., 2020).

Head and neck squamous cell carcinoma (HNSCC) represents approximately 90% of all head and neck malignancies. It is the sixth most prevalent cancer globally and is characterized by its recurrence tendency post-treatment. Cancers in the oral cavity and larynx are commonly linked to the use of tobacco, excessive alcohol consumption, or a combination of both. In terms of infectious agents, persistent infection with human papillomavirus (HPV) and Epstein–Barr virus (EBV), are risk factor for HNSCC arising from the oropharynx and nasopharynx (Johnson et al., 2020).

In recent research, TLR3 has been linked with the development of EBV-induced nasopharyngeal carcinoma (Li et al., 2015). External factors, including viral infections, toxins, and radiation, cause inflammation in the TME. During chronic inflammation, this persistent state leads to ROS factors release, and pro-inflammatory cytokines, which results in DNA damage or mutation in tumor suppressor genes, including *TP53*, which promotes tumor progression (Gudkov & Komarova, 2016).

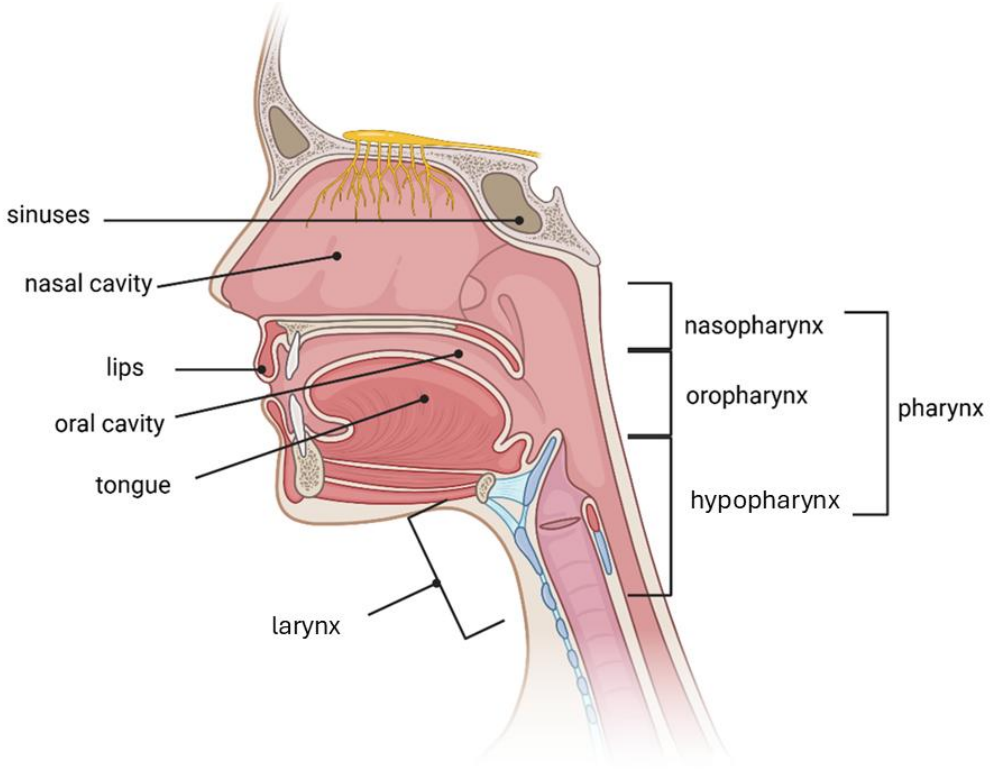

Figure 2.8. The Anatomy of the head and neck. The oral cavity includes the lips, mouth, anterior tongue, buccal mucosa, and hard palate. Surrounding anatomical regions include the nasal cavity, sinuses, pharynx, which is divided into nasopharynx, oropharynx, hypopharynx, and the larynx with vocal cords. The image was created with biorender.com.

2.5.1. Challenges in current HNSCC therapies

Regardless of many existing therapy modalities, a significant number of patients show inadequate responses to treatment, resulting in recurrent disease. HNSCC is characterized by the high incidence of local recurrence and distant metastasis, which may be attributed to CSCs (Chinn et al., 2012). HNSCC is often very aggressive and diagnosed in the late stages of the disease, when metastasis has already occurred. Current treatments often include surgery, chemotherapy, radiotherapy, immunotherapy, or their combinations.

Despite the development of cancer treatment, HNSCC still has a poor prognosis, and overall, the 5-year survival rate for HNSCC can range from 40% to 60%. Head and neck tumor cells often develop radio- and chemotherapy resistance, which results in the recurrence of disease (Li et al., 2023). Epithelial–mesenchymal transition (EMT) plays a significant role in tumor migration and metastasis. EMT is a physiological mechanism that causes cells to lose their epithelial traits. This allows them to loosen and lose a strong, adhesive bond with surrounding cells. These cells then gain the ability to migrate, which causes invasion of surrounding tissues and metastasis. EMT is believed to be crucial in head and neck malignancies (Pal et al., 2021).

Recent studies showed that metastasis in HNSCC is associated with several molecular mechanisms. This involves immune invasion, extracellular matrix reorganization, and involvement of hypoxia-induced factors. Hypoxia in TME activates HIF-1α, which enhances metastatic potential by promoting angiogenesis in TME (Wicks & Semenza, 2022). Additionally, (Li et al., 2016) showed that the exosomal miRNA in TME derived from hypoxic HNSCC can reach normal cells and induce pro-metastatic characteristics in nonhypoxic cells. Moreover, HNSCC metastases most commonly occur in cervical lymph nodes (Burusapat et al., 2015).

2.6. Radiation therapy

Radiation therapy is one of the main treatment options for HNSCC. Radiotherapy is often combined with chemotherapy and surgery. Pre-treatment by chemotherapy can make cancer cells more susceptible to irradiation by inducing radiosensitivity (Yeh, 2010). Radioactive decay generates three types of radiation: alpha and beta particles, and γ-rays (Springer, 2004). Gamma (γ) irradiation is based on γ-rays that are obtained from radioactive isotopes of Cobalt-60, a common source of γ-rays in medical use. Gamma radiation has a very high ability of tissue penetration and is only stopped by very dense materials such as thick lead shields (Brinston & Norton, 1994). It is also damaging healthy tissue, so common side effects include irritation, vomiting, and hair loss. Radiotherapy damages the cancer cells' DNA, which leads to cell death and disruption of the TME in terms of damage to endothelial cells, stromal cells, and activation of the immune response.

In HNSCC, it can be used as the final treatment after surgery, as definitive treatment (instead of surgery), or pre-operatively. Cancer cells often become resistant to radiation therapy due to enhanced DNA damage repair, specific changes in the TME, such as hypoxia or immune suppression, or by the activation of pro-survival pathways and apoptosis evasion. Radiotherapy resistance in HNSCC is common because of increased DNA repair capacity and tumor hypoxia (low oxygen levels). Hypoxia reduces the generation of reactive oxygen species (ROS), which are crucial for radiation-induced damage. EGFR and PI3K/AKT signaling pathways are frequently dysregulated in cancer and are known to promote cell survival, DNA repair, and contribute to radioresistance (Glorieux et al., 2020). To enhance anti-tumor response and overcome resistance in HNSCC, a promising approach would involve sensitization of cancer cells to radiation, targeting hypoxia-related mechanisms, and combining radiation treatment with immune checkpoint inhibitors (Kao et al., 2023; dos Santos et al., 2021).

2.7. Proton therapy

Proton beam therapy is an innovative form of radiation treatment that employs positively charged particles – protons to deliver a focused dose of radiation directly to cancerous tissue. Unlike conventional radiation cancer treatments, such as γ-ray radiation and X-ray irradiation, which lack precision, protons target cancer cells with high precision, releasing most of their energy exactly where the tumor is located. This leads to less destructive irradiation side effects since it preserves normal surrounding tissues. Bragg's peak is the distinct ability of charged particles to deposit most of their energy at the end of their path as they travel through matter. This results in a sharp, localized peak for radiation dose delivery. Bragg's peak was first mentioned in 1904 by William Henry Bragg when he observed that ionization with radium alpha particles was more effective towards the end of its course (Bragg & Kleeman, 1904). Bragg's peak was first mentioned in a medical context by Wilson in 1946. He proposed the idea that proton beam therapy could be used for cancer treatment. He explained first that the proton beam travels through healthy tissue before it reaches the target cancer, depositing low amounts of energy. Then it releases a large amount of radiation energy to the target and kills cancer cells (Wilson, 1946). To compare, X-rays release and deposit energy along their path, causing damage to surrounding tissues and organs, before and after the target tumor tissue. Protons were effective in lung cancer CSCs eradication, where they significantly decreased the cell survival of tumor cells resistant to chemotherapy, reduced the number and survival of tumor spheres, and downregulated migration and invasiveness. Moreover, CSC markers were reduced, and apoptosis and ROS were increased (Zhang et al., 2013).

For HNSCC, Nuyts et al. (2022) show that proton beam therapy could be a treatment option for patients with mucosal SCC that is situated superior to the hyoid bone because of their complex structure and different critical organs at risk. For patients with recurrent disease, the re-irradiation therapy with proton beam could be the sole treatment approach with a curative outcome. It allows a higher dose of irradiation for tumor targeting, but without affecting the previously irradiated healthy tissue (Romesser et al., 2016). Another study indicated that re-irradiation in HNSCC was effective for the tumor site, but it comes with the risk of potentially developing osteoradionecrosis (Hsieh et al., 2024). Mumaw et al. (2024) state that there are only a few cases of cancer recurrence on the contralateral neck after the unilateral proton beam therapy in patients with HNSCC.

2.8. UFMylation

UFMylation is a form of posttranslational modification, similar to ubiquitination, that was described in the early 2000s. It was first characterized by Komatsu et al. (2004). who showed that all the major proteins that take part in UFMylation are ubiquitously expressed across various tissues, indicating their fundamental role in cellular processes. The process of UFMylation begins with the activation of ubiquitin fold modifier-1 (UFM1), a small protein (9 kDa) that is similar to ubiquitin in its tertiary structure. UFM1 is synthesized as a precursor and requires proteolytic cleavage (processing). It is cleaved by UFSP1 and UFSP2, which are UFM1-specific peptidases. Three types of enzymes, which are preserved in most eukaryotes, play a role in the process of UFMylation, similarly to ubiquitination: E1 (activating), E2 (conjugating), and E3 (ligase). The process begins with the E1, ubiquitin-like modifier activating enzyme 5 (UBA5) activation of UFM1 by binding adenosine triphosphate (ATP).

Next, the E2, ubiquitin-fold modifier conjugating enzyme 1 (UFC1), transports active UFM1 from E1 to E3. Subsequently, E3, UFM1-specific ligase 1 (UFL1) recognizes specific target proteins (substrate) and, along with regulatory proteins DDRGK domain containing 1 (DDRGK1), acts as a docking hub for substrate UFMylation. UFM1 binds to lysine residues on target proteins. UFSP1 and UFSP2 also act as de-UFMylating enzymes and can remove UFM1 from the substrate to make the process of UFMylation reversible (Kang et al., 2007) (Figure 2.9).

Besides UFM1, UBA5 is found in the cytoplasm and is specific for UFMylation as the only E1 protein found in this process. UFC1 is found in the nucleus and the cytoplasm and acts as the E2 enzyme. UFL1 is identified as the E3 ligase, which is specific for UFM1 and is located on the membrane of the endoplasmic reticulum. The DDRGK1 and CDK5 regulatory subunit-associated protein 3 (CDK5RAP3) participate in the final step of substrate recruitment (Millrine et al., 2023).

UFSP2, together with UFSP1, is a protease specific to UFM1 that belongs to the novel cysteine protease subgroup. They cleave the C-terminal Ser-Cys dipeptide so it can reveal the glycine residue. They are involved in the process of protein UFM1 activation and UFM1 removal from the substrate. It is generally assumed that UFSP2 plays a more important role in the removal of UFM1 from the substrate, which enables the recycling of UFM1, while UFSP1 might have a role in UFM1 maturation. UFSP1 is found in the cytoplasm, while UFSP2 is found in the

cytoplasm and nucleus and can be associated with the endoplasmic reticulum (ER) (Millrine et al., 2023).

The function of UFMylation is still not completely clear, but it has been linked to DNA damage response, protein biogenesis, telomere maintenance, autophagy, and ER homeostasis. The role of UFMylation in tumorigenesis is still poorly explained, and the role depends on the type of cancer. In some tumors, it plays a role in tumor suppression, while in others, it has a pro-tumorigenic effect (Millrine et al., 2023). Only a few UFMylation substrates have been described. Tumor suppressor p53 protein is one of them, and it has been demonstrated that UFM1 can covalently modify p53 and inhibit its ubiquitination and proteasomal degradation. This leads to stabilization of the p53 protein and activation of tumor suppression. It has been shown that the downregulation of DDRGK1 and UFL1 reduces the stability of p53, which leads to increased cell proliferation and tumor formation (Liu et al., 2020).

We showed that in HNSCC, UFMylation could play an important role in cancer stem cells. Proteomic analysis and further confirmation by western blot showed different expressions of DDRGK1 and UFSP2 proteins, involved in UFMylation. Bioinformatic analysis revealed us a correlation of UFM1 with EMT genes that indicate poor prognosis. UFM1 silencing decreased tumor sphere number and stemness, demonstrating its possible role in maintaining CSC characteristics. Based on bioinformatics analysis, which identified Sp1 as the main TF in UFMylation, mithramycin, a known Sp1 inhibitor, was used to target CSCs. Mithramycin reduced tumor sphere survival, targeted key UFMylation genes and *RPL26*, a known UFMylation substrate, and induced apoptosis. Overall, downregulating UFMylation proteins could inhibit HNSCC progression by acting on CSCs (Derfi et al., 2024).

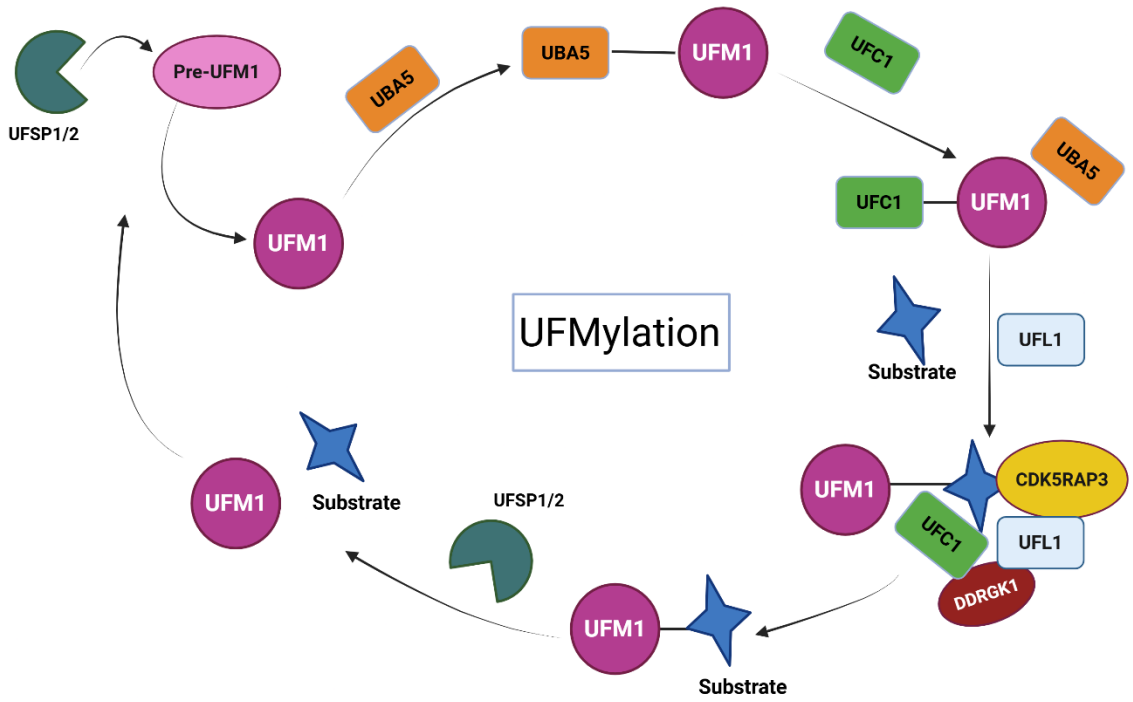

Figure 2.9. The UFMylation process. The UFM1 precursor (pre-UFM1) is cleaved by the UFM1-specific peptidases (UFSP1 and UFSP2), while the UBA5 activates the mature UFM1 by starting the cascade of UFM1 transfer to the substrate through UFC1 and UFL1 proteins. The regulatory proteins CDK5RAP3 and DDRGK1 participate in the final step of substrate recruitment. UFSP1 and UFSP2 can cleave UFM1 from the substrate to make the process reversible. The image is adapted from Jing et al. (2022) and created with biorender.com.

2.9. Kynurenine pathway

The kynurenine pathway plays a role in the tryptophan (Trp) degradation cascade (Figure 2.10). According to Badawy (2017) it participates in 95% of the Trp metabolism. Kynurenine Aminotransferase 3 (KYAT3, KAT3) is a key enzyme that plays a role in the tryptophan degradation cascade. KYAT3 facilitates the irreversible transamination of L-kynurenine, which leads to the production of kynurenic acid (Human Protein Atlas, 2024, accessed on 10.05.2025). According to The Human Protein Atlas, KYAT3 is found to be a prognostic marker for breast carcinoma, kidney carcinoma, and colon adenocarcinoma. Overall, little is known about KYAT3 and its role in cancer stem cells.

A preliminary study from 2006 (Tankiewicz et al.) showed that in oral squamous cell carcinoma, Trp breakdown has been associated with the regulation of tumor cell proliferation. The kynurenine pathway has been linked with tumor escape from immune recognition. Increased indolamine 2,3-dioxygenase (IDO), one of the key enzymes of the Trp/kynurenine pathway, causes a drop in Trp levels and a buildup of the breakdown product, kynurenine, within the TME. This leads to immunosuppressive settings where T cells are unresponsive and apoptotic, while their differentiation is inhibited (León-Letelier et al., 2023). In recent studies, targeting tryptophan metabolism has been proposed as a potential new strategy for cancer treatment (Platten et al., 2019; Yan et al., 2024).

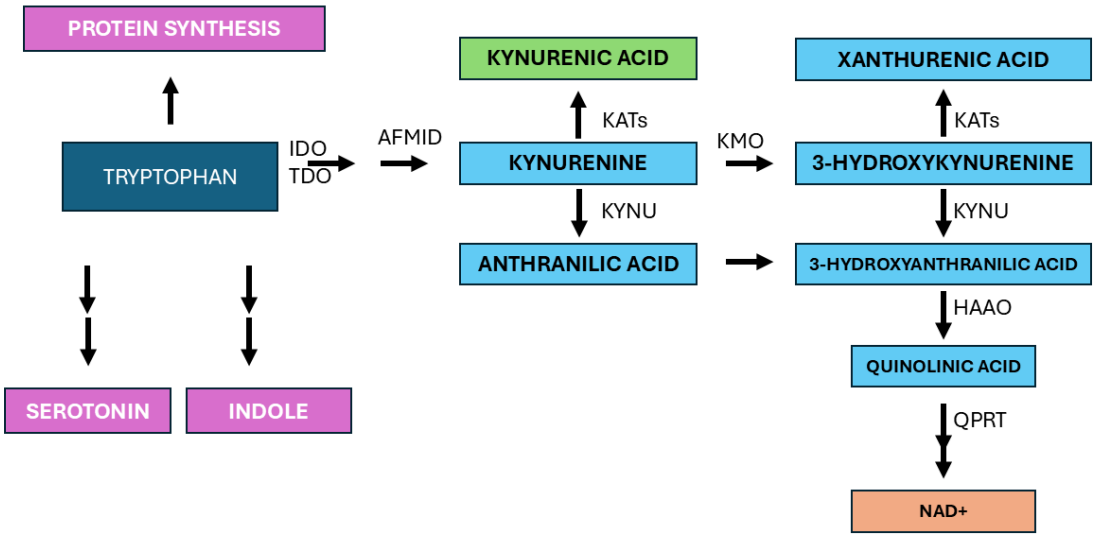

Figure 2.10. Kynurenine pathway. The overview of the tryptophan metabolism and the kynurenine pathway. Tryptophan (Trp) is metabolized by indolamine 2,3-dioxygenase (IDO) (or tryptophan 2,3-dioxygenase (TDO) to kynurenine (Kyn). It can then be converted to several metabolites (kynurenic acid, anthranilic acid or quinolinic acid), and also to other metabolites (xanthurenic acid, 3-hydroxykynurenine, 3-hydroxyanthranilic acid and quinolinic acid. Pathway includes several enzymes including arylformamidase (AFMID), kynurenine aminotransferases (KATs/KYATs), kynureninase (KYNU), kynurenine 3-monooxygenase (KMO), 3-hydroxyanthranilate 3,4-dioxygenase (HAAO), and quinolinate phosphoribosyltransferase (QPRT). The image is adapted from Walczak et al. (2020).

3. MATERIALS AND METHODS

3.1. Tumor cell lines

Human head and neck squamous cell carcinoma (HNSCC) derived cell lines were analyzed in this research (pharyngeal cancer cell lines Detroit 562 and FaDu, and laryngeal cancer cell line SQ20B). The pharyngeal cells were obtained from ATCC (LGC Standards) in 2018 (part of the head and neck cancer panel, TCP-1012), and the laryngeal cancer cell line SQ20B (CVCL 7138) was a gift from Prof. Pierre Busson (Gustave Roussy Institute, Villejuif, France). The Detroit 562 (CCL-138™, ATCC, Manassas, Virginia, USA) (CVCL 1171) epithelial cell line is derived from pleural effusion of pharyngeal metastatic carcinoma. FaDu (ATCC® HTB-43™, ATCC, Manassas, Virginia, USA) (CVCL 1218) is an epithelial cell line derived from primary hypopharyngeal squamous cell carcinoma. The SQ20B cell line, derived from a laryngeal tumor, is frequently used as a radiation-resistant HNSCC model.

3.2. Cell culture

3.2.1. Routine cell culturing

Detroit 562, FaDu, and SQ20B cells were stored at -196°C in liquid nitrogen for long-term storage. To introduce the cells into the cell culture, they were rapidly thawed using a water bath at 37°C. Then, the cells were transferred into a 15 mL Falcon tube containing 5 mL of cell growth medium (DMEM, Dulbecco's Modified Eagle Medium Low Glucose (Sigma Aldrich, St. Louis, Missouri, USA); supplemented with 1% penicillin and streptomycin (Sigma Aldrich, St. Louis, Missouri, USA), 1% L-glutamine (Sigma Aldrich, St. Louis, Missouri, USA), and 10% fetal bovine serum (FBS, Sigma Aldrich, St. Louis, Missouri, USA)). The cells were centrifuged (Heraeus Megafuge 1.0 R, Thermo Fisher Scientific, Waltham, Massachusetts, USA) at 300 x g for 5 minutes at room temperature. The cell pellet was resuspended in fresh DMEM and transferred to the cell culture flask (T75, TPP Techno Plastic, Trasadingen, Switzerland). Finally, the cell culture flask was kept in the incubator at 37°C, with 5% CO_2 volume fraction (Heraeus HERAcell 150, Thermo Fisher Scientific, Waltham, Massachusetts, USA). All *in vitro* procedures were performed under sterile conditions inside a laminar flow hood (Iskra HK16, Klimaoprema, Samobor, Croatia).

3.2.2. Tumor sphere formation

The tumor sphere formation technique was applied to enrich CSCs. This assay is considered a well-established model for CSC research (Lee et al., 2016). The assay was based on the ability of cancer cells to form 3D spherical structures when grown in low-attachment cell culture plates in a serum-free, antibiotic-free medium MEBM (Mammary Epithelium Basal Medium, Lonza Bioscience, Basel, Switzerland), supplemented with vitamin B27 supplement (50X) serum free (1:50) (Thermo Fisher Scientific, Waltham, Massachusetts, USA), epidermal growth factor (EGF, 20 ng/mL) (PeproTech, Thermo Fisher Scientific, Waltham, Massachusetts, USA) and fibroblast growth factor (FGF, 10 ng/mL) (PeproTech, Thermo Fisher Scientific, Waltham, Massachusetts, USA) (Figure 3.1). To prepare plates for tumor sphere growing conditions, different types and sizes of TPP® tissue culture dishes (Techno Plastic, Trasadingen, Switzerland) were coated with BIOFLOAT™ FLEX coating solution (faCellitate, Mannheim, Germany). For 96 wells, ready-to-use BIOFLOAT™ 96-well plates with U-bottom were used.

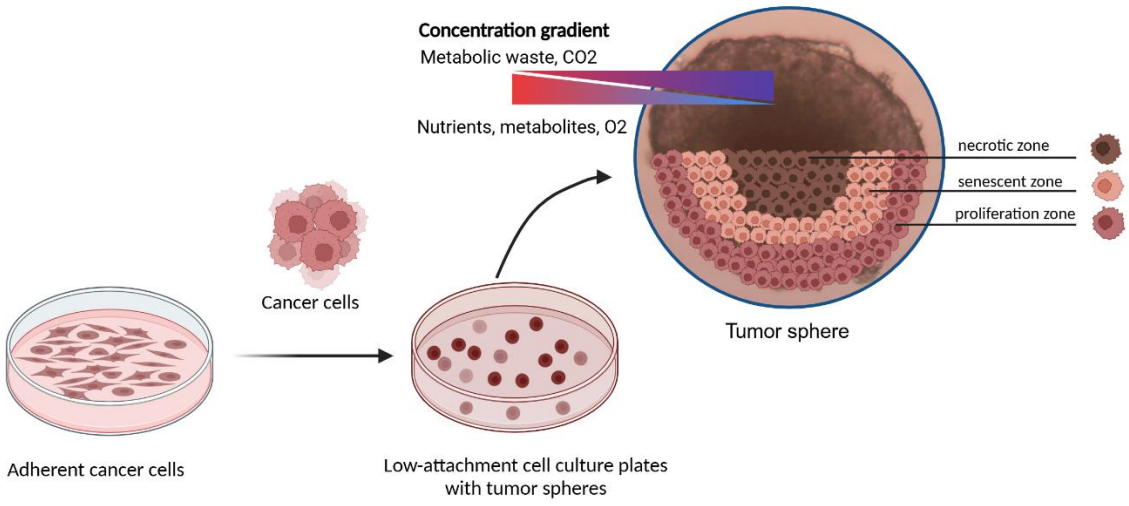

Figure 3.1. Formation of tumor spheroids. Adherent cancer cells are transferred into the low-attachment culture plates, where they aggregate and form 3D tumor spheroids. Tumor spheroids have an established concentration gradient. Oxygen and nutrients decrease towards the center, while metabolic waste and CO_2 accumulate. This creates a proliferative zone at the periphery, senescent middle zone and the necrotic core. The image was sourced from Gilazieva et al. (2020), and adjusted using biorender.com.

3.2.2.1. Tumor sphere size and morphology

Detroit 562, FaDu, and SQ20B cells were cultured in ultra-low attachment plates and serum-free MEBM with the addition of EGF, FGF, and B27 to form tumor spheres. Three days after seeding, tumor spheres were treated with poly(I:C) or poly(A:U) and were quantified based on number and size after the stimulation of TLR3. The number of tumor spheres was quantified at 2, 4, and 7 days after the treatment. Spheres were counted using an inverted phase-contrast microscope, with particular focus on larger spheres. Tumor spheres were divided into three groups based on size. The first was 0 - 50 μm in diameter, the second was 150 - 200 μm in diameter, and the third was ≥300 μm in diameter. The effects of the treatment on sphere size and morphology were assessed by comparing the number of spheres in the treated versus control groups.

3.3. Tumor sphere generations

Aldehyde dehydrogenase (ALDH) is a marker for cancer stem cells that plays a significant role in cell survival. The expression of ALDH1A1 was analyzed after prolonged cultivation and tumor spheres enrichment through a series of passages of tumor spheres. Detroit 562 cells were seeded in low-adhesion conditions and special MEBM medium for tumor spheres cultivation. Several generations of tumor spheres were grown, and the expressions of ALDH1A1 and CD133 were determined for each generation. Increased expression and activity of ALDH are linked to enhanced stem-like properties in tumor spheres, and CD133 is a CSC marker that plays an important role in tumorigenicity and metastasis. Generations 1-3 were obtained by cultivating the spheres for 72 hours after which a portion of tumor spheres was removed for expression analysis and the rest was dissociated into single-cell suspension using TrypLE™ Express Enzyme (Thermo Fisher Scientific, Waltham, Massachusetts, USA) with EDTA without phenol red, which reduces damage to cells. The dissociated cells were then cultured again to form tumor spheres under the same conditions for another 3 days, and the whole process was repeated for 3 generations. Proteins were isolated from tumor spheres, and ALDH1A1 and CD133 expressions were detected using western blot.

3.4. Transfection

Transfection is a technique utilized to distribute external nucleic acids into eukaryotic cells. RNA interference (RNAi) is an RNA-dependent gene silencing method that is regulated by RNA-induced silencing complex (RISC) and is activated by short double-stranded RNA molecules (small hairpin RNA (shRNA), small interfering RNA (siRNA), and microRNA (miRNA)). It is being utilized by eukaryotes for antiviral defense, gene modulation, and gene regulation. Many methods for shRNA and siRNA delivery into the cell are available (Agrawal et al., 2003). Different vectors and commercially available plasmids are being used. In most cases, transfection is transient, meaning that the introduced DNA remains in the cell cytoplasm without integrating into the chromosomal DNA of the cell. The introduced DNA will be lost after a few cell divisions, unlike in stable transfection, where the plasmid is integrated into the genome (Chong et al., 2021).

3.4.1. pTRIPZ stable transfection

FaDu and SQ20B cell lines with stably transfected pTRIPZ were a gift from Prof. Pierre Busson of the Institut Gustave Roussy, Villejuif, France. The pTRIPZ plasmid was used for stable transfection (Thermo Scientific, Waltham, Massachusetts, United States) (Figure 3.2). pTRIPZ can induce shRNA expression in the presence of doxycycline (Tet-On configuration) . The Tet-On system is based on two features for induction: a modified tetracycline response element (TRE) and a transactivator. This transactivator, reverse tetracycline transactivator 3 (rtTA3), is bound to the TRE in the presence of doxycycline, activating transcription from the TRE promoter. The pTRIPZ plasmid contains a coding region for TurboRFP (tRFP, red fluorescent protein), the operator gene, which is located upstream of the shRNA gene and downstream of TRE. Additionally, the plasmid contains a puromycin resistance gene, allowing the establishment of stably transfected cell lines. Cells without the plasmid will not survive when puromycin is added to the medium.

FaDu and SQ20B cell lines were stably transfected with the pTRIPZ plasmid containing shRNA targeting TLR3. More specifically, FaDu-shTLR3 and SQ20B-shTLR3 cell clones were stably transfected with the pTRIPZ plasmid, which carries a gene for shRNA that specifically targets TLR3 mRNA. The addition of doxycycline induces the expression of shRNA in transfected cells, allowing conditional TLR3 knockdown. This activates the RNAi pathways, ultimately

leading to mRNA degradation and silencing of TLR3 expression. FaDu-shcontrol and SQ20B-shcontrol cell clones contain a stably transfected empty plasmid.

For protein isolation, 10^6 cells were seeded in 6-well plates per well for tumor spheres and 0.5 x 10^6 cells in 6-well plates per well for adherent cells. Doxycycline (Sigma Aldrich, St. Louis, Missouri, USA) was added at a concentration of 2 µg/mL, and puromycin (Sigma Aldrich, St. Louis, Missouri, USA) at a concentration of 0.4 µg/mL. Antibiotics were mixed with the medium before being added to the cells. Cells were incubated for 72 hours to form tumor spheres before the tumor spheres were treated with poly(I:C) or poly(A:U) and doxycycline to silence TLR3. Proteins were isolated after 24 hours, and a western blot was performed.

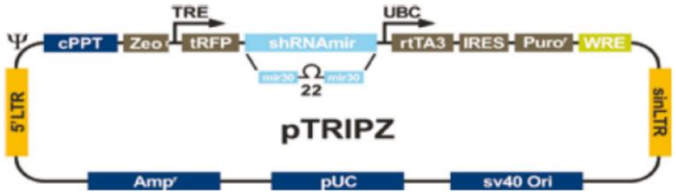

Figure 3.2. pTRIPZ lentiviral vector. Source: Thermo Fisher pTRIPZ technical manual.

3.4.2. Transient transfection

siRNAs are often used to silence and regulate the expression of target genes in eukaryotes. siRNAs are assembled into RISCs through the Argonaute 2 (Ago2) protein. When siRNA is being processed, it is separated into two strands. One is the guide strand that matches the target messenger RNA (mRNA), and the other, the passenger strand, is discarded. Once RISCs are activated, they bind to complementary mRNA. The bound mRNA is cleaved, resulting in gene silencing (Alshaer et al., 2021) (Figure 3.3).

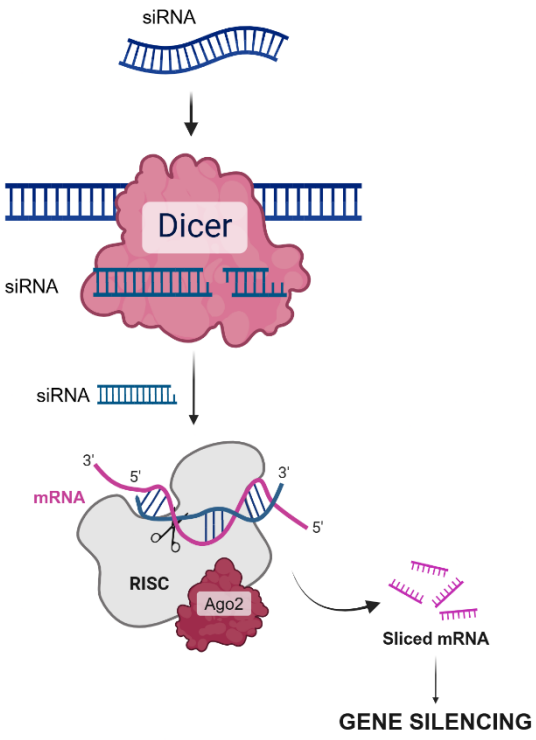

Figure 3.3. The RNAi cascade reaction from the siRNA to mRNA degradation and gene silencing. siRNAs are incorporated into the RISCs via the Ago2 protein, which keeps the guided strand and degrades the passenger strand. Activated RISC binds to complementary mRNA and cleaves it, leading to gene silencing. The image was created in biorender.com.

A literature search revealed that the transfection of tumor spheres may not be as effective as that of adherent cells (de Caro et al., 2023). Therefore, the transfection was performed on adherent Detroit 562 cells, and tumor spheres were grown subsequently (Figure 3.4). Double-stranded siRNA for knocking down the endogenous TLR3 (sc-36685, Santa Cruz Biotechnology, Dallas, Texas, USA) and scrambled-sequence control siRNA (Control siRNA-A, sc-37007, Santa Cruz Biotechnology, Dallas, Texas, USA) were used. To determine the most suitable transfection conditions for gene silencing, the efficiency of different concentrations of siRNA and transfection reagent was evaluated.

To obtain visible results, control siRNA labeled with fluorescein isothiocyanate was used (FITC-siRNA, sc-36869, Santa Cruz Biotechnology, Dallas, Texas, USA). Various molar concentrations of FITC-siRNA (10 nM, 20 nM, 50 nM, and 80 nM) were combined with different volumes (4 µL, 6 µL, and 8 µL) of TransFectin™ Lipid Reagent (Bio-Rad Laboratories, Hercules, California, USA). For siRNA transient transfections in adherent cells, serum-free DMEM supplemented with L-glutamine was used. The FLoid™ Cell Imaging

Station (Thermo Fisher Scientific, Waltham, Massachusetts, USA) fluorescence microscope was used to capture images of transfected cells. The conditions where a substantial reduction in gene expression was demonstrated were replicated in experiments with the target gene. We have determined that for transfection experiments, Detroit 562 cells, which were seeded at 8 x10^5 cells in 6-well plates, the best results are obtained with 80 nM of TLR3 siRNA or control siRNA and 8 µL of TransFectin™ Lipid Reagent. Twenty-four hours following transfection, cells were seeded in low adherent plates and MEBM medium to form tumor spheres, and one day later, spheres were treated with poly(I:C)/poly(A:U) for 24 hours, followed by protein isolation.

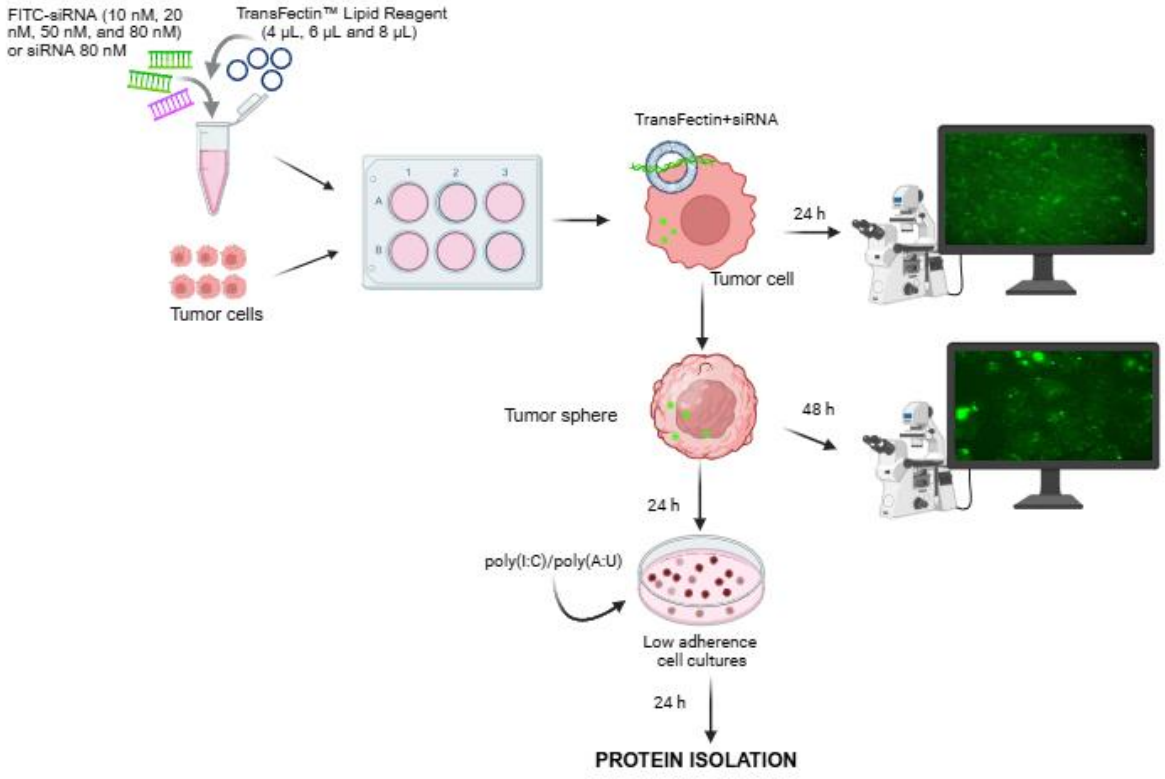

Figure 3.4. Experimental setup for transient transfections. The image was created with biorender.com.

3.5. Protein isolation

Proteins were isolated from Detroit 562, siRNA Detroit 562, siTLR3 Detroit 562, FaDu shCTRL, FaDu shTLR3, SQ20B shCTRL, and SQ20B shTLR3 cells cultured in adherent conditions and tumor spheres. Adherent cells or tumor spheres were grown for 3 days and treated with 10 µg/mL of poly(I:C) or poly(A:U) for 24 hours before protein isolation. Adherent cells were detached from the flask using a 0.25% trypsin-EDTA solution (Sigma Aldrich, St. Louis, Missouri, USA), and tumor spheres were collected from the flask.

Once the cell pellet was collected by centrifugation at 300 x g for 5 minutes at room temperature, it was resuspended in a 50 - 100 µL of RIPA buffer (1M Tris pH 7,4-8,0; 5M NaCl; Triton X; 10% SDS; sodium deoxycholate, sterile dH_2O) supplemented with protease inhibitor cocktail (complete Tablets Mini, Roche, Basel, Switzerland).

To prepare the 7X concentrated stock solution, one cOmplete Mini Protease inhibitor tablet was dissolved in 1.5 mL PBS (Dulbecco's phosphate buffered saline without Ca^{2+} and Mg^{2+}) (Sigma Aldrich, St. Louis, Missouri, USA). The stock solution was diluted 7 times in the RIPA buffer to generate lysis buffer.

After the lysis in RIPA buffer, cells were sonicated for 10 seconds per sample at an amplitude of 80 with the probe of 1 mm in diameter using Labsonic M (B. Braun Biotech International, Melsungen, Germany). Samples were centrifuged (Centrifuge 5415R, Eppendorf, Hamburg, Germany) at 15300 x g for 15 minutes and 4°C, and the supernatants were collected. Isolated proteins were used immediately or stored at -80°C.

3.5.1. Determination of protein concentration using Bradford assay

To determine the concentration of isolated proteins, the Bradford colorimetric protein quantification assay was performed. The Coomassie Brilliant Blue G-250 dye is bound to proteins through electrostatic interactions with basic amino acids and hydrophobic interactions, causing a shift in its absorbance spectrum and a visible color change from reddish-brown to blue. The absorbance is measured at 595 nm.

For Bradford assay, isolated protein samples were diluted 10X in MilliQ water and measured in duplicates. For the standard curve, BSA (bovine serum albumin) was used in concentrations of 1000 µg/ml, 800 µg/ml, 400 µg/ml, 200 µg/ml, 100 µg/ml, and 0 µg/ml, which was blank

containing qH2O. A final volume of 10 µL of prepared proteins and standards was mixed with 200 µL of Bradford reagent (Bio-Rad Laboratories, Hercules, California, USA), which had been previously diluted 5 times with MilliQ water. Samples were incubated for 3 minutes in the dark, shaken by a microtitre plate shaker, and the absorbance was measured using the microplate reader (Labsystems Multiscan MS, Ascent software 2.6, Thermo Fisher Scientific, Waltham, Massachusetts, USA). The absorbance measured at 595 nm is proportional to protein concentration. Higher absorbance indicates higher protein concentration.

Protein concentration was calculated by generating a standard curve based on the absorbance of known BSA concentrations. The linear regression equation (Y = AX + B) was derived from the standard curve. X represents protein concentration; Y is absorbance, A is the slope, and B is the Y intercept. The absorbance of proteins was measured, and the concentration was calculated by solving the X. The final concentration was adjusted based on the dilution factor. Protein concentration was calculated using Microsoft Excel.

3.6. Western blot

Western blot is a widely used and highly specific method for detecting and quantifying specific proteins. Proteins are separated according to molecular weight using the Sodium Dodecyl Sulfate-Polyacrylamide Gel Electrophoresis (SDS-PAGE). SDS is an anionic detergent, which means that it binds to proteins, giving them a negative charge. This allows proteins to denature and migrate through the gel, based solely on their molecular weight, and move towards the positively charged electrode during electrophoresis. The separated proteins are transferred from the gel onto the 0.2 µm nitrocellulose membrane using the wet transfer. The wet transfer involves an electric current in a buffer system, which allows proteins to migrate from the gel onto the membrane. The proteins are detected using primary and secondary antibodies, and the presence of target proteins is visualized using chemiluminescence. The signal was generated through an enzymatic reaction of horseradish peroxidase (HRP) with a substrate.

3.6.1. SDS-PAGE - protein gel electrophoresis

Isolated proteins were mixed 1:1 with 2x Laemmli buffer (1M Tris pH 6.8; 1M DTT; 10% SDS; glycerol; 0.1 mg/ml bromophenol blue, dH2O) and boiled for 4 min at 95°C on the thermoblock (Thermomixer comfort, Eppendorf, Hamburg, Germany). 20-40 µg of protein was loaded onto

a 5% polyacrylamide stacking gel (1.0M Tris pH 6.8; 10% SDS; 30% acrylamide mix; 10% ammonium persulfate; 1% TEMED, dH_2O), which allowed proteins to concentrate before entering the resolving gel. Next, the proteins migrate into polyacrylamide resolving gels. Depending on the molecular weight of the analyzed proteins, resolving gels with different acrylamide concentrations (ranging from 8% to 15%) (1.5M Tris pH 8.8; 10% SDS; 30% acrylamide mix; 10% ammonium persulfate; 1% TEMED, dH_2O) were prepared in separate experiments. For the molecular weight identification, 3.5 µL of protein maker (Precision Plus Protein Dual Color, Bio-Rad Laboratories, Hercules, California, USA) was used. The SDS page was performed in a 1X running buffer (25 mM Tris base, 192 mM Glycine; 1% SDS, dH_2O 1 L) for 20 minutes at the 90 V current (electrophoresis, PowerPac HC, Bio-Rad Laboratories, Hercules, California, USA) to pack together the proteins in the stacking gel, followed by 110 V current for around 90 minutes or until the samples reached the lower edge of the gel to separate the proteins.

3.6.2. Wet transfer

Once the proteins were separated on SDS-PAGE, the gel was put into the cassette containing the nitrocellulose membrane with a pore size of 0.2 µm (Protran BA83, Whatman, Dassel, Germany). The transfer cassette was assembled by first placing a sponge on the black side of the cassette, followed by two filter papers and the gel. A wet nitrocellulose membrane soaked in transfer buffer was placed on the gel, followed by two more filter papers and another sponge. Before closing the cassette, air bubbles were removed by gently rolling a glass tube over the top sponge with light pressure.

The transfer was performed in wet conditions with a cool 1X transfer buffer (TB) (700 mL dH_2O, 200 mL MetOH, 100 mL 10X TB (184 mM Tris, 140 mM glycine, 1 L dH_2O)). The closed cassette was placed into the Bio-Rad system with a spinning magnet to ensure continuous buffer circulation and a cool environment for consistent and efficient transfer. The system was filled with a cold 1X TB with an ice insert to keep it cool during the transfer. The transfer was conducted for 40-80 minutes at 90-110 V (PowerPac HC, Bio-Rad Laboratories, Hercules, California, USA), depending on the size of the protein of interest. After the transfer, the membrane was shortly dyed with naphthol blue solution (10% MetOH, 2% CH_3COOH, 0.1% naphthol blue in dH_2O) for visualization and loading control acquisition. The membrane was further washed with the decolorizing solution (40% MetOH, 8% CH_3COOH in dH_2O) twice,

and once in 1x TBST (900 mL dH_2O, 100 mL 10X TBST (1M Tris pH 8; 5M NaCl; 20% Tween 20)). The drying and washing of the membrane were performed on a shaker (Thermolyne Specimix, Thermo Fisher Scientific, Waltham, Massachusetts, USA). Next, the membrane was incubated in a blocking solution which was specific for each antibody used, and was applied as described in Table 3.1, containing milk, BSA (Tocris Bioscience, Bristol, UK) or both in 1x TBST for 20 minutes.The primary antibody was incubated overnight at 4°C. It was diluted 1:400 - 1:000, depending on the antibody type, in the blocking solution (Table 3.1).

3.6.3. DAMP detection

For detection of DAMPs in adherent cells and tumor spheres treated with poly(I:C) or poly(A:U). Adherent cells or tumor spheres were grown for 3 days and treated with 10 µg/mL of poly(I:C) or poly(A:U) for 24 hours before DAMP collection and protein isolation. Western blot was performed, and DAMPs expressed after the TLR3 activation in adherent cells and tumor spheres were detected using antibodies against S100A9, HMGB1, HSP70, RAGE, and TLR4 (Table 3.1) by western blot.

Table 3.1. List of primary antibodies

Target (clone)	Molecular weight	Host species	Dilution for WB	Blocking buffer	Transfer time	Manufacturer (cat. no.)
HSP70 (W27)	70 kDa	Mouse	1:1000	4% milk	60 min	Santa Cruz Biotechnology (sc-24)
HMGB1 (HAP46.5)	30 kDa	Mouse	1:500	2% milk + 2.5% BSA	35 min	Santa Cruz Biotechnology (sc-56698)
S100A9 (Calgranulin B; B-5)	14 (25) kDa	Mouse	1:400	5% BSA	35 min	Santa Cruz Biotechnology (sc-376772)
TLR4 (25)	100 kDa	Mouse	1:400	4% milk	80 min	Santa Cruz Biotechnology (sc-293072)
RAGE (A-9)	46 kDa	Mouse	1:500	2% milk + 2.5% BSA	60 min	Santa Cruz Biotechnology (sc-365154)
ALDH1A1 (H-4)	56 kDa	Mouse	1:500	5% BSA	60 min	Santa Cruz Biotechnology (sc-374076)
UFSP2 (G-11)	53 kDa	Mouse	1:1000	4% milk	60 min	Santa Cruz Biotechnology (sc-376084)
PARP (46D11)	89 (116) kDa	Rabbit	1:1000	2% milk + 2.5% BSA	70 min	Cell signaling technology (9532)
KYAT3	40 kDa	Rabbit	1:1000	2% milk + 2.5% BSA	40 min	Sigma-Aldrich (HPA027168)
GRWD1 (B-7)	49 kDa	Mouse	1:1000	2% milk + 2.5% BSA	40 min	Santa Cruz Biotechnology (sc-514125)

STARD10 (C-11)	35 kDa	Mouse	1:1000	2% milk + 2.5% BSA	35 min	Santa Cruz Biotechnology (sc-365580)
Gasdermin (H-6)	49 kDa	Mouse	1:1000	2% milk + 2.5% BSA	40 min	Santa Cruz Biotechnology (sc-376318)
GSTT1 (D-1)	27 (54) kDa	Mouse	1:1000	2% milk + 2.5% BSA	40 min	Santa Cruz Biotechnology (sc-393035)
TSG101 (2H18)	44 (20) kDa	Rabbit	1:1000	2% milk + 2.5% BSA	40 min	Sigma-Aldrich (ZRB1244)
NUP62 (C-9)	62 kDa	Mouse	1:1000	2% milk + 2.5% BSA	60 min	Santa Cruz Biotechnology (sc-48373)
UCH-L5 (C-4)	38 kDa	Mouse	1:1000	2% milk + 2.5% BSA	40 min	Santa Cruz Biotechnology (sc-271002)
syntenin-1 (C-3)	32 kDa	Mouse	1:1000	2% milk + 2.5% BSA	35 min	Santa Cruz Biotechnology (sc-515538)
CD133 (17A6.1)	100 kDa	Mouse	1:500	5% BSA	80 min	Merck (MAB4399-I)

After the incubation of the membrane with primary antibody, it was washed 3 times for 5-10 minutes in 1x TBST buffer. Further, the secondary antibody was diluted 1:3000 for mouse (Anti-mouse IgG-HRP conjugated antibody, GE Healthcare, Chicago, Illinois, USA) and 1:5000 for rabbit (Anti-rabbit IgG HRP-conjugated antibody, Cell Signaling Technology, Danvers, Massachusetts, USA) in blocking solution. Proteins bound to the membrane were detected using the imaging system (Alliance Q9 Mini, Uvitec, Cambridge, UK) after incubation with the luminol-based substrate for HRP-catalyzed detection (Western Lightning Plus-ECL, PerkinElmer, Waltham, Massachusetts, USA) for 5 minutes in the dark. An image of the membrane stained with naphthol blue was used as a loading control.

3.7. Treatments

3.7.1. TLR3 agonists

Since TLR3 is activated by dsRNA, synthetic dsRNA ligands, polyinosinic:polycytidylic acid (poly(I:C)) and polyadenylic-polyuridylic acid (poly(A:U)) (InvivoGen, San Diego, California, USA) were used as TLR3 agonists to stimulate the signaling pathway. Working concentrations of poly(I:C) and poly(A:U) were 10 µg/mL. Poly(I:C) activates TLR3, RIG-I and MDA5, while poly(A:U) is a selective TLR3 agonist (Perrot et al., 2010).

3.7.2. DAMP inhibitors

We investigated if certain DAMP inhibitors as potential cancer treatment since TLR activation can trigger DAMP release, and this may contribute to tumor metastasis and inflammation. In this study, several renowned drugs were evaluated for use as potential DAMP inhibitors to explore their ability to control these processes. These drugs are already being used as dietary supplements or as pharmaceutical agents to treat different illnesses. The idea was to repurpose them for new therapeutic applications to target CSCs and determine if CSC properties could be decreased by the treatment with pharmacological inhibitors of endogenous ligands, including ASA (acetylsalicylic acid, Aspirin), kahweol (KW), paquinimod (PAQ), and metformin (MF). DAMP inhibitors were dissolved either in DMSO or qH_2O and filtered to ensure sterility.

Table 3.2. List of DAMP inhibitors.

Drug	Inhibition target	Solvent	Mr (g/mol)	Stock conc. (mM)	*Working conc. (μM)	Manufacturer
Aspirin (ASA)	HMGB1	DMSO	180	55	100 and 1000	Sigma Aldrich, St. Louis, Missouri, USA
Kahweol (KW)	HSP70	DMSO	314	1.6	10	Abcam, Cambridge, UK
Metformin (MF)	RAGE	qH_2O	130	310	10000	Sigma Aldrich, St. Louis, Missouri, USA
Paquinimod (PAQ)	S100A9	DMSO	350.41	5.7	10	Sigma Aldrich, St. Louis, Missouri, USA

*Working concentrations were adapted to the Detroit 562 cell line.

3.7.2.1. The determination of DAMP inhibitor concentrations

The IC_{50} for each DAMP inhibitor was determined in Detroit 562 cells using the MTT assay (described in 3.9.1.), and these concentrations were employed in all subsequent experiments: ASA 1000 μM and 100 μM, paquinimod 10 μM, kahweol 10 μM, and metformin 10000 μM.

3.7.3. Gamma irradiation

Gamma irradiation is a highly effective form of ionizing radiation which has been used in cancer therapy. It utilizes gamma rays from cobalt-60 (^{60}Co) and can easily interact with biological materials and reach deep tissues. It causes DNA damage and denatures proteins through direct ionization and the production of reactive oxygen species.

Detroit 562 adherent cells and tumor spheres were irradiated with gamma rays in a panoramic ^{60}Co source (Rudjer Boskovic Institute, Division of Materials Chemistry, Radiation Chemistry

and Dosimetry Laboratory,). The ^{60}Co isotope is a radioactive source of irradiation. Adherent cells were irradiated with 2.5 Gy or 5 Gy, and tumor spheres were irradiated with 2 Gy and 5 Gy. Gy (Gray) is the unit of absorbed radiation dose. Gy measures the amount of ionizing radiation energy deposited in a mass. One Gray equals the absorption of one joule (J) per kilogram of matter. Cells were irradiated at 220 cm from the irradiation source. Total time was 242 - 253 seconds for 5 Gy (20 mGy/s), 121 seconds for 2.5 Gy (20 mGy/s), and 92 - 110 seconds for 2 Gy (20 mGy/s).

3.7.4. Proton irradiation

Conventional cancer treatments, such as gamma and X-ray irradiation, lack precision and have limitations due to their non-specific targeting and damage to surrounding healthy tissues. Proton therapy, a type of particle therapy, offers more targeted treatment by using high-energy protons. The Bragg peak effect allows precise energy delivery to the tumor while minimizing harm to surrounding tissue. This means that, unlike gamma rays, protons can direct most of the energy to a specific depth in the targeted tissue. The energy can be deposited in a very localized manner. Proton therapy was explored as a potential strategy for targeting tumor spheres. For this specific research, Teflon chambers were designed (Figure 3.5) in collaboration with the Laboratory for Ion Beam Interactions, Division of Experimental Physics at Rudjer Boskovic Institute. A day before proton irradiation, Detroit 562 cells were seeded in these chambers on a special 3 μm Mylar transparent foil (Spex Industries, Metuchen, New Jersey, USA) coated with collagen (Rat Tail Collagen Coating Solution: Type I Collagen, Cell Applications, San Diego, California, USA). Before the collagen coating, chambers and Mylar foil were assembled and sterilized using 70% EtOH for 30 minutes. Once it was completely dry, the chambers were exposed to UV light for 10 minutes. All preparation was done in sterile conditions under the laminar flow and using the Bunsen burner with an open flame. Once the chambers were sterilized, 600 μL of collagen was added inside the chamber to cover the bottom. It was incubated in a cell culture incubator at 37°C, 5% CO_2 for 2 hours. The excess of collagen was removed from the chamber and washed twice with PBS before $1x10^6$ cells were seeded per well in 4 mL DMEM. The next day, cells were then exposed to a proton beam to deliver a dose of 2 Gy. Before the irradiation, chambers were filled completely with DMEM to cover the cells and sealed with covers. Irradiations were performed at the Ruđer Bošković Institute (Laboratory for Ion Beam Interactions, Division of Experimental Physics). The 1.0 MV Tandetron accelerator provided 2

MeV protons inside the Dual Microprobe (DuMi) end station (Jakšić et al., 2023). The beam passed through a 1 μm-thick nickel foil, and the samples were positioned in the air at 25 mm from the exit window. The final proton energy on the samples was 700 keV with a circular-shaped beam of 1 cm in diameter. After the irradiation, cells were incubated to recover at 37°C, 5% CO_2 for 24 hours. The next day, irradiated cells were cultured as tumor spheres in 12-well plates under ultra-low attachment conditions with 1.5 x10^5 cells per well in 2 mL MEBM for RNA and protein isolation. For the cytotoxicity assay 3x 10^3 cells of the irradiated cells were seeded in 200 μL MEBM and cultured as tumor spheres in 96 wells. Tumor spheres were grown for 72 hours before the treatment with DAMP inhibitors (Aspirin 1000 μM, and Kahweol 10 μM), which were added alone or in combination with poly(I:C). The effects of proton irradiation on CSC viability and self-renewal capacity were evaluated using a cytotoxicity assay, poly (ADP-ribose) polymerase (PARP) cleavage, and further studied by RNA expression analysis of CSC markers by qPCR. RNA isolation was performed 24 hours after the treatment, while protein isolation and cytotoxicity assay were carried out 48 hours after the treatment. Apoptosis was assessed with western blot by measuring PARP cleavage.

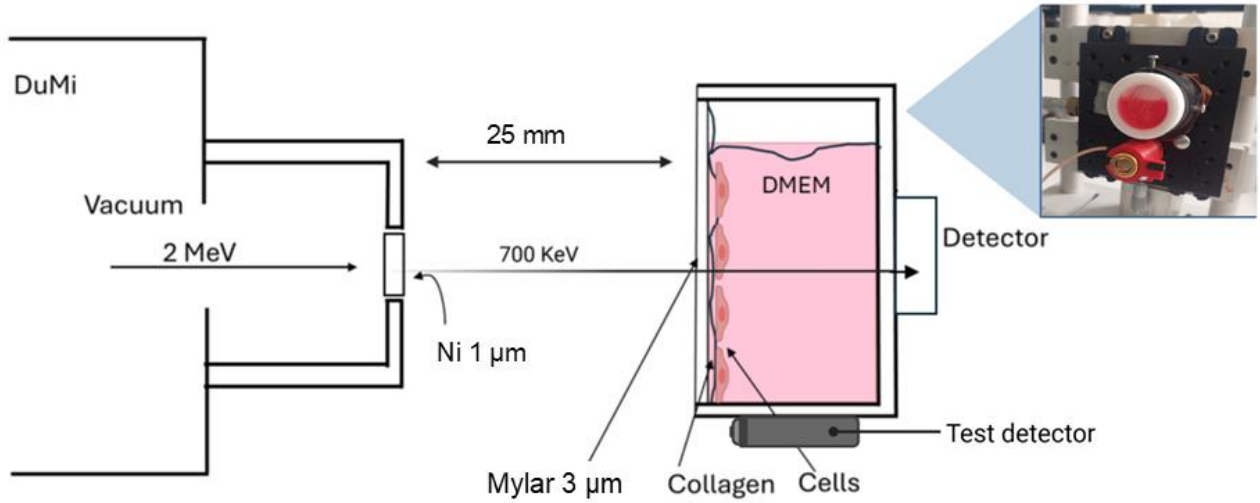

Figure 3.5. Proton irradiation experimental setup. Irradiations were performed at the Ruđer Bošković Institute (Laboratory for Ion Beam Interactions, Division of Experimental Physics). The 1.0 MV Tandetron accelerator provided 2 MeV protons inside the Dual Microprobe (DuMi) end station. The beam passed through a 1 μm-thick nickel foil, and the samples were positioned in the air at 25 mm from the exit window. The final proton energy on the samples was 700 keV with a circular-shaped beam of 1 cm in diameter. The image was created using PowerPoint in combination with biorender.com.

3.8. Migration and invasion

To determine whether CSCs release factors (DAMPs) into the environment that can induce migration and invasion of tumor cells, Detroit 562 adherent tumor cells were treated with supernatants (conditioned media) obtained from tumor sphere cultures and monitored for their migration and invasion capacity. DAMP inhibitors were investigated to determine if they can abolish this effect.

3.8.1. Cell migration

Cell migration is involved in various biological mechanisms, including wound healing, immune response, and cancer metastasis. This experimental technique is used to study the movement of cells in response to chemical, biological, and mechanical stimuli. Usually, chamber-based systems such as Boyden chambers or transwells are used for migration assays (Grada et al., 2017). In this study, the Radius™ 96-Well Cell Migration Assay kit (Cell Biolabs, San Diego, California, USA) was used (Figure 3.6). This assay uses a special cell culture plate with a central gel spot, which is made of biocompatible, non-toxic hydrogels. Cells can't adhere to the gel spots. After the seeding, cells attach everywhere except on the gel, creating a cell-free zone. The gel was then removed, allowing cells to close the gap by migrating across the area. This method was compatible with cells of all sizes, which eliminates problems with finding the corresponding pore size. Also, it supports both quantitative and qualitative analysis of migrated cells in real time or at the endpoint imaging. Altogether, this kit was a highly effective tool for detecting cell migration.

A total of 0.75 x 10^5 Detroit 562 cells were seeded in 700 µL of MEBM using 24-well plates for tumor sphere formation. A total of 1x10^5 of adherent cells were seeded in 1 mL of DMEM in 12 wells. The cells were treated 96 hours after the initial seeding. Tumor spheres were treated with DAMP inhibitors using working concentrations from Table 3.2 in combination with 10 µg/mL poly(I:C)/poly(A:U) or with poly(I:C)/poly(A:U) alone. The next day, migration plates were prepared according to the manufacturer's instructions. The gel spot was removed at the beginning of the experiment by dissolving it using the 1X Radius™ Gel Removal Solution (Part No. 112504), allowing the cells to fill the circular space after seeding. 7.4 x 10^4 adherent cells were seeded per well in migration plates in 100 µL of DMEM and incubated at 37°C, 5% CO_2 for 24 hours. The migration experiment was performed in triplicate. The next day, 48 hours

after the treatment, 170 µL of conditioned media from treated tumor spheres was added to the adherent cells on the migration plate. Cell migration was evaluated after 0, 11, and 24 hours. Images were captured using a Dino-Eye microscope camera at the inverted microscope (Invertoscope ID 03 Zeiss, Jena, Germany), and analyzed by measuring the closing of the cell-free area in Image J.

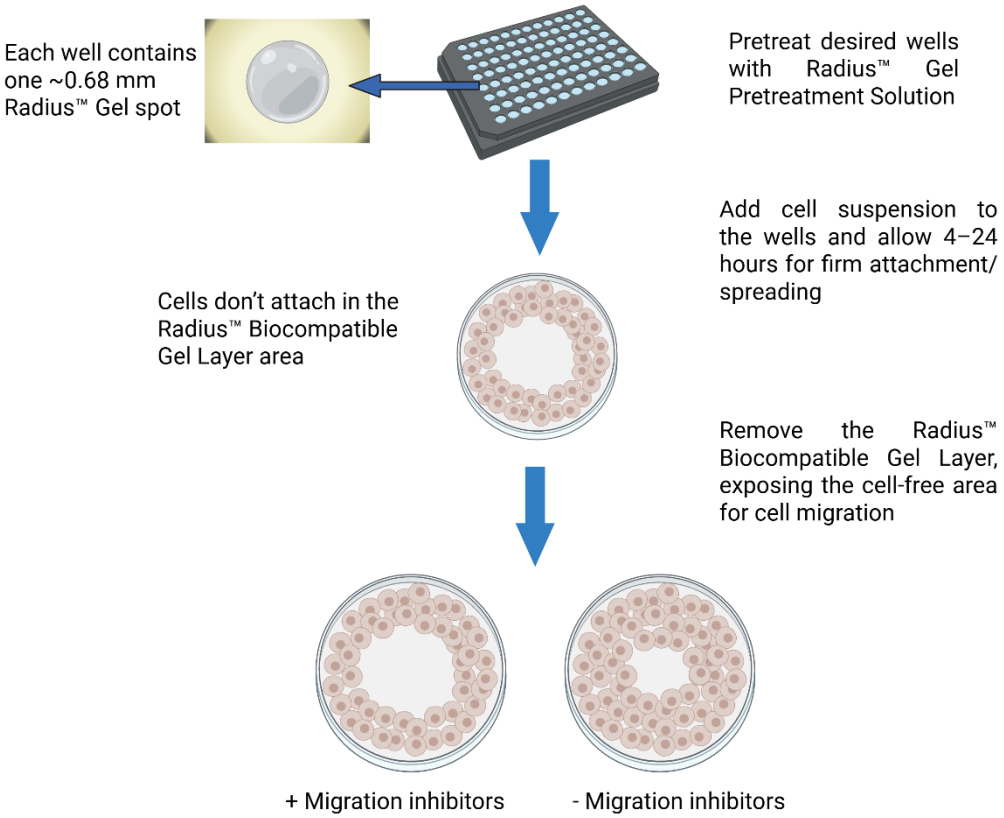

Figure 3.6. Cell migration assay. The image was acquired from the Radius™ 96-Well Cell Migration Assay kit (Cell Biolabs, San Diego, California, USA) and adjusted with biorender.com.

3.8.2. Cell invasion

The acquisition of invasive properties enables cells to penetrate surrounding tissues and migrate through the extracellular matrix (ECM) (Fares et al., 2020). For the invasion assay, the Corning® Matrigel® Basement Membrane Matrix for 3D Culture In Vitro (Corning, New York, USA) was used for gel formation, which mimics ECM, along with Millicell Cell Culture Inserts (transwell inserts, Merck Millipore, Darmstadt, Germany). This method was based on chambers with porous membranes that allow cells to migrate through the pores and reach the chemoattractant (Figure 3.7).

0.15 x 10^6 Detroit 562 cells per well were seeded in 800 µL MEBM using 24-well plates to form tumor spheres. Additionally, 0.5x10^5 adherent cells per well were seeded in 1 mL DMEM. Tumor spheres were treated 96 hours after the initial seeding with DAMP inhibitors using working concentrations from Table 3.2. and with 10 µg/mL poly(I:C)/poly(A:U) or with 10 µg/mL poly(I:C)/poly(A:U) alone, and incubated at 37°C, 5% CO_2 for 72 hours. A day before the invasion experiment, Matrigel was transferred from -20°C to +4°C to liquify. Pipette tips were placed in -20°C to cool overnight. Matrigel contains thermosensitive extracellular matrix components, which include collagen IV, laminin, and entactin, that form a gel network at room temperature. This results in quick solidification of the gel (Hughes et al., 2010). To avoid this, and to keep the gel in liquid form, all the equipment was kept cool during the experiment.

On the day of the invasion experiment, 24-well plates and transwell inserts were prepared. Everything was kept on ice, especially Matrigel and tips. Matrigel mix was prepared by mixing it with DMEM without FBS in a 1:3 ratio. The 60 µL of the Matrigel/DMEM mix was added onto the transwells, which were placed inside the 24-well plate and incubated for 1 hour at 37°C, 5% CO_2. Next, the supernatants were prepared by transferring to 1.5 mL microfuge tubes and centrifuged (Centrifuge 5415R, Eppendorf, Hamburg, Germany) at 13000 x g for 5 minutes. At the same time, Detroit 562 cells were prepared for seeding into the Matrigel. The cells were trypsinized, centrifuged, and resuspended at a concentration of 1x10^6 cells in 1 mL of migration buffer (DMEM + 10 mM HEPES (N- [2-Hydroxyethyl] piperazine-N'- [2-ethanesulfonic acid]) + 0.1% bovine serum albumin (BSA), pH 7.4). A total of 100 µL of cell suspension was added to the Matrigel inside the transwell. After incubation for 10 minutes, 600 µL of chemoattractant (tumor spheres supernatant with all the treatment conditions) was added to the bottom of the 24-well plate. After 24 hours, transwells were gently washed with PBS, and migrated cells were fixed for 5 minutes with 4% paraformaldehyde in PBS and stained for

5 minutes with 0.2% crystal violet staining solution. Transwells were washed with PBS to remove excess dye, and the Matrigel excess was removed with a cotton swab. Images were captured using a Dino-Eye microscope camera at the inverted microscope, and analyzed by counting the migrated cells in Image J. The experiment was based on the *Transwell In Vitro Cell Migration and Invasion Assays* (Justus et al., 2023) protocol and adjusted for the Detroit 562 cancer cell line.

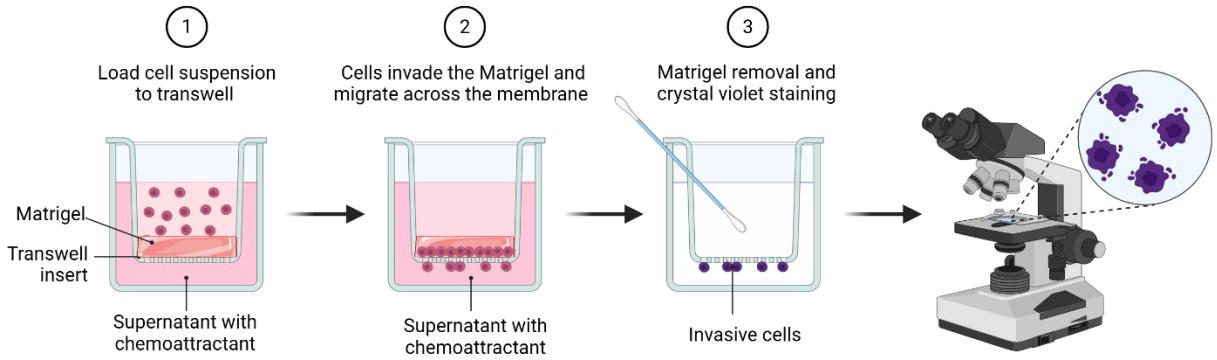

Figure 3.7. Cell invasion experiment set up. The image was created with biorender.com.

3.9. Cytotoxicity assays

3.9.1. Adherent cell proliferation assay (MTT assay)

The cytotoxicity after the irradiation and the treatment with pharmacological DAMP inhibitors alone or in combination with poly(I:C) was determined using the MTT assay. Living cells can convert the yellow, water-soluble tetrazolium salt MTT [3-(4,5-dimethylthiazol-2-yl)-2,5-diphenyltetrazolium bromide] to formazan, a purple substance soluble in dimethyl sulfoxide (DMSO). The MTT assay relies on the activity of NAD(P)H-dependent oxidoreductase enzymes, which are primarily found in the mitochondria of metabolically active cells. Detroit 562 cells ($1x10^4$ cells per well) were seeded into 96-well plates 16 hours before treatment and irradiation. After the irradiation and/or the treatment with DAMP inhibitors, cells were grown for 72 hours. The supernatants were then removed, and 40 µL of diluted MTT reagent (1:10 in DMEM) was added to the cells, including the blind control (only diluted MTT reagent). Cells were incubated for 4 hours in the dark at 37°C, 5% CO_2. Before the absorbance measurement, 160 µL of DMSO was added to each well to dissolve the formazan produced during the assay. After mixing the plate on a microtitre plate shaker (ASAL, Milan, Italy), the absorbance was measured at 570 nm wavelength using the microplate reader (Labsystems Multiscan MS, Ascent program 2.6, Thermo Fisher Scientific, Waltham, Massachusetts, USA) (Figure 3.8). Cell survival (percentage of growth) was calculated using the formula and expressed in relation to the control.

$$PG = 100 \times \frac{\text{mean OD}_{sample} - \text{mean OD}_{t0}}{\text{mean OD}_{control} - \text{mean OD}_{t0}}$$

OD sample = the measured absorbance value of the samples
OD control = the measured absorbance value of the control samples
OD t0 = measured absorbance value of the samples without the treatment at time point 0

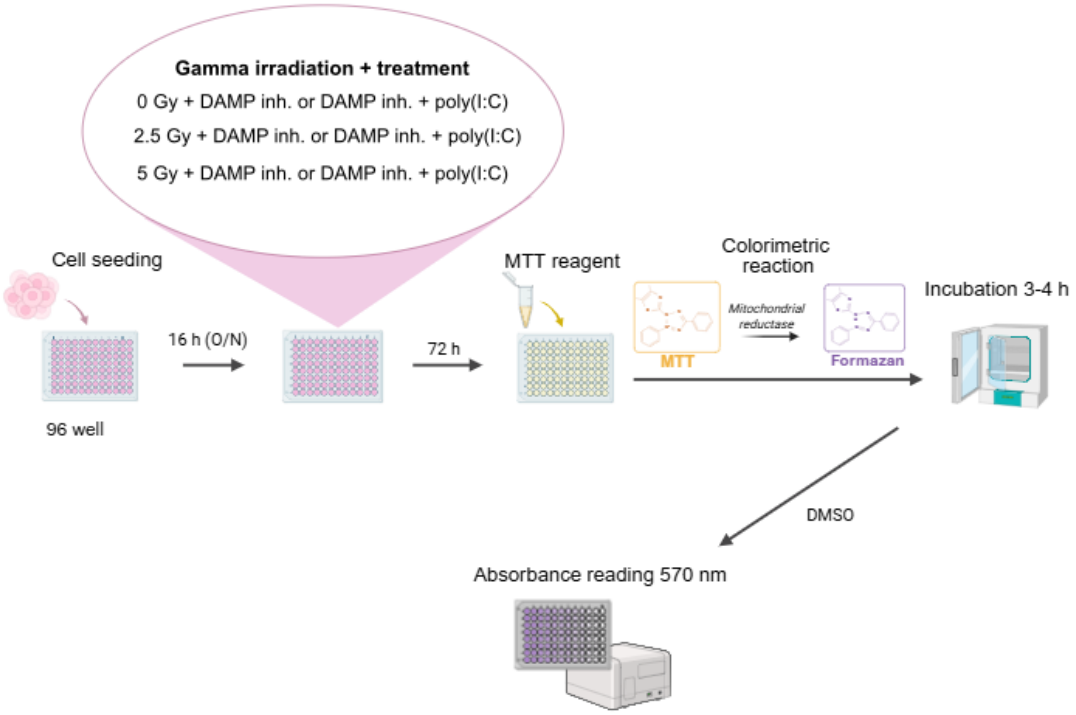

Figure 3.8. The MTT assay experiment set up. The image was created with biorender.com

3.9.2. Tumor spheres proliferation assay (ViaLight™ Plus Cell Proliferation and Cytotoxicity BioAssay Kit)

The viability of tumor spheres was measured using ViaLight™ Plus Cell Proliferation and Cytotoxicity BioAssay Kit (Lonza Bioscience, Basel, Switzerland). The cell survival of tumor spheres could not be determined using the MTT assay, as they grow in clusters of cells and in a suspension, so alternative evaluation options had to be explored. The ViaLight™ Plus kit as a good option for the measurement of the viability of cells in a suspension. This kit provides sensitive and highly reproducible measurement of tumor sphere viability based on intracellular ATP levels, which reflects metabolic function and consequently cell viability.

ViaLight assay tracks the survival of tumor spheres by using a bioluminescent ATP assay, which relies on the firefly luciferase enzymatic reaction to generate light photons from ATP released upon lysis of viable cells. Luciferase enzyme catalyzes the production of light from luciferin and ATP. The detectable light intensity demonstrates the concentration of ATP.

To determine the viability, 3 x 10^3 Detroit 562 cells were seeded per well in 200 µL MEBM in BIOFLOAT™ 96-well U-bottom plates (faCellitate, Mannheim, Germany) and cultured for 72 hours to form tumor spheres. The spheres were then treated with DAMP inhibitors in

combination with 10 µg/mL poly(I:C) or with poly(I:C) alone and incubated at 37°C, 5% CO_2 for 72 hours. To evaluate the tumor sphere survival, the manufacturer's protocol was followed: 50 µl of cell lysis reagent was added to each well, and the plate was incubated for 75 minutes at room temperature to lyse the tumor spheres and release the ATP. To ensure better lysis, the protocol was slightly modified, and 45 minutes after the addition of lysis reagent, the solution was mixed 10 times with a pipette, and the lysis buffer with spheres was incubated for another 30 minutes (Figure 3.9). The original protocol from the kit was adjusted to ensure complete tumor sphere lysis; so, the lysis step was prolonged from 10 minutes to 75 minutes. Then, 100 µl of the cell lysate was transferred to white Nunclon Surface flat-bottom 96-well plates (Nunc, Roskilde, Denmark), and 100 µl of the ATP monitoring reagent (AMR plus) was added. This reagent was prepared by adding the assay buffer from the kit to the lyophilized AMR Plus. It was gently mixed and left for 15 minutes at room temperature to equilibrate. After 2 minutes of incubation of lysed cells with ATP monitoring reagent, the luminescence was measured using a Spark multimodal microplate reader (Tecan, Männedorf, Switzerland) and Magellan data analysis software (Tecan, Männedorf, Switzerland). Results were analyzed using Excel.

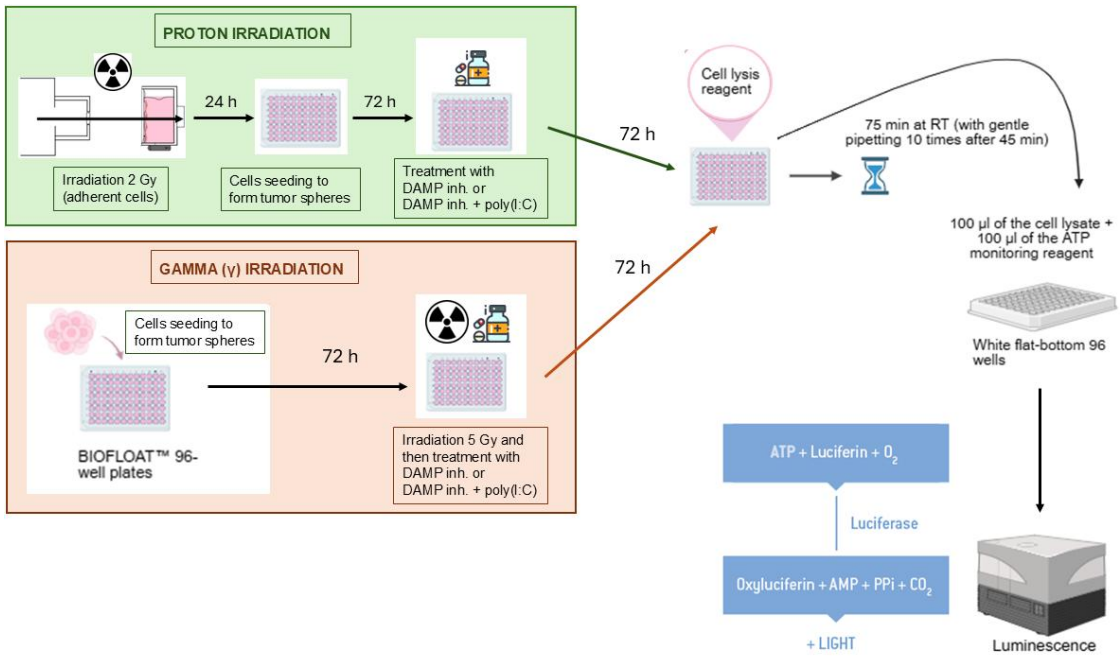

Figure 3.9. Vialight assay for tumor spheres set up. The image was created using the ViaLight Plus kit images and biorender.com.

3.10. Gene expression

3.10.1 RNA isolation

RNA was isolated using the GenElute Mammalian Total RNA Miniprep Kit (Sigma Aldrich, St. Louis, Missouri, USA). 1.5 x 10^5 cells of Detroit 562 cells were seeded in 2 ml of MEBM. 72 hours after the seeding, the cells were treated with DAMP inhibitors (ASA 1000 µM or KW 10 µM) alone or in combination with 10 µg/mL poly(I:C) for 24 hours, followed by RNA isolation. Medium with tumor spheres was collected into a 15 mL Falcon tube and spun in the centrifuge at 300 x g for 5 minutes at room temperature to pellet the spheres and remove the excess medium. The tumor sphere pellet was lysed using the lysis buffer with the addition of β-mercaptoethanol (BME). Lysed cells were transferred onto the filtration column in a collection tube and centrifuged at maximum speed for 2 minutes. Next, 70% EtOH was added directly to the filtered lysate and transferred to the binding column and centrifuged at maximum speed for 15 seconds. In the next step, the column with samples was washed with the manufacturer's washing solution 1, centrifuged, and for each sample, 10 µL DNase 1 enzyme was dissolved in 70 µL DNase Digest Buffer, which was then added to the column and incubated for 15 minutes at RT. The columns were then washed again once with washing solution 1 and twice with washing solution 2. The binding column was transferred to the new collection tube. The 23 µl of Elution Solution (provided with the kit) was added to the membrane, and RNA was eluted by centrifugation for 1 minute at maximum speed. RNA concentration and quality were measured by the spectrophotometer NanoPhotometer N60 (Implen, Munich, Germany). The ratio of A260/280 measures the RNA purity by indicating protein contamination, with expected values around 2.0. A260/230 ratio analyzes RNA sample purity, reflecting contamination with organic compounds, with the optimal range around 2.0 - 2.2. The elution solution provided by the kit was used as a blank. Isolated RNA was used immediately or stored at -80°C.

3.10.2. Complementary DNA (cDNA) synthesis

Complementary DNA (cDNA) is a double-stranded DNA that is synthesized from RNA that serves as a synthesis template through the action of the enzyme reverse transcriptase. The cDNA synthesis was performed with 0.3 µg of isolated RNA using random primers (hexamer), short 6-nucleotide-long sequences. These primers bind randomly across the RNA template, enabling the synthesis of cDNA. The High-Capacity cDNA Reverse Transcription kit (Applied

Biosystems, Thermo Fisher Scientific Baltics, Vilnius, Lithuania) was used according to the manufacturer's instructions (Table 3.3).

Table 3.3. Mastermix for cDNA synthesis

Mastermix for cDNA	**1 X (µL)**
dNTP mix	1.0
RT buffer	2.5
RNAse inhibitor	1.25
Reverse transcriptase	1.25
random primers	2.5
qH_2O	4.0
Total mastermix per reaction	**12.5**
0.3 µg RNA + qH_2O per sample	12.5
Total volume	**25.0**

cDNA synthesis was performed in an Applied Biosystems PCR machine, 2720 Thermal Cycler (Applied Biosystems, Foster City, California, USA) under the following conditions: 25°C for 10 minutes (random primers bind to the RNA template before the reverse transcription), 37°C for 120 minutes (reverse transcriptase enzyme converts RNA into cDNA), 85°C for 5 minutes (denaturing the reverse transcriptase enzyme for inactivation). The cDNA was stored at -20°C before further use.

3.10.3. Real-time PCR (qPCR)

Quantitative polymerase chain reaction (qPCR), also known as real-time PCR, is a method that is used to amplify and quantify specific DNA sequences in real time. It uses fluorescent dyes (SYBR Green) or probe-based detection (TaqMan). SYBR Green is a sensitive fluorescent dye that binds double-stranded DNA molecules by intercalating between the DNA bases. During the PCR reaction, DNA polymerase amplifies the target DNA sequence, therefore doubling the amount of target sequence with each cycle . SYBR Green dye binds to each newly formed copy of dsDNA, resulting in increased fluorescent intensity, which is proportional to the amount of PCR products. Melting curve analysis confirms the specificity of the PCR product and ensures that the fluorescence detected during the reaction comes from a single amplicon.

The PCR reactions were performed with SsoAdvanced Universal Sybr® Green Supermix (Bio-Rad Laboratories, Hercules, California, USA) on a QuantStudio™ 3 Real-Time PCR System (Applied Biosystems, Foster City, California, USA). Primer (table 3.4) stock solutions were diluted 1:10 in qH_2O to prepare working solutions. cDNA was diluted 1:3 to obtain a 0.1 µg ng RNA (25 µL of cDNA was diluted with 50 µL of qH_2O). 10 µL of qPCR mix (9 µL of master mix and 1 µL of 0.1 µg cDNA sample) (Table 3.5) was added to the white 96-well plate (Hard-Shell PCR White Plates 96-well, thin-wall) (Bio-Rad Laboratories, Hercules, California, USA) using a 96-Well Plate Cooling Block. Plates were sealed with PCR Plate Seals (Bio-Rad Laboratories, Hercules, CA, USA) and briefly centrifuged before being inserted into the QuantStudio 3 Real-Time PCR System. The amplification program was used: 95°C for 10 min (initial denaturation), 95°C for 30 s (denaturation), 62°C for 30 s and 60°C for 30 s (annealing and elongation), in total 44 cycles. The CT values were normalized to the 28S rRNA gene. The results were calculated according to a $2^{-\Delta\Delta Ct}$ method for relative quantification, following verification that all primer sets amplified their respective target sequences with comparable efficiencies.

Table 3.4. Primer sequences

Gene	Nucleotide sequence	Accession number	Manufacturer
28S rRNA	F: 5'-CGCGACCTCAGAGATCAGAC-3'	NR_003287	Sigma Aldrich, St. Louis, Missouri, USA
	R: 5'-GGCCTCGATCAGAAGGAC-3'		
OCT4	F: 5'-GTGGAGGAAGCTGACAACAA-3'	NM_002701	Sigma Aldrich, St. Louis, Missouri, USA
	R: 5'-ATTCTCCAGGTTGCCTCTCA-3'		
ABCG2	F: 5′-TACCTGTATAGTGTACTTCAT-3'	NM_004827	Merck, Sigma Aldrich, St. Louis, Missouri, USA
	R: 5′-GGTCATGAGAAGTGTTGCTA-3		

Table 3.5. Mastermix for qPCR reaction

Mastermix for qPCR	Volume (µL)
Sybr green	5.0
F primer	0.3
R primer	0.3
qH_2O	3.4
Total mastermix volume per reaction	**9.0**
0.1 µg cDNA	1.0
Total volume	**10.0**

3.11. Proteomic analysis

Proteomic analysis was performed within this HRZZ project to determine the changes in the proteome of tumor spheres after the stimulation of TLR3, in comparison to the adherent cells. This included Detroit 562 untreated adherent tumor cells, untreated tumor spheres, tumor spheres treated with poly(I:C), and tumor spheres treated with poly(A:U). The focus was on identifying the proteins that were altered after TLR3 activation in tumor spheres. $1.5x10^6$ of Detroit 562 cells were seeded in 6 cm low-adherence plates. Tumor spheres were grown for 72 hours and treated with 10 μg/mL poly(I:C) or poly(A:U) for 24 hours. Adherent cells, as the control cells, were seeded 24 hours before sample collection. Cell pellets were washed several times with PBS and transferred to Biocentar (Zagreb) for proteomic analysis. Samples were stored at -80°C before the analysis. Once the results of the proteomic analysis were obtained, validation of detected proteins was performed by western blot. The validated proteins included GRWD1, STARD10, Syntenin-1, TSG101, GSTT1, Gasdermin, UCH-L5, NUP62, UFSP2 and KYAT3 listed in Table 3.1.

3.12. Microscope image capturing

Images of adherent and tumor spheres were captured during treatments using a camera for a microscope called Dino-Eye (AnMo Electronics Corporation, Taipei, Taiwan) with image capturing software DinoCapture 2.0 (Dino-Lite Europe, Almere, The Netherlands). Images were captured using 2.5x and 10x magnification, which were multiplied by the optical zoom of the camera, which was 72.5x.

3.13. Data analysis

3.13.1. Statistics

The statistical analysis was conducted using Excel. The Student two-tailed t-test was used to assess statistical significance. A p-value of less than or equal to 0.05 was considered statistically significant.

3.13.2. Image analysis

Images were analyzed and edited using ImageJ (1.53 Java 8) (National Institutes of Health, USA) (Schindelin et al., 2012). ImageJ was used for basic image processing and editing, but also for analyzing results.

4. RESULTS

4.1. Determination of TLR3 role in tumor sphere formation and maintenance of stemness

4.1.1. Stimulation of TLR3 enhances tumor sphere formation and growth in HNSCC cell lines

Tumor spheres were grown in special conditions using serum-free medium with the addition of EGF, FGF, and B27. To determine whether TLR3 activation plays a role in the formation and maintenance of tumor spheres, Detroit 562 (Figure 4.1), FaDu (Figure 4.2), and SQ20B (Figure 4.3) cell lines were used as experimental models. The cells were treated with 10 μg/mL poly(I:C) or poly(A:U). Tumor spheres were quantified based on number and size. Treatment with poly(A:U) has significantly affected tumor sphere size and shape in all cell lines, but especially in Detroit 562 (Figure 4.1). It is particularly notable when comparing larger tumor spheres, those over 300 μm in diameter, with the control group 7 days after the treatment.

Detroit 562 cells were changed in morphology and size after the treatment. Control spheres (Figure 4.1D) on day 2 and day 4 had a more defined shape. They had spherical shapes and were similar in size. The control spheres, 7 days after the treatment, were bigger and had an irregular shape. They were also darker in the center compared to the outer layers. Detroit 562 tumor spheres after the treatment with poly(I:C) (Figure 4.1E) begin to dissociate, which is especially visible on day 2 and day 4 after the treatment. At day 4, spheres were bigger, and some were even around 500 μm in diameter. Detroit 562 tumor spheres treated with poly(A:U) (Figure 4.1F), 2 days after the treatment, were already bigger than the control samples. On day 4, they were exceeding 500 μm in diameter. On day 7 after the treatment, the number of spheres over 300 μm increased. On day 7 after the treatment, there was a total of 47 control tumor spheres, 60 tumor spheres treated with poly(I:C), and 82 tumor spheres treated with poly(A:U) bigger than 300 μm.

FaDu tumor spheres were also changed in morphology and size after the treatment. Control spheres (Figure 4.2D) on day 2 were small and round. On day 4, they were bigger and had already developed a necrotic core. On day 7, they were exceeding 500 μm in size with a dark center. FaDu spheres after the treatment with poly(I:C) (Figure 4.2E) were still smaller in size, similar to the size of spheres without the treatment. However, they started to dissociate. On day

4 and day 7 after the poly(I:C) treatment, the spheres exceeded 500 μm in size and developed a dark necrotic center. FaDu spheres treated with poly(A:U) (Figure 4.2F) on day 2 after the treatment were similar size compared to poly(I:C) treatment, but they were not dissociated. On day 4 and day 7, they started to grow, exceeding 500 μm in diameter, and they began to scatter, which was especially visible on day 7. On day 7 after the treatment, there were 8 control tumor spheres, 4 tumor spheres treated with poly(I:C), and 3 tumor spheres treated with poly(A:U) bigger than 300 μm.

On day 2, the SQ20B control tumor sphere size was similar to the size of treated spheres. The difference was noticed in spheres treated with poly(I:C), on day 7 after the treatment, where they were darker compared to the control and poly(A:U) treatment. On day 7, control spheres (Figure 4.3D), tumor spheres treated with poly(I:C) (Figure 4.3E), and tumor spheres treated with poly(A:U) (Figure 4.3F) developed a dark necrotic core. On day 7 after the treatment, there were 15 control tumor spheres, 13 tumor spheres treated with poly(I:C), and 28 tumor spheres treated with poly(A:U) bigger than 300 μm.

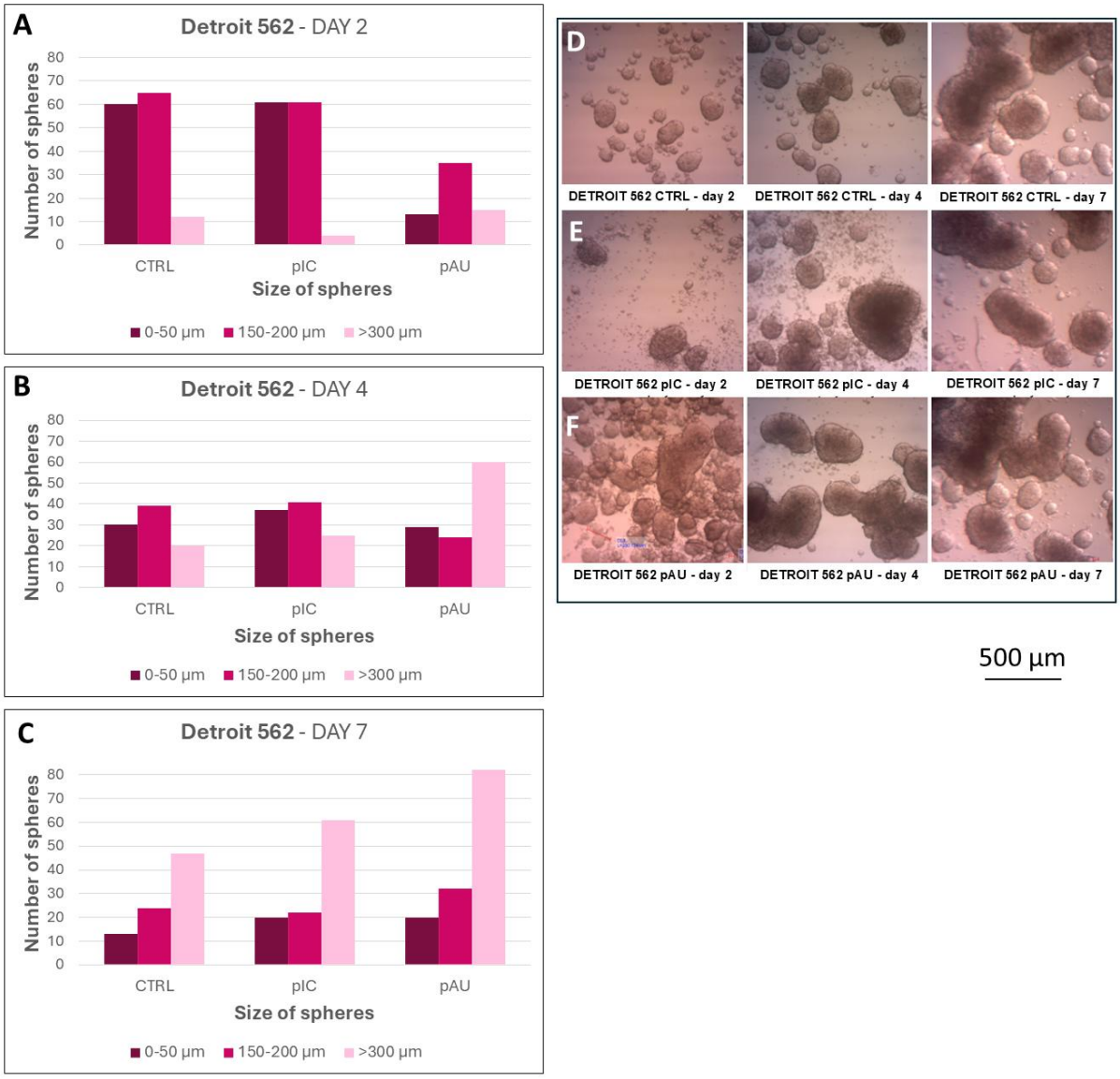

Figure 4.1. Detroit 562 tumor sphere growth and morphology. Changes in tumor sphere size and number over the timeline of 7 days. The sphere size on day 2 (**A**), day 4 (**B**), and day 7 (**C**), following the poly(I:C)/poly(A:U) (pIC/pAU) treatment. **(D, E, F)** Figures represent microscopic analysis of tumor spheres morphology on days 2, 4, and 7 without the treatment (**D**) and with 10 µg/mL poly(I:C) (**E**) or poly(A:U) (**F**). CTRL are untreated tumor spheres grown in MEBM. Magnification is 2.5X times 72,5 for a digital camera objective. At least five separate microscopic fields were examined.

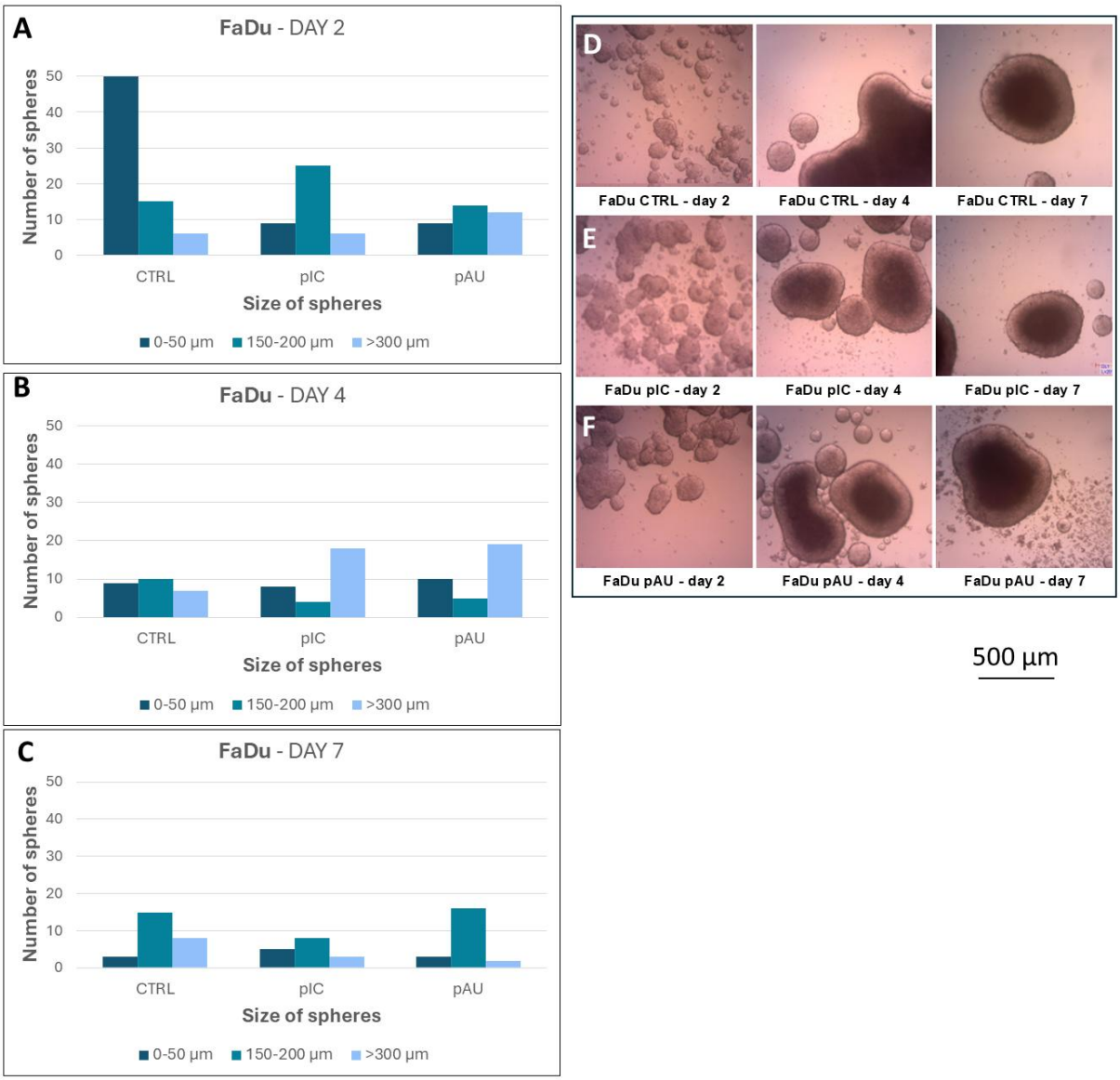

Figure 4.2. FaDu tumor sphere growth and morphology. Changes in tumor sphere size and number over the timeline of 7 days. The sphere size on day 2 (**A**), on day 4 (**B**), and day 7 (**C**), following the poly(I:C)/poly(A:U) (pIC/pAU) treatment. (**D, E, F**) Figures represent microscopic analysis of tumor spheres morphology on days 2, 4, and 7 without the treatment (**D**) and with 10 µg/mL poly(I:C) (**E**) or poly(A:U) (**F**). CTRL are untreated tumor spheres grown in MEBM. Magnification is 2.5X times 72,5 for a digital camera objective. At least five separate microscopic fields were examined.

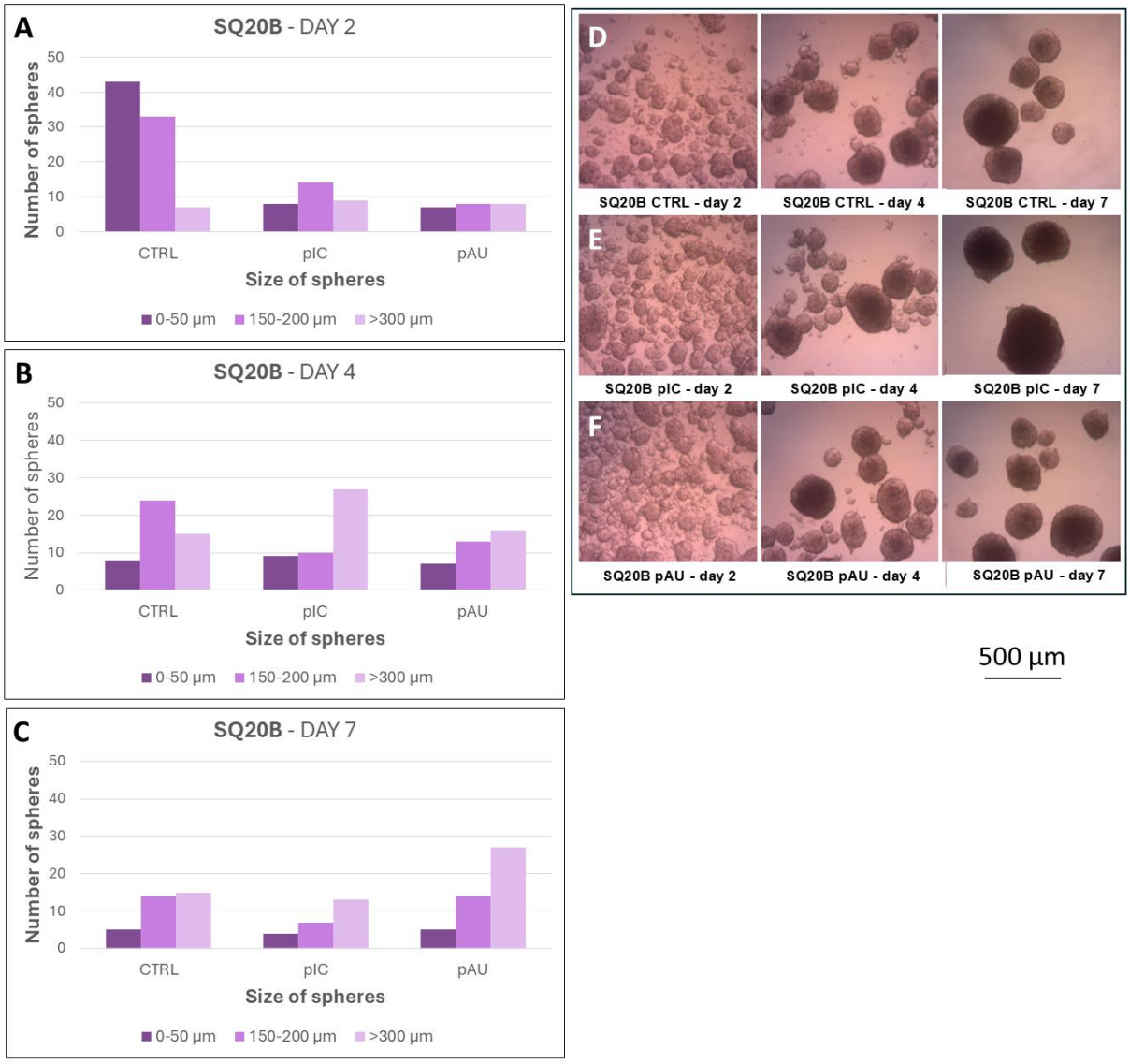

Figure 4.3. SQ20B tumor sphere growth and morphology. Changes in tumor sphere size and number over the timeline of 7 days. The sphere size on day 2 (**A**), on day 4 (**B**), and day 7 (**C**), following the poly(I:C)/poly(A:U) (pIC/pAU) treatment. (**D, E, F**) Figures represent microscopic analysis of tumor spheres morphology on days 2, 4, and 7 without the treatment (**D**) and with 10 µg/mL poly(I:C) (**E**) or poly(A:U) (**F**). CTRL are untreated tumor spheres grown in MEBM. Magnification is 2.5X times 72,5 for a digital camera objective. At least five separate microscopic fields were examined.

4.1.2. The expression of stemness markers in Detroit 562 is enhanced through tumor sphere generations

After confirming Detroit 562 tumor sphere formation, the expression of stemness markers through tumor sphere generations was evaluated by western blot analysis, focusing on the detection of ALDH1A1 and CD133 proteins.

ALDH1A1 was expressed in all tumor spheres equally, regardless of TLR3 stimulation. However, it was not expressed in adherent cells (Figure 4.4A). During several tumor sphere generations, ALDH1A1 expression increased with every generation. The highest expression is observed in generations two and three. ALDH1A1 was again not expressed in adherent cells (Figure 4.4B). The expression of CD133 was observed in adherent cells in the 1st generation; however, it was absent in subsequent generations. CD133 was expressed in all generations of tumor spheres. The strongest expression was in the first generation, and it slightly decreased in the following two generations (Figure 4.4C). This confirms that stemness properties in Detroit 562 tumor spheres were stable or even increased through generations.

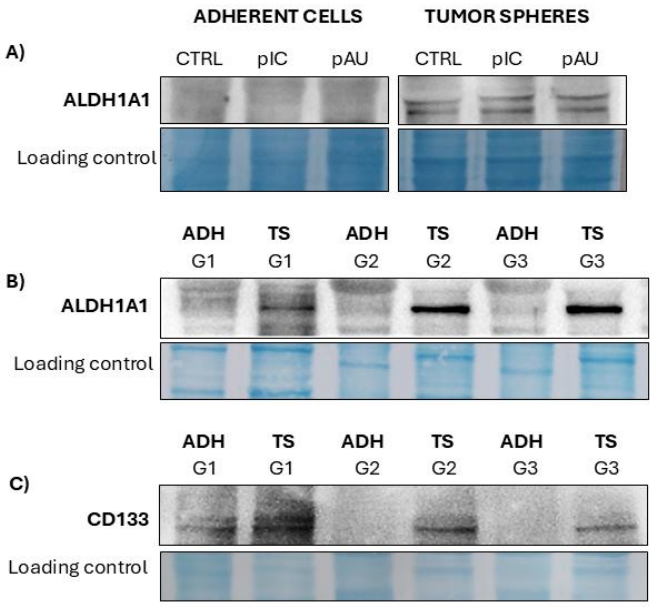

Figure 4.4. ALDH1A1 and CD133 expression after prolonged cultivation through generations (G1–G3) of Detroit 562 tumor spheres. ALDH1A1 expression in adherent cells and tumor spheres after the stimulation of TLR3 with pIC/pAU (10 μg/mL of poly(I:C) or poly(A:U)) (**A**). In tumor spheres (TS), ALDH1A1 expression is increased through generations (**B**). The CD133 expression was rather constant through tumor sphere generations (**C**). The loading controls were membranes stained with naphthol blue.

4.2. Release of endogenous ligands (DAMPs) into the microenvironment by CSC promotes the migration of surrounding tumor cells

4.2.1 TLR3 stimulation induces the expression of DAMPs in Detroit 562 cells

We have demonstrated that CSCs release endogenous ligands (DAMPs) into the microenvironment, thereby enhancing the migration and invasion of tumor cells. Significantly higher expression of DAMPs in tumor spheres and adherent cells was observed after TLR3 activation with 10 µg/mL of poly(I:C)/poly(A:U). Among the DAMPs, S100A9 showed the highest upregulation following both treatments with poly(I:C) and poly(A:U) in tumor spheres and adherent cells compared to the control. HMGB1 was induced by poly(A:U) treatment in tumor spheres and by poly(I:C) in adherent cells, whereas RAGE, as a receptor for HMGB1, exhibited robustly expressed bands when treated with poly(A:U) in tumor spheres and with poly(I:C) in adherent cells. HSP70 displayed modest upregulation with poly(I:C) treatment in tumor spheres and no change in expression in adherent cells. TLR4 was slightly upregulated in tumor spheres compared to adherent cells (Figure 4.5). These results demonstrate that TLR3 stimulation induces the expression of DAMPs in Detroit 562 tumor spheres.

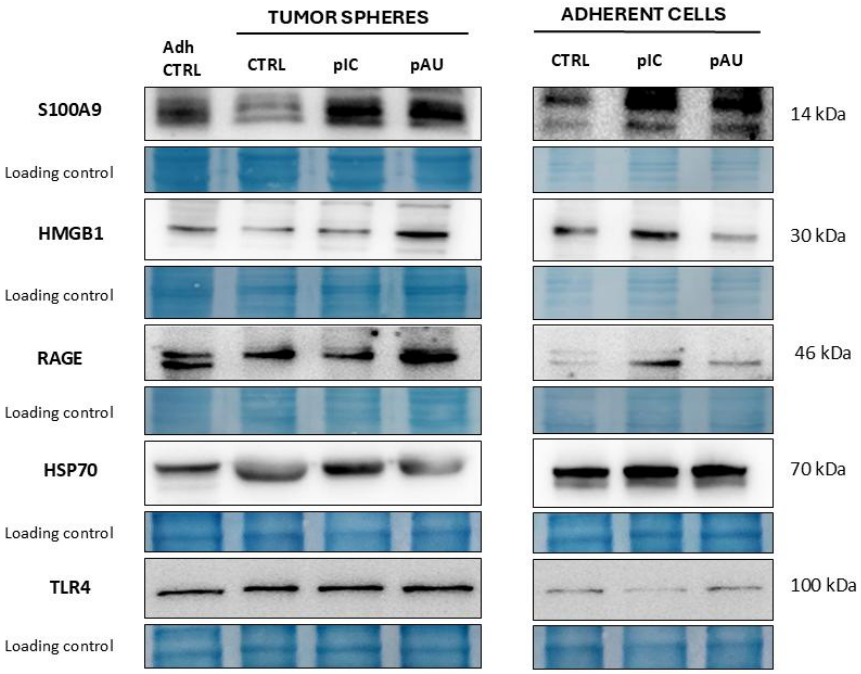

Figure 4.5. DAMP expression in Detroit 562 tumor spheres and adherent cells after the TLR3 activation with poly(I:C) or poly(A:U). The expression of S100A9 (14 kDa), HMGB1 (30 kDa), RAGE (46 kDa), HSP70 (70 kDa), and TLR4 (100 kDa) was determined. Poly(I:C) and poly(A:U) (pIC/pAU) were used in a concentration of 10 µg/mL. The loading controls were membranes stained with naphthol blue.

4.2.2. The effect of DAMP inhibitors in combination with poly(I:C) on the survival of Detroit 562 cell line

The impact of DAMPs in the TME could be repressed using specific DAMP inhibitors. An MTT assay was performed to determine whether the survival of tumor cells and tumor spheres can be reduced with pharmacological inhibitors of endogenous ligands, including ASA (acetylsalicylic acid, aspirin, inhibits HMGB1), kahweol (inhibits HSP70), paquinimod (inhibits S100A9), and metformin (inhibits RAGE), combined with 10 µg/mL poly(I:C).

Aspirin is a widely used non-steroidal anti-inflammatory medication (NSAID) for treating pain, fever, and inflammation. In individuals at high risk, it also serves to prevent blood clotting, ischemic and heart attacks. It mainly inhibits the cyclooxygenase (COX) enzymes COX-1 and COX-2, resulting in reduced prostaglandins and inflammation (Vane & Botting, 2003). Yang et al. (2015) found that the anti-inflammatory effect of ASA is regulated via HMGB1-dependent pathways that are independent of COX-2.

Kahweol is a diterpene that is found in coffee. It belongs to the group of bioactive molecules known as cafestol (kahweol), which are present in coffee beans. The health benefits of kahweol include antioxidant, anti-inflammatory, and anti-cancer properties. Choi et al. (2015) demonstrated that kahweol-induced HSP70 suppression has an increased cytotoxic effect by inducing apoptosis in colorectal cancer cells. Some studies indicate that kahweol inhibits the MAPK signaling pathway, which is involved in cell survival and proliferation (Kwon et al., 2024).

Paquinimod inhibits S100A8/A9 by binding to the S100A9 subunit, which prevents receptor binding to RAGE and TLR4. The inhibition reduces the inflammatory response, including the release of cytokines and chemokines. This effect is particularly recognized in different autoimmune diseases, including systemic lupus erythematosus (Bengtsson et al., 2012).

Metformin is widely used for the treatment of diabetes mellitus. It has also been found that metformin inhibits RAGE receptors through the activation of the AMP-activated protein kinase (AMPK) pathway. When RAGE is inhibited, metformin helps in reducing inflammation and oxidative stress (Ishibashi et al., 2012).

Poly(I:C) was used in these experiments because it can induce apoptosis (Salaun et al., 2006). Our results indicated that adherent cells treated with ASA and metformin alone can inhibit the

growth of tumor cells, which was further decreased in combination with poly(I:C). Cell survival after the treatment of ASA alone was 70%, but it decreased to only 7% when combined with poly(I:C). Cell survival with metformin treatment was 50% but decreased to 20% when combined with poly(I:C). Kahweol and paquinimod did not have strong effects when applied alone. Kahweol did not have an inhibitory effect on cell growth, while paquinimod decreased cell survival to 85%. On the other hand, the survival of tumor cells was 30-40% when paquinimod or kahweol were combined with poly(I:C). Overall, ASA and metformin, when combined with poly(I:C) showed the most effective results, with only 7% and 20% survival of tumor cells, respectively, and with demonstrated significance compared to the poly(I:C) treatment alone (Figure 4.6).

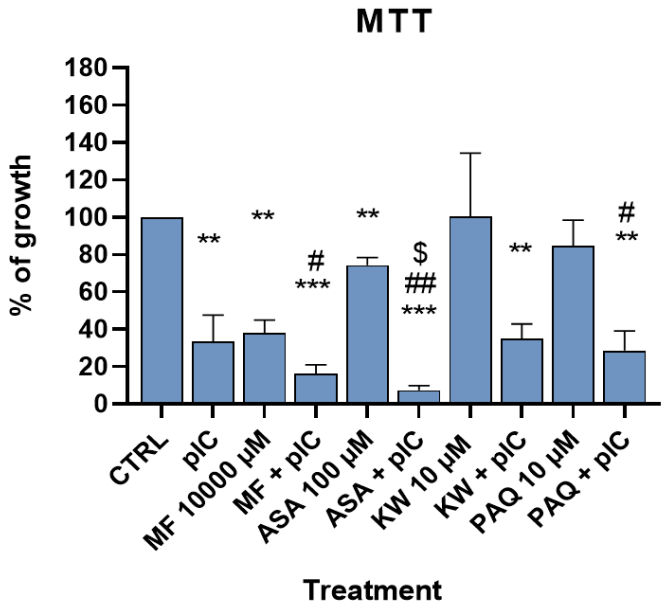

Figure 4.6. The survival of Detroit 562 tumor cells after the treatment with DAMP inhibitors. Tumor cell survival after the treatment with DAMP inhibitors 100 µM acetylsalicylic acid (ASA), 10000 µM metformin (MF), 10 µM kahweol (KW), and 10 µM paquinimod (PAQ), either alone or in combination with pIC (10 µg/mL poly(I:C)). Statistical significance was determined using t-test: * $p \leq 0.05$, ** $p \leq 0.01$, *** $p \leq 0.001$ (compared to control (CTRL)); # $p \leq 0.05$, ## $p \leq 0.01$ (compared to DAMP inhibitor treatment alone); $ $p \leq 0.05$ (compared to poly(I:C)). CTRL are untreated adherent tumor cells grown in DMEM.

4.2.3. Combined treatment with DAMP inhibitors and poly(I:C) reduces the viability of tumor spheres and changes their morphology

The treatment of tumor spheres with DAMP inhibitors, when combined with 10 µg/mL poly(I:C), resulted in reduced survival and changed morphology of tumor spheres. ASA and metformin alone or in combination with poly(I:C) altered the morphology of tumor spheres, which appeared smaller compared to the control and other treatments. Spheres treated with ASA+poly(I:C) showed disrupted outer margins, and tumor spheres appeared dispersed without a firm structure (Figure 4.7). The treatment with ASA, metformin, and kahweol alone reduced the viability of tumor spheres to 85-90%, and paquinimod reduced it to 70%. The strongest effect was observed in treatment with poly(I:C) combined with metformin or ASA, where the survival was only 20-25% when compared to the control. Kahweol and paquinimod in combination with poly(I:C) reduced the viability of tumor spheres to 35-40% (Figure 4.8).

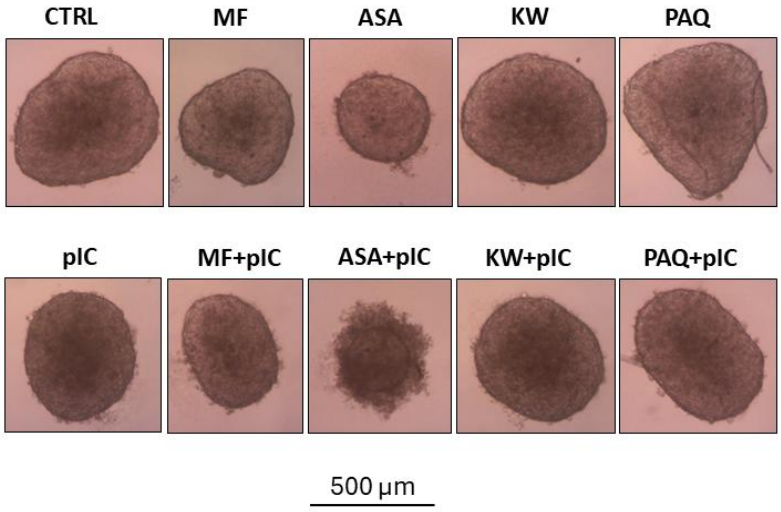

Figure 4.7. Photomicrographs of Detroit 562 tumor spheres. Tumor spheres were treated with 1000 µM acetylsalicylic acid (ASA), 10000 µM metformin (MF), 10 µM kahweol (KW), and 10 µM paquinimod (PAQ), either alone or in combination with pIC (10 µg/mL poly(I:C)). CTRL are untreated tumor spheres. Magnification is 2.5X times 72,5 for a digital camera objective.

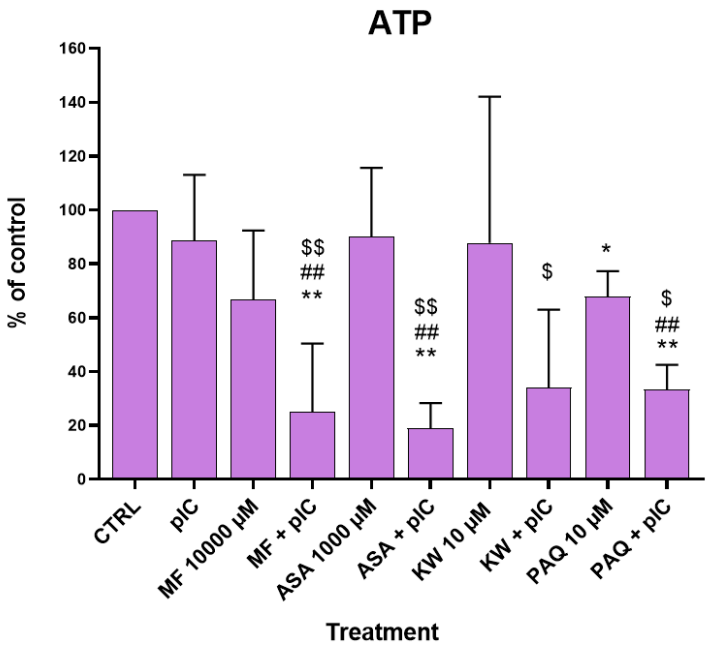

Figure 4.8. The viability of Detroit 562 tumor spheres after the treatment with DAMP inhibitors and poly(I:C). DAMP inhibitors: 1000 µM acetylsalicylic acid (ASA, aspirin), 10000 µM metformin (MF), 10 µM kahweol (KW), and 10 µM paquinimod (PAQ), either alone or in combination with pIC (10 µg/mL poly(I:C)). Statistical significance was determined using t-test: * $p \leq 0.05$, ** $p \leq 0.01$ (compared to control (CTRL)), # $p \leq 0.05$, ## $p \leq 0.01$ (compared to DAMP inhibitor treatment alone). $ $p \leq 0.05$, $$ $p \leq 0.01$ (compared to poly(I:C)). CTRL are untreated tumor spheres.

4.2.4. DAMPs released from cancer stem cells enhance head and neck cancer cell migration

To determine whether CSCs release certain factors (DAMPs) into the environment that can induce migration and invasion of tumor cells, Detroit 562 adherent tumor cells were treated with supernatants (conditioned media) obtained from tumor sphere cultures and monitored for their migration capacity. DAMP inhibitors aspirin (ASA), metformin, kahweol, and paquinimod were investigated to determine if they can abolish this effect. Matijevic Glavan et al. (2017) showed previously that poly(I:C) induces migration of adherent Detroit 562 cells. Here, we have further explored whether Detroit 562 tumour spheres release factors into the medium and TME that can induce the migration of neighbouring tumour cells.

The migration of tumor cells was followed under the microscope at two different time points: 0 hours (the beginning of the experiment) and 11 hours after treatment (the end of the experiment). At time point 0, only the empty circular, uninvaded spot, surrounded by tumor cells, was visible. At 11 hours post-treatment, tumor cells have either migrated or their migration was inhibited (Figure 4.9). ADH represents the control, which is supernatant from adherent Detroit 562 cells, and all the results were normalized to this value.

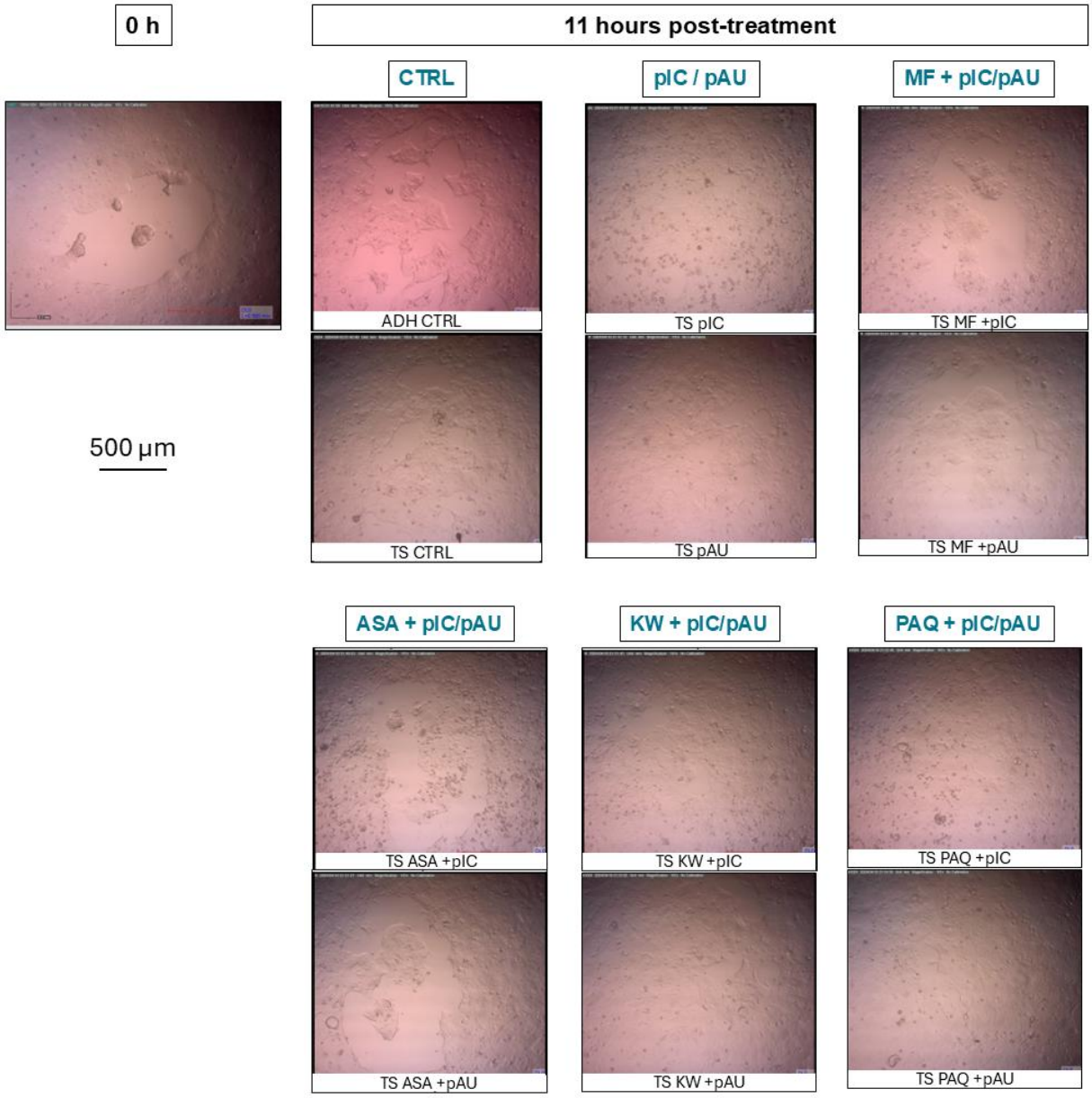

Figure 4.9. Microscopic analysis of Detroit 562 tumor cell migration 11 hours post-treatment. 0-hour time point represents tumor cells at the beginning of the treatment addition. It serves as the baseline reference showing the initial state of the gap closure. Variations in cell migration status are visible across different treatments. DAMP inhibitors: 1000 µM acetylsalicylic acid (ASA, aspirin), 10000 µM metformin (MF), 10 µM kahweol (KW), and 10 µM paquinimod (PAQ) in combination with pIC/pAU (10 µg/mL poly(I:C)/poly(A:U)). ADH are untreated adherent cells grown in DMEM (control conditioned medium), and TS CTRL are untreated tumor spheres. Magnification is 2.5X times 72,5 for the digital camera objective.

The migration of Detroit 562 cells was assessed 11 hours following the treatment. Increased migration of tumor cells was observed for adherent cells treated with supernatants from untreated tumor spheres (TSctrl), but also in samples treated with conditioned media from tumor spheres treated with poly(I:C) and poly(A:U) compared to the adherent control (ADH). Supernatants from poly(I:C)-treated spheres induced higher migration even in comparison to TSctrl.

Significant inhibition of migration was observed in cells treated with supernatants from tumor spheres treated with DAMP inhibitors metformin and aspirin in combination with poly(I:C) or poly(A:U), compared to poly(I:C) or poly(A:U) treatment alone. Cells treated with supernatants from tumor spheres treated with aspirin in combination with poly(I:C) or poly(A:U) showed more noticeable migration inhibition compared to poly(I:C) or poly(A:U) treatment alone, where the migration was reduced to ADH control levels. The treatment with paquinimod and kahweol did not inhibit the migration of the cells. These results indicate that DAMPs derived from CSCs may play a role in promoting tumor cell migration, suggesting their potential involvement in cancer progression, which can be suppressed by metformin and aspirin (Figure 4.10).

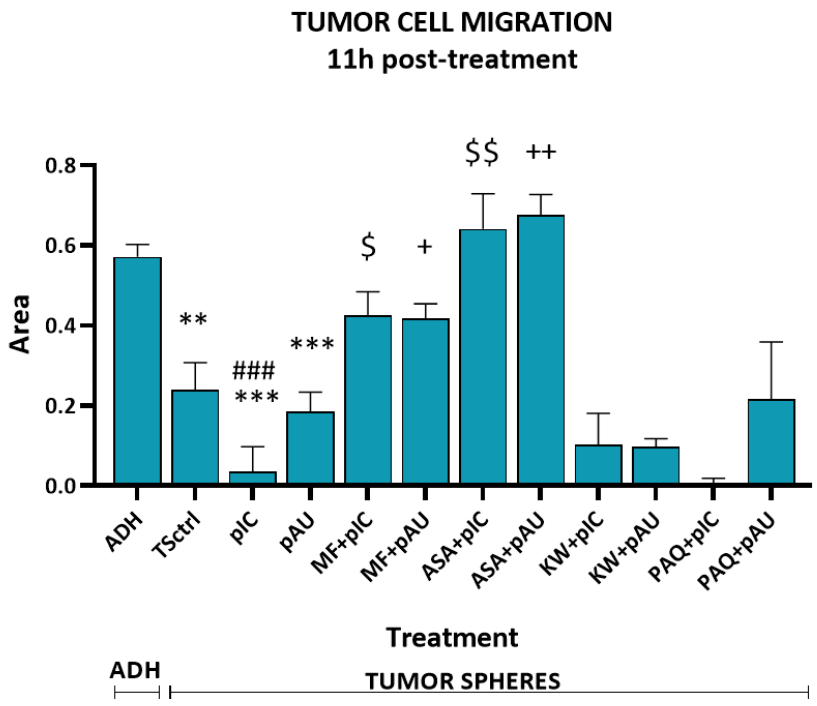

Figure 4.10. Quantitative analysis of Detroit 562 tumor cell migration 11 hours post-treatment with supernatants from tumor spheres. Supernatant from adherent cells (ADH) was used as a control and a baseline. The increased migration is represented by lower values of area. 1000 µM acetylsalicylic acid (aspirin, ASA), 10000 µM metformin (MF), 10 µM kahweol (KW), 10 µM paquinimod (PAQ), and pIC (10 µg/mL poly(I:C)). Statistical significance was determined using t-test: ** $p \leq 0.01$, *** $p \leq 0.001$ (compared to adherent control (ADH)); ### $p \leq 0.001$ (compared to TSctrl); \$ $p \leq 0.05$, \$\$ $p \leq 0.01$ (compared to poly(I:C)); + $p \leq 0.05$, ++ $p \leq 0.01$ (compared to poly(A:U)). ADH are untreated adherent tumor cells, and TSctrl are untreated tumor spheres.

4.2.5. Tumor cell invasion after the treatment of cells with supernatants from tumor spheres

Detroit 562 tumor cell invasion was increased when cells were treated with supernatants from tumor spheres induced by 10 µg/mL poly(I:C)/poly(A:U) compared to the control, and the trend of decrease of the invasion after the treatment with aspirin, metformin, and kahweol in combination with poly(I:C) was observed but it was not statistically significant (Figure 4.11). Paquinimod in combination with poly(I:C) did not reduce cell invasion. Even though in some experiments it was effective, in other experiments it was not, as evidenced by large deviations in error bars, suggesting significant variability (Figure 4.12). The inhibition of DAMPs did not affect invasion in a statistically significant manner. This indicates that while DAMPs may be important for the migration of tumor cells, invasion may be induced by other mechanisms.

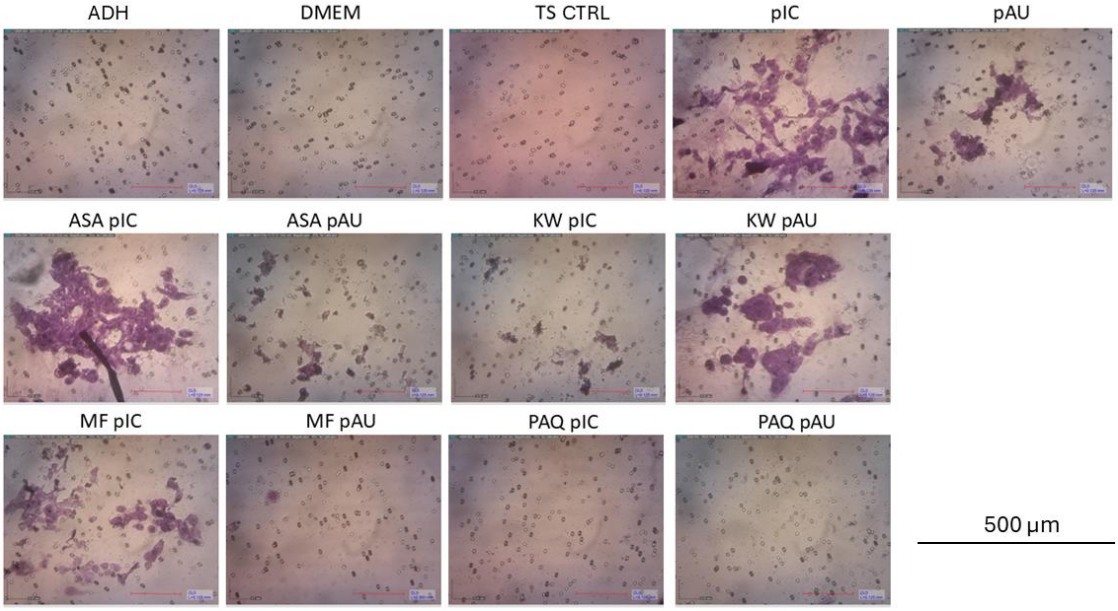

Figure 4.11. Detroit 562 tumor cell invasion 24 hours post-treatment with different treatment conditions. Tumor cells were treated with supernatants from tumor spheres treated with 1000 µM acetylsalicylic acid (ASA), 10000 µM metformin (MF), 10 µM kahweol (KW), 10 µM paquinimod (PAQ), and pIC/pAU (10 µg/mL poly(I:C)/poly(A:U)). ADH are untreated adherent cells, and TS CTRL are untreated tumor spheres. Magnification is 10X times 72,5 for a digital camera objective.

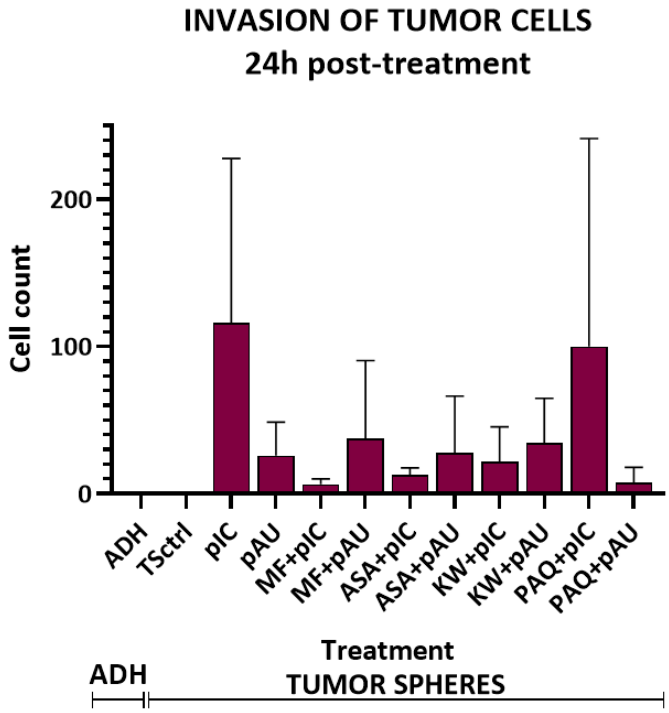

Figure 4.12. Invasion of Detroit 562 tumor cells 24 hours after the treatment. The graph represents the cell count of invasive cells across different treatment conditions. Tumor cells were treated with supernatants from tumor spheres treated with 1000 µM acetylsalicylic acid (ASA), 10000 µM metformin (MF), 10 µM kahweol (KW), 10 µM paquinimod (PAQ), and pIC/pAU (10 µg/mL poly(I:C)/poly(A:U)). ADH are untreated adherent cells, and TSctrl are untreated tumor spheres.

4.3. Combining DAMP inhibitors with irradiation and poly(I:C) to determine the effect on cancer stem cell survival and stemness properties

4.3.1. Combining DAMP inhibitors with γ-irradiation and TLR3 activation to target head and neck cancer stem cells

The therapeutic effect of DAMP inhibitors combined with **γ-**irradiation and TLR3 activation with a known apoptotic inducer poly(I:C), was assessed on Detroit 562 adherent tumor cells and tumor spheres. The impact of the combined treatment on adherent tumor cells was assessed using the MTT assay, and the effect of the combined treatment on tumor spheres was evaluated using the Vialight assay. For poly(I:C), it was previously shown that it has a radiosensitizing effect on HNSCC tumor cells alone (Mikulandra et al., 2019).

Treatment with ASA 100 μM, kahweol, paquinimod, and metformin, in combination with 10 μg/mL poly(I:C) and 5 Gy irradiation, demonstrated enhanced cytotoxicity, resulting in the elimination of tumor cells. Moreover, metformin combined with poly(I:C) decreased tumor cell growth down to 35% in non-irradiated cells and led to complete tumor cell proliferation block upon irradiation with both 2.5 Gy and 5 Gy. ASA 100 μM+poly(I:C) reduced the tumor cell survival to 50% even without irradiation and further to 20% when irradiated with 2.5 Gy and completely eliminated tumor cells when irradiated with 5 Gy. The treatment with 1000 μM aspirin was excessive for adherent cells, but we have included this concentration for easier comparison of adherent cells and tumor spheres, which were not that sensitive to aspirin treatment which was expected, since CSCs are resistant to radiotherapy. KW and PAQ alone demonstrated a protective effect against radiation. When they are combined with poly(I:C), the only effect comes from poly(I:C), except at the highest dose of radiation (5 Gy) where a complete proliferation block was observed.

Treatments with DAMP inhibitors alone without poly(I:C) in all irradiation conditions didn’t have a significant effect on tumor cell survival, except for metformin, and ASA in the concetration of 1000 μM, which was included only for comparison to spheres (Figure 4.13).

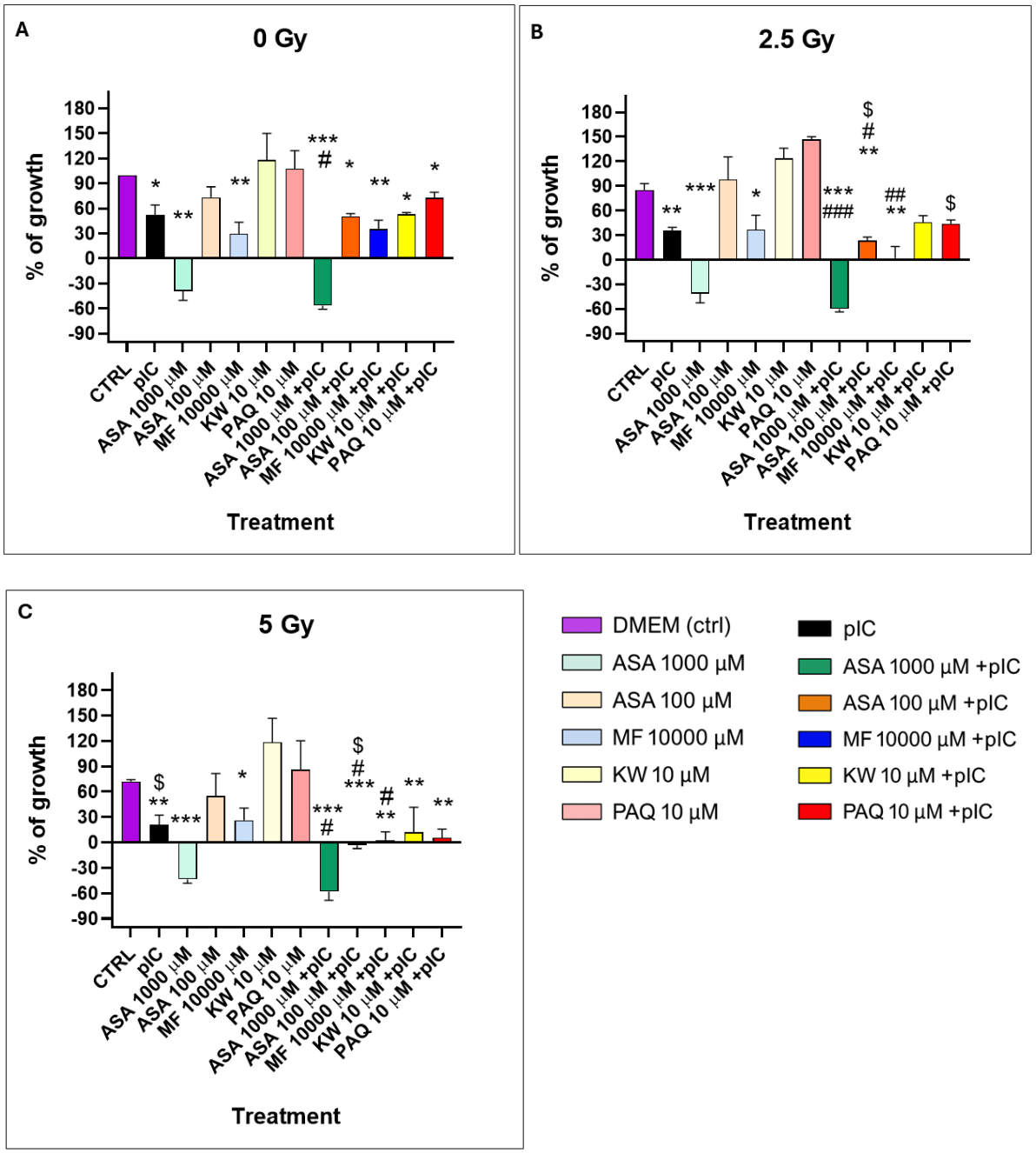

Figure 4.13. The viability of adherent Detroit 562 cells following treatment with DAMP inhibitors, poly(I:C), and γ-irradiation was determined by MTT assay. (**A**) The survival of tumor cells treated with DAMP inhibitors alone or combined with poly(I:C) without irradiation. (**B**) The survival of tumor cells treated with DAMP inhibitors alone or combined with poly(I:C) irradiated with 2.5 Gy. (**C**) The survival of tumor cells treated with DAMP inhibitors alone or combined with poly(I:C) irradiated with 5 Gy. Statistical significance was determined using t-test: * $p \leq 0.05$, ** $p \leq 0.01$, *** $p \leq 0.001$, *** $p \leq 0.0001$ (compared to control (CTRL)); # $p \leq 0.05$, ## $p \leq 0.01$, ### $p \leq 0.001$ (compared to DAMP inhibitor treatment alone); $ $p \leq 0.05$ (irradiated cells compared to the non-irradiated cells). MF=metformin, ASA=aspirin, KW=kahweol, PAQ=paquinimod, pIC (10 µg/mL poly(I:C)). CTRL are untreated tumor cells.

When tumor spheres were irradiated with γ-irradiation (5 Gy), the photomicrograph analysis showed changes in tumor sphere size and morphology after the treatment with ASA 1000 μM alone and ASA 1000 μM + poly(I:C), regardless of irradiation, demonstrating the cytotoxic effect of the treatment. Photomicrograph analysis showed that the treatment with ASA 1000 μM reduced the tumor sphere size by 50%. The addition of poly(I:C) caused a disrupted margin of the tumor sphere. Also, metformin treatment reduced tumor sphere size. Other treatment combinations did not affect sphere morphology, but 5 Gy irradiation caused changes in sphere morphology, resulting in a more distressed margin in all conditions (Figure 4.14).

The viability of tumor spheres after irradiation decreased by 30%. The treatment with 1000 μM ASA alone without the irradiation decreased the cell viability to 65%, which was further decreased to 60% with irradiation. The combination of ASA 1000 μM + poly(I:C) caused a decrease in viability to 50% regardless of the irradiation. Poly(I:C) alone, when combined with irradiation, reduced the cell survival to 60%. ASA 100 μM alone was not cytotoxic to tumor spheres, while the irradiation treatment reduced proliferation by 40%. Cell viability remained 70% after the treatment with ASA 100 μM + poly(I:C), but was slightly reduced with irradiation. Metformin alone decreased the viability of tumor spheres down to 80%, and metformin + poly(I:C) only slightly reduced the viability. Irradiation in treatment with metformin and poly(I:C) reduced cell viability to 60%. Kahweol alone and after irradiation with 5 Gy did not significantly reduce the viability. Also, the treatment with kahweol + poly(I:C) alone or in combination with irradiation did not affect the viability compared to pIC alone. Paquinimod treatment alone did not affect cell viability. Paquinimod + poly(I:C) alone or in combination with the irradiation did not cause a reduction in cell viability compared to poly(I:C) alone (Figure 4.15).

Overall, the results indicate that the combined treatment, especially with ASA and metformin, enhances the radiosensitivity of adherent Detroit 562 tumor cells to γ-irradiation, leading to a significant reduction in cell viability. In contrast, tumor spheres exhibited relative radioresistance, with only a slight reduction in tumor sphere viability after the irradiation and limited morphology changes after the treatment with ASA 1000 + poly(I:C). These findings suggest that tumor spheres may have activated some intrinsic pathways to induce radioresistance.

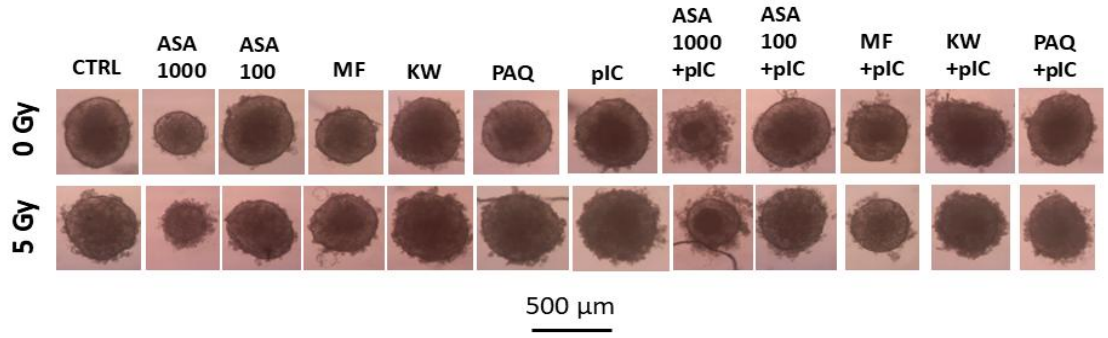

Figure 4.14. Photomicrograph analysis: morphology of Detroit 562 tumor spheres following the treatment with DAMP inhibitors, poly(I:C), and γ-irradiation. Tumor spheres were treated with DAMP inhibitors alone or in combination with poly(I:C). The top row represents tumor spheres without irradiation (0 Gy), and the bottom row represents tumor spheres irradiated with 5 Gy. 1000 µM acetylsalicylic acid (ASA), 10000 µM metformin (MF), 10 µM kahweol (KW), and 10 µM paquinimod (PAQ), 10 µg/mL poly(I:C) (pIC). CTRL are untreated tumor spheres. Magnification is 2.5X times 72,5 for a digital camera objective.

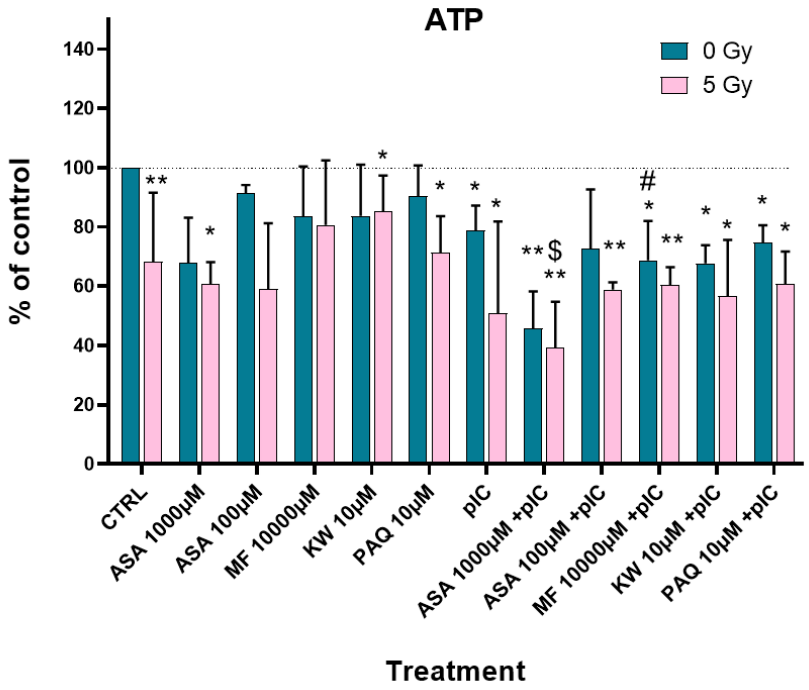

Figure 4.15. The viability of Detroit 562 tumor spheres after the treatment with DAMP inhibitors, poly(I:C), and γ-irradiation was determined using the Vialight assay. Blue represents the survival of tumor spheres without irradiation (0 Gy), and pink represents the survival of tumor spheres irradiated with 5 Gy. Statistical significance was determined using t-test: * $p \leq 0.05$, ** $p \leq 0.01$ (compared to the control (CTRL)); # $p \leq 0.05$ (compared to DAMP inhibitor treatment alone); $ $p \leq 0.05$ (irradiated TS compared to non-irradiated TS). 1000 µM acetylsalicylic acid (ASA), 10000 µM metformin (MF), 10 µM kahweol (KW), and 10 µM paquinimod (PAQ), 10 µg/mL poly(I:C) (pIC). CTRL are untreated tumor spheres.

4.3.1.1. Expression of CSC-related genes following combined treatment with poly(I:C), DAMP inhibitors, and γ-irradiation

Next, we investigated if the combination of DAMP inhibitors with poly(I:C) and γ-irradiation has an inhibitory effect on gene expression. The expression of *OCT4* (stemness marker) and *ABCG2* (drug resistance marker) was determined following the combined treatment with 10 μg/mL poly(I:C), DAMP inhibitors, and **γ-**irradiation.

The qPCR results show a significant decrease in the expression of *OCT4* and *ABCG2* following ASA and ASA+poly(I:C) treatment. Without irradiation, treatment with ASA reduced the expression of *OCT4* by 50%, and ASA+poly(I:C) reduced the expression of *OCT4* to 30%.

The expression of *ABCG2* was reduced to 20% after the treatment with ASA or ASA+poly(I:C) without the irradiation, suggesting a reduction of CSC characteristics. Irradiation did not affect the expression (Figure 4.16).

Also, no significant reduction in *OCT4* expression was observed in cells treated with KW or KW+poly(I:C) with or without irradiation. Irradiation even increased the expression of *OCT4* in combination with KW and KW+pIC. KW+poly(I:C) treatment reduced *ABCG2* expression by 50% regardless of irradiation, but this was not significant compared to poly(I:C) treatment alone.

The 2 Gy radiation dose was used to compare the effect of γ-irradiation and proton beam irradiation. In the proton irradiation experiment (further in the results, Figure 4.20), a stronger effect was observed with the same dose.

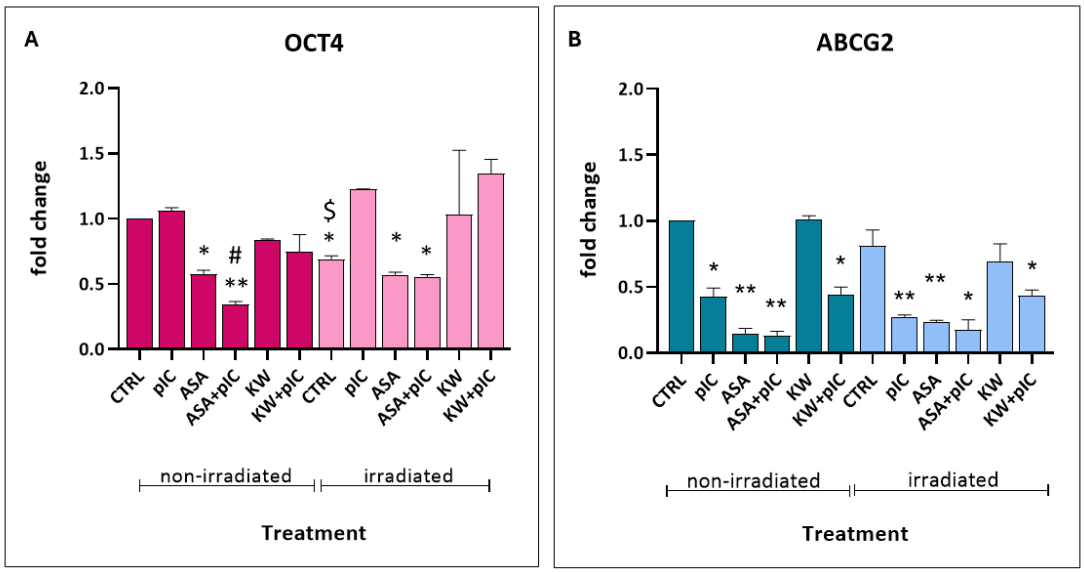

Figure 4.16. Expression of CSC-related genes in Detroit 562 tumor spheres. (**A**) The expression of *OCT4*, the stemness marker, and (**B**) *ABCG2*, the multidrug resistance marker. Tumor spheres were treated with DAMP inhibitors alone or in combination with poly(I:C) and were either irradiated with 2 Gy or not irradiated (0 Gy). Statistical significance was determined using t-test: *p ≤ 0.05, **p ≤ 0.01 (compared to the control (CTRL)); # p ≤ 0.05 (compared to DAMP inhibitors treatment alone); $ p ≤ 0.05 (irradiated TS compared to non-irradiated TS). 1000 µM acetylsalicylic acid (ASA), 10 µM kahweol (KW), and 10 µg/mL poly(I:C) (pIC). CTRL are untreated tumor spheres.

4.3.2. Combined proton therapy, DAMP inhibitors and TLR3 activation effectively targets head and neck cancer stem cells

4.3.2.1. The effect of DAMP inhibitors with poly(I:C), and proton irradiation on Detroit 562 cancer stem cells

A difference in size and morphology of tumor spheres was observed after different treatments and proton irradiation. Non-irradiated control tumor spheres 24 hours after the treatment were bigger compared to the control (spheres before the treatment), and they started to develop a necrotic center. Tumor spheres treated with ASA and ASA+poly(I:C) were significantly smaller compared to the untreated spheres, and also smaller than spheres treated with KW and poly(I:C). Irradiated spheres had disrupted the tumor sphere margin, and their morphology significantly changed 24 hours after the treatment. The outer border of the spheres was beginning to dissociate, which was especially visible in the tumor spheres treated with ASA and ASA+poly(I:C). The two controls (CTRL) were similar in size, but the outer border of the irradiated spheres was beginning to dissociate, suggesting proton irradiation has a cytotoxic effect on tumor spheres. (Figure 4.17).

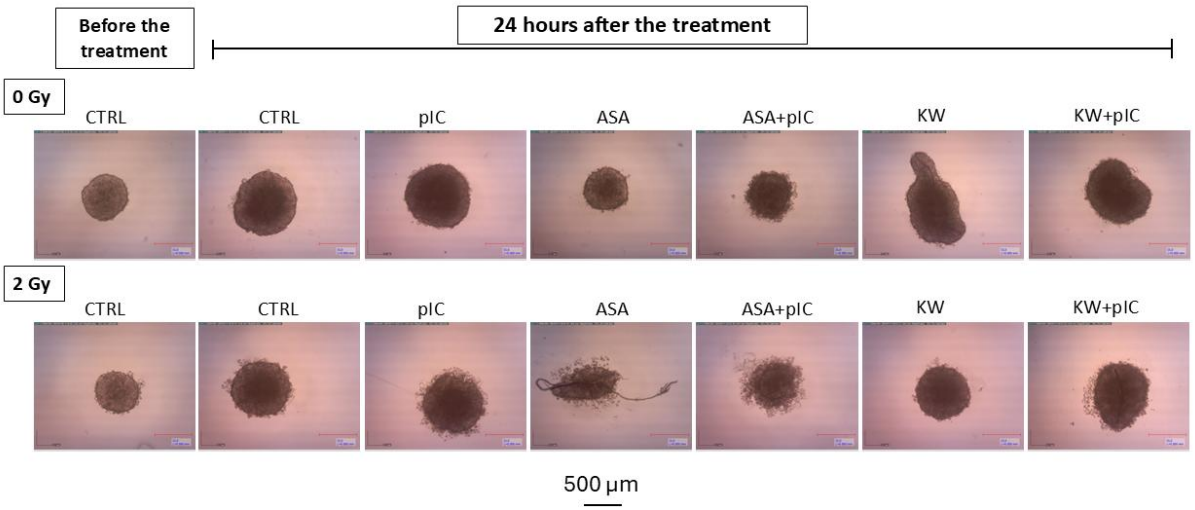

Figure 4.17. Photomicrograph analysis: single Detroit 562 tumor sphere size and morphology. The effect of different treatments and proton irradiation on tumor sphere formation 24 hours following different treatment and irradiation conditions. The top row shows non-irradiated tumor spheres (0 Gy) while the bottom row shows tumor spheres irradiated with 2 Gy. 1000 µM acetylsalicylic acid (ASA), 10 µM kahweol (KW), and pIC (10 µg/mL poly(I:C)). CTRL are untreated tumor spheres. Magnification is 2.5X times 72,5 for a digital camera objective.

Decreased viability of tumor spheres without and with proton irradiation was observed in spheres treated with ASA alone and with ASA+poly(I:C). The viability was reduced to 50% with ASA treatment and to 45% with ASA+poly(I:C) treatment without irradiation. Irradiation decreased the viability of tumor spheres to 45% with ASA treatment alone and 35% for ASA+poly(I:C) treatment. The proliferation of irradiated spheres treated with KW+poly(I:C) was also decreased. In tumor spheres without irradiation, KW treatment did not have an effect, while KW+poly(I:C) reduced tumor sphere viability to 80% (Figure 4.18). Overall, the ViaLight assay showed reduced tumor sphere viability after the treatment with ASA alone and with the combination of ASA+poly(I:C), and the viability was further reduced after proton irradiation.

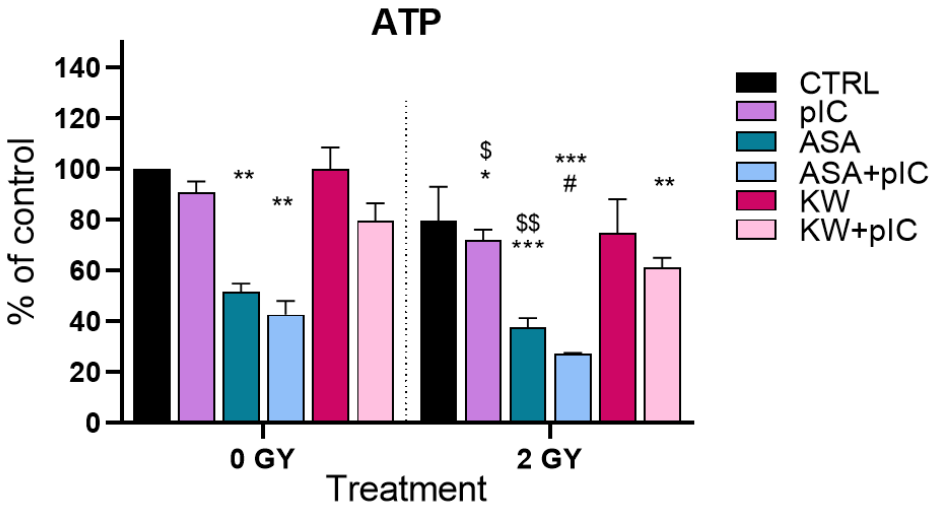

Figure 4.18. The viability of Detroit 562 tumor spheres following proton irradiation, treatment with DAMP inhibitors, and poly(I:C) was determined using the ViaLight assay. Tumor spheres were treated with DAMP inhibitors alone or in combination with poly(I:C) without irradiation (0 Gy) or irradiated with 2 Gy. Statistical significance was determined using t-test: * $p \leq 0.05$, ** $p \leq 0.01$, *** $p \leq 0.001$ (compared to the control (CTRL)); # $p \leq 0.05$ (compared to DAMP inhibitor treatment alone); \$ $p \leq 0.05$, \$\$ $p \leq 0.01$ (irradiated TS compared to non-irradiated TS). 1000 µM acetylsalicylic acid (ASA), 10 µM kahweol (KW), and 10 µg/mL poly(I:C) (pIC). CTRL are untreated tumor spheres.

4.3.2.2. Expression of CSC-related genes following combined treatment with poly(I:C), DAMP inhibitors, and proton irradiation

Next, we investigated if the combination of DAMP inhibitors with poly(I:C) and proton irradiation has an inhibitory effect on stemness marker expression. Overall, the qPCR showed reduced expression of CSC-related markers *ABCG2* and *OCT4* after the ASA+poly(I:C) treatment, which was further downregulated after the irradiation.

In non-irradiated spheres, *OCT4* expression was reduced in response to ASA treatment to 40%, but it was also further reduced with ASA+poly(I:C) treatment to 35%. This was not significant to poly(I:C) treatment alone. Treatment with KW alone did not change *OCT4* expression, and reduced expression with KW+poly(I:C) was not significant compared to poly(I:C) treatment alone.

After irradiation with 2 Gy, *OCT4* expression was further decreased in spheres treated with ASA+poly(I:C) to 25%. The treatment KW and KW+poly(I:C) did not have a significant effect on gene expression.

The treatment with ASA reduced *ABCG2* gene expression to 25%, and treatment with ASA+poly(I:C) reduced gene expression to 20%. KW+poly(I:C) reduced gene expression to 30% when compared to the non-irradiated control, but it was not significant compared to poly(I:C) treatment alone.

After irradiation (2 Gy), the reduction of gene expression became even more pronounced in cells treated with ASA+poly(I:C), where expression was decreased to 5%, while *ABCG2* expression in spheres treated with ASA alone was not affected by irradiation. The treatment with KW+poly(I:C) even leads to slightly increased expression of *ABCG2* after the irradiation. (Figure 4.19).

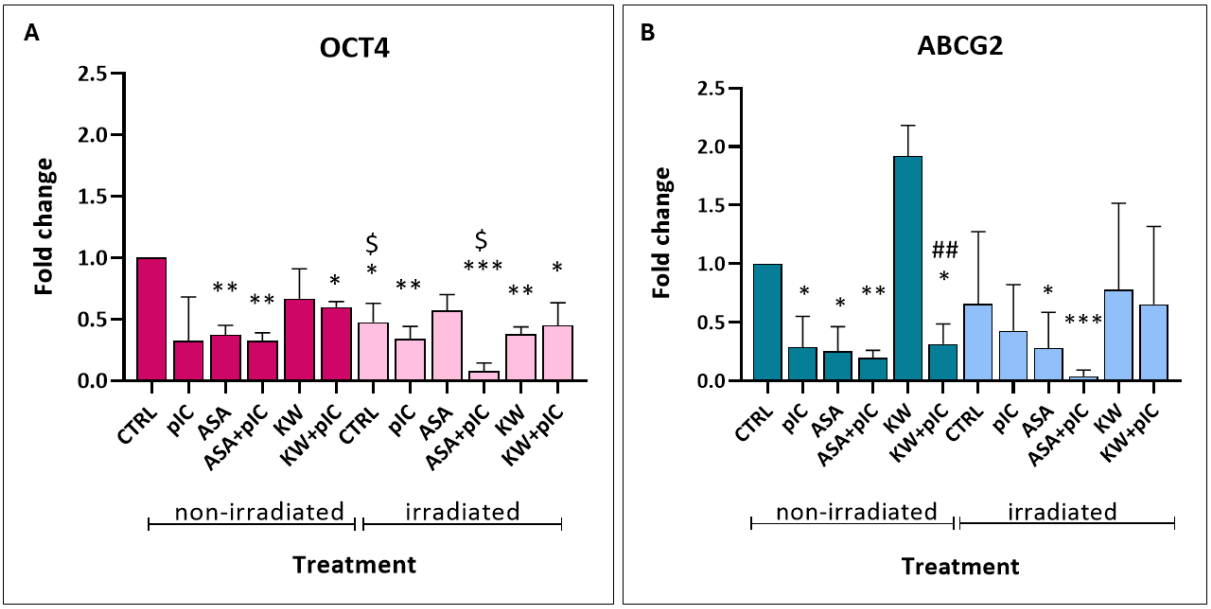

Figure 4.19. Expression of CSC-related genes in Detroit 562 tumor spheres. Tumor spheres were treated with DAMP inhibitors alone or in combination with poly(I:C), and either irradiated with protons (2 Gy) or not irradiated (0 Gy). qPCR results of the expression of (**A**) *OCT4* and (**B**) *ABCG2*. Statistical significance was determined using t-test: *p ≤ 0.05, **p ≤ 0.01, ***p ≤ 0.001 (compared to the control (CTRL)). ## p ≤ 0.01 (compared to DAMP inhibitors treatment alone); $ p ≤ 0.05 (irradiated TS compared to non-irradiated TS). 1000 µM acetylsalicylic acid (ASA), 10 µM kahweol (KW), and 10 µg/mL poly(I:C) (pIC). CTRL are untreated tumor spheres.

4.3.2.3. Effects of different treatments and proton irradiation on tumor sphere apoptosis induction

Using the western blot, we determined PARP cleavage (cleaved fragment, 89 kDa), which indicates apoptosis. No significant PARP cleavage was observed in untreated and non-irradiated (CTRL) cells. On the contrary, poly(I:C), ASA, ASA+poly(I:C), and KW+poly(I:C) induced increased PARP cleavage compared to the control, with the strongest cleaved band in tumor spheres treated with ASA+poly(I:C). Proton irradiation induced PARP cleavage in all samples, including the control, which was only irradiated, indicating apoptosis induction. The strongest cleaved PARP band was present in the spheres treated with ASA+poly(I:C) (Figure 4.20). These results demonstrated that combining proton therapy with poly(I:C) and ASA significantly enhances the treatment efficacy and may eliminate HNSCC CSCs.

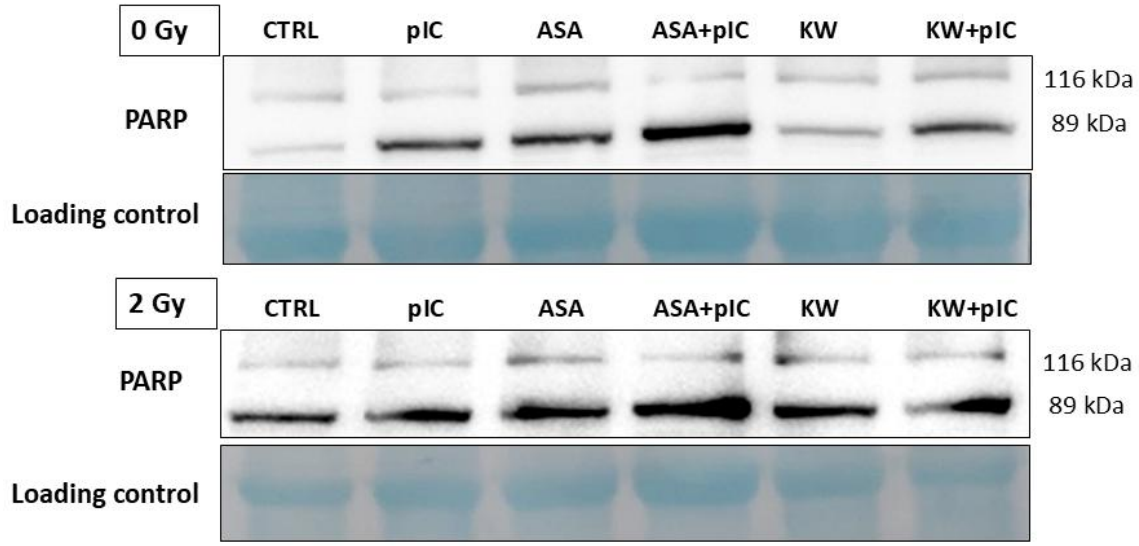

Figure 4.20. Western blot demonstrating PARP cleavage in Detroit 562 tumor spheres. Tumor spheres were treated with DAMP inhibitors (1000 µM acetylsalicylic acid (ASA), 10 µM kahweol (KW)) alone or in combination with pIC (10 µg/mL poly(I:C)), and either irradiated with protons (2 Gy) or not irradiated (0 Gy). Full-length PARP protein is 116 kDa in size, while the cleaved PARP fragment is 89 kDa in size. CTRL are untreated tumor spheres. The loading controls were membranes stained with naphthol blue.

4.4. Exploration of potential novel CSC biomarkers

4.4.1. Proteomic analysis validation

To determine new potential biomarkers for HNSCC CSC, proteomic analysis was performed. Proteomic analysis included 4 different samples: adherent control, untreated tumor spheres, tumor spheres treated with poly(I:C), and tumor spheres treated with poly(A:U). Several proteins (Table 4.1) exhibited significant changes in tumor spheres compared to the adherent cells, but some changes were also noticeable in poly(I:C)- or poly(A:U)- treated spheres. Table 4.1. shows the list of proteins changed after proteomic analysis, which we decided to further explore. A complete list of proteins with altered expressions can be found in our publication (Derfi et al., 2024).

Table 4.1. List of proteins chosen for further validation, including their principal role and their role in cancer.

Protein	Abbreviation	Principal role	Role in cancer
Nucleoporin 62	NUP62	It is essential for preserving proper chromosomal stability (Chien et al., 2020).	Plays a role in the growth and progression of squamous cell carcinomas (Hazawa et al., 2018).
StAR-related lipid transfer domain containing 10	StarD10	It is a phospholipid transfer protein that enables their movement across intracellular membranes (Olayioye et al., 2005).	Its expression is associated with increased malignancy in breast cancers related to alcohol consumption (Floris et al., 2019).
Gasdermin	GSDM	It is known for its dual role; it is involved in pyroptosis (Yuan et al., 2024) but also plays a role in chronic inflammation leading to tumor progression (Gao et al., 2024).	In HNSCC, expression is elevated and linked to poor prognosis (Yuan et al., 2024).
Tumor susceptibility gene 101	TSG101	It is involved in the ESCRT pathway, which enables the formation of multivesicular bodies that deliver cargo to lysosomes for degradation (Henne et al., 2011).	In HNSCC, its overexpression induces metastasis through cell cycle regulation (Yang et al., 2025).
Glutathione S-transferase theta 1	GSTT1	A GST family member that catalyzes the conjugation of reduced glutathione to diverse hydrophobic and electrophilic molecules (Mazari et al., 2023).	Plays a role in tumor metastasis and dissemination but is not necessary for primary tumor development (Ferrer et al., 2024).
Glutamate-rich WD repeat-containing 1	GRWD1	Plays a role in cellular regulation and growth control. It also has a role in ribosomal biosynthesis (Kayama et al., 2017).	In HNSCC, it demonstrated altered expression compared to healthy tissues, indicating its potential role as a diagnostic biomarker (Gill et al., 2024).

Ubiquitin C-terminal hydrolase L5	UCHL5	Functions as a deubiquitinating enzyme and regulates the degradation of proteins (Deol et al., 2020).	It regulates apoptosis and cell proliferation in cancer and plays a role in the proliferation and survival of HNSCC cells (Morgan et al., 2023).
Syndecan-binding protein	Syntenin	Plays a role in cytoskeletal organization, cell-to-cell adhesion, intracellular protein transport, and transcription factor activation (Zimmermann et al., 2001).	It is a membrane protein that facilitates the invasion and progression of HNSCC (Cui et al., 2016).

Proteomic results were validated by Western blot. NUP62 was overexpressed in TS in comparison to the adherent cells and was strongly expressed but slightly reduced compared to the untreated tumor spheres in poly(I:C)-treated TS, with almost complete absence in TS treated with poly(A:U). StarD10 was strongly expressed in tumor spheres treated with poly(I:C) and poly(A:U). Gasdermin had the strongest expression in adherent control cells, which was reduced in tumor spheres, independent of the treatment. TSG101 expression was the same in all samples. GSTT1 was detected only in tumor spheres and was slightly reduced in tumor spheres treated with poly(A:U). GRWD1 was highly expressed in adherent controls compared to tumor spheres, and its expression was not dependent on TLR3 activation. UCHL5 expression was increased in the tumor spheres compared to the adherent cells. It was also reduced after TLR3 activation, especially with poly(A:U). Syntenin was strongly expressed in adherent control, and its expression was reduced in tumor spheres, especially spheres treated with poly(A:U) (Figure 4.21). Using a proteomic approach, potential novel biomarkers that might play an important role in HNSCC CSCs were identified.

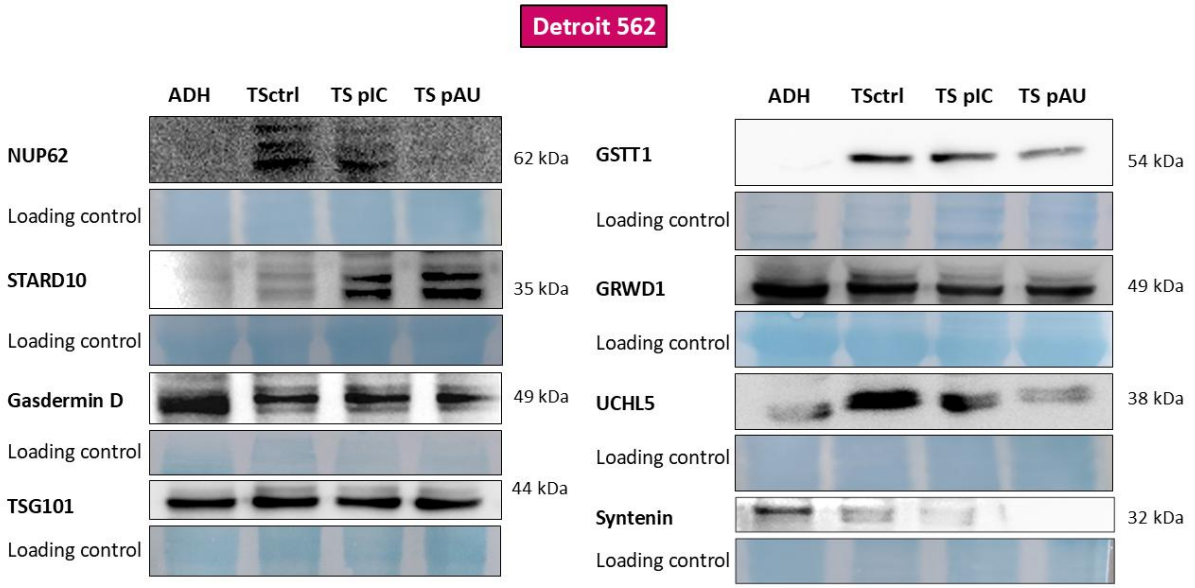

Figure 4.21. Validation of proteomic analysis by Western blot. Expression of proteins NUP62 (62 kDa), STARD10 (35 kDa), Gasdermin D (49 kDa), TSG101 (44 kDa), GSTT1 (54 kDa), GRWD1 (49 kDa), UCHL5 (38 kDa) and Syntenin (32 kDa) in adherent cells (ADH), control tumor spheres (TSctrl), tumor spheres treated with poly(I:C) (TS pIC), and tumor spheres treated with poly(A:U) (TS pAU). Poly(I:C) and poly(A:U) were used in a concentration of 10 µg/mL. The loading controls were membranes stained with naphthol blue.

4.4.2. The expression of UFSP2 and KYAT3 in Detroit 562 tumor spheres

The significant changes of UFM1 Specific Peptidase 2 (UFSP2) and Kynurenine Aminotransferase 3 (KYAT3, KAT3) were observed during the validation of proteomic analysis, which we decided to further explore. UFSP2 is a protease that is involved in the UFMylation process, a posttranslational modification in which ubiquitin-fold modifier-1 (UFM1), a protein similar to ubiquitin, is covalently attached to target proteins (Jing et al., 2022). KYAT3 is one of the key enzymes involved in the tryptophan metabolism from kynurenine to kynurenic acid, and in recent studies, tryptophan metabolism has been detected as a potential target for cancer treatment. Furthermore, kynurenine can promote tumor growth (León-Letelier et al., 2023).

In tumor spheres, stimulation of the TLR3 receptor caused a decrease in expression of the UFSP2. The effect was most pronounced in cells treated with poly(A:U) when compared to untreated tumor spheres. Control tumor spheres showed upregulated UFSP2 compared to adherent cells, while in adherent cells, UFSP2 was expressed equally across the treatments. KYAT3 expression was decreased in adherent Detroit 562 cells treated with poly(I:C). On the other hand, in untreated tumor spheres, KYAT3 expression was increased compared to the adherent tumor cells, while it was reduced after the poly(A:U) treatment (Figure 4.22).

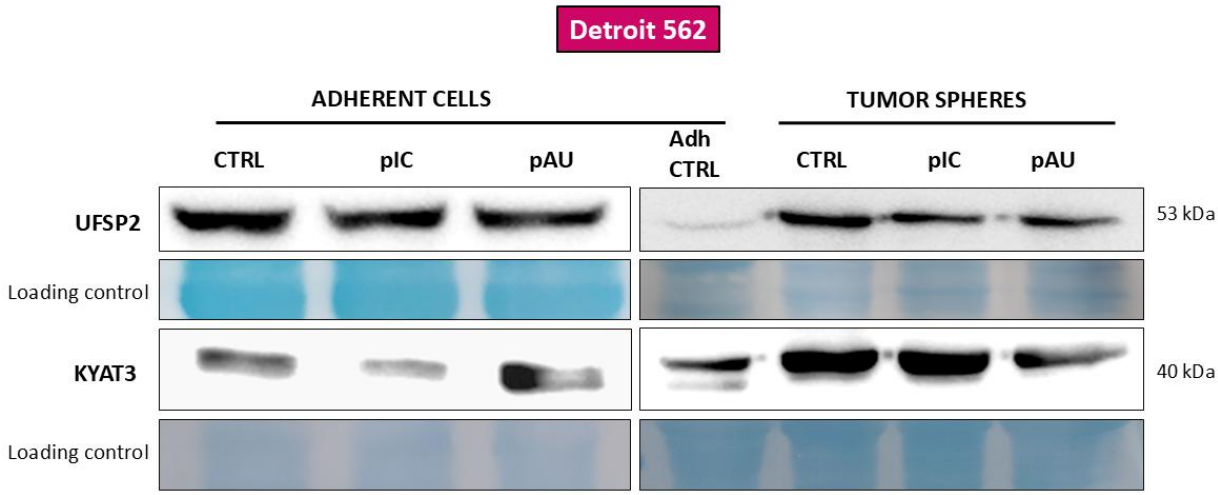

Figure 4.22. Expression of UFSP2 and KYAT3 in Detroit 562 adherent cells and tumor spheres. Samples include adherent cells control (CTRL), adherent cells treated with poly(I:C) (pIC) adherent cells treated with poly(A:U) (pAU); and tumor spheres including control (CTRL), tumor spheres treated with poly(I:C) (pIC), and tumor spheres treated with poly(A:U) (pAU). Poly(I:C) and poly(A:U) were used in a concentration of 10 µg/mL. The loading controls were membranes stained with naphthol blue.

4.4.3. Optimization of the siRNA transfection in tumor spheres

To determine whether the observed effects in UFSP2 and KYAT3 change in expression are TLR3-dependent, the silencing of TLR3 was performed using siRNA.

The optimal transfection conditions for the Detroit 562 cell line were determined using Control siRNA labelled with fluorescein isothiocyanate (FITC-siRNA). The transfection protocol was optimized, and adherent cells and tumor spheres were examined under the fluorescence microscope. The highest efficiency was observed with 80 nM FITC-siRNA and 8 µL TransFectin reagent; therefore, we followed these conditions as most suitable for further transfections. The transfection was performed with adherent cells (Figure 4.23 & Figure 4.24). Once transfected, cells were seeded to form tumor spheres (Figure 4.25). We concluded that siRNA silencing can be performed in adherent cells and will remain effective in tumor spheres.

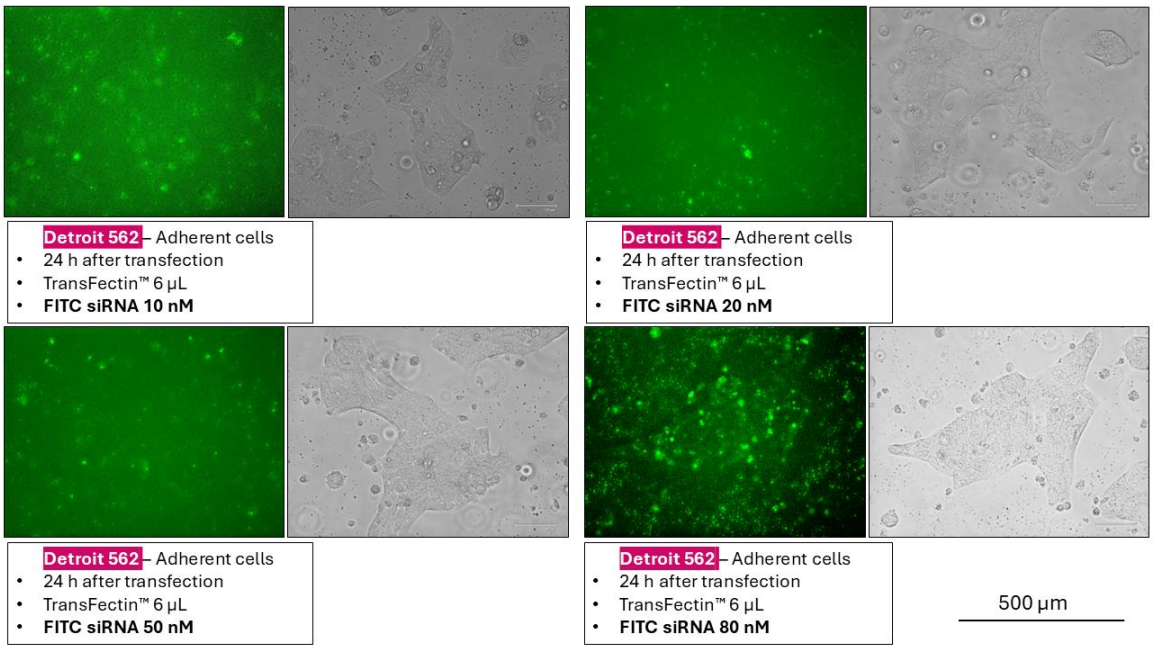

Figure 4.23. Photomicrograph of Detroit 562 tumor cells 24 hours after transfection. Validation of transfection efficiency with different concentrations of control FITC-labelled siRNA (Fluorescein Conjugate)-A (10 nM, 20 nM, 50 nM, and 80 nM) and 6 µL of TransFectin™ Lipid Reagent. Fluorescein is a light-reactive dye visible using fluorescent microscopy, showing transfected tumor cells in green color. The light source (right) displays the general morphology and number of the cells.

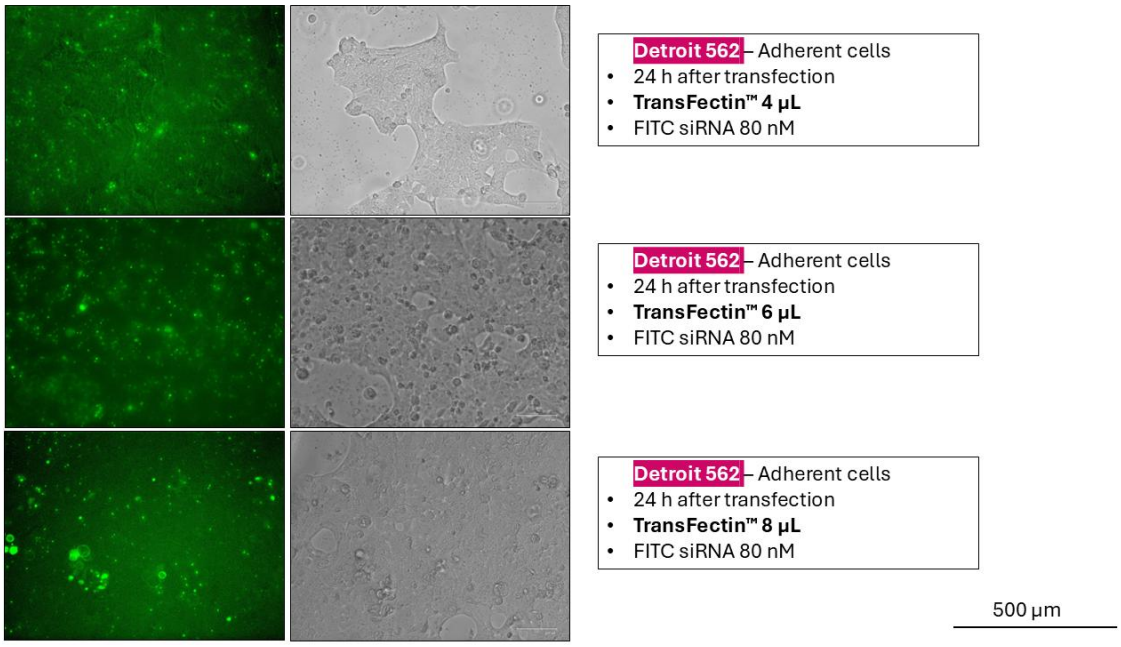

Figure 4.24. Photomicrograph of Detroit 562 cells 24 hours after transfection. The highest concentration of 80 nM Control FITC-labelled siRNA (Fluorescein Conjugate)-A with different amounts of TransFectin™ Lipid Reagent (4 µL, 6 µL, and 8 µL). Fluorescein is a light-reactive dye visible using fluorescent microscopy, showing transfected tumor cells in green color (left). The light source (right) displays the general morphology and number of the cells.

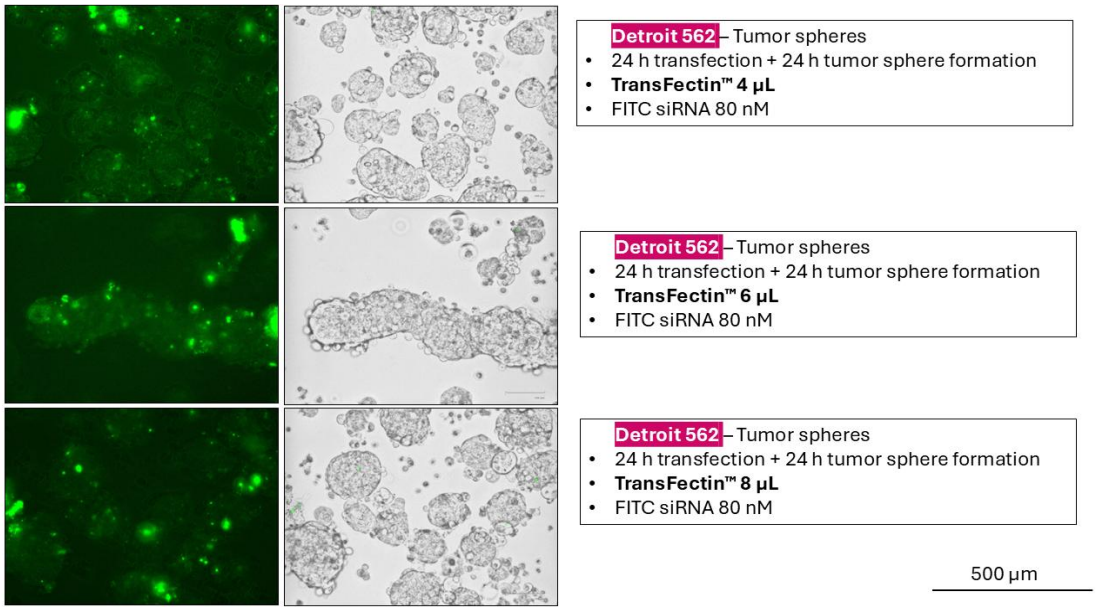

Figure 4.25. Photomicrograph of Detroit 562 tumor spheres 48 hours after transfection. The highest concentration of 80 nM Control FITC-labelled siRNA (Fluorescein Conjugate)-A with different amounts of TransFectin™ Lipid Reagent (4 µL, 6 µL, and 8 µL). 24 hours after transfection, cells were seeded in tumor sphere media to form tumor spheres. Fluorescein is a light-reactive dye visible using fluorescent microscopy, showing transfected tumor spheres in green color (left). Tumor spheres were visible with a white light source (right).

4.4.4. The role of TLR3 activation in the regulation of UFSP2 and KYAT3 expression

To obtain additional confirmation of the previous results, we performed a transient transfection using siRNA for TLR3.

Western blot analysis of proteins from transfected cells revealed that UFSP2 expression was reduced after the treatment with poly(I:C) and poly(A:U) in tumor spheres transfected with scrambled sequence (SCR) compared to untreated control (CRTL SCR) spheres, with the most pronounced reduction observed after poly(I:C) treatment. In contrast, in spheres where TLR3 was silenced, it was shown that the UFSP2 expression was unchanged across all conditions and its expression is lower in CTRL siTLR3 compared to the CTRL SCR.

KYAT3 expression was reduced in poly(I:C)- and poly(A:U)-treated spheres transfected with SCR compared to the control spheres. In spheres where TLR3 was silenced, the expression of KYAT3 was similar in control and poly(I:C)-treated spheres, but it was reduced in poly(A:U)-treated spheres. Its expression is lower in CTRL siTLR3 compared to CTRL SCR (Figure 4.26).

We conclude that TLR3 silencing prevents the decrease of UFSP2 expression. As for KYAT3, its decreased expression is abolished in tumor spheres treated with poly(I:C), but this was not observed in spheres treated with poly(A:U). This suggests a different effect on expression that is dependent on the TLR3 agonist.

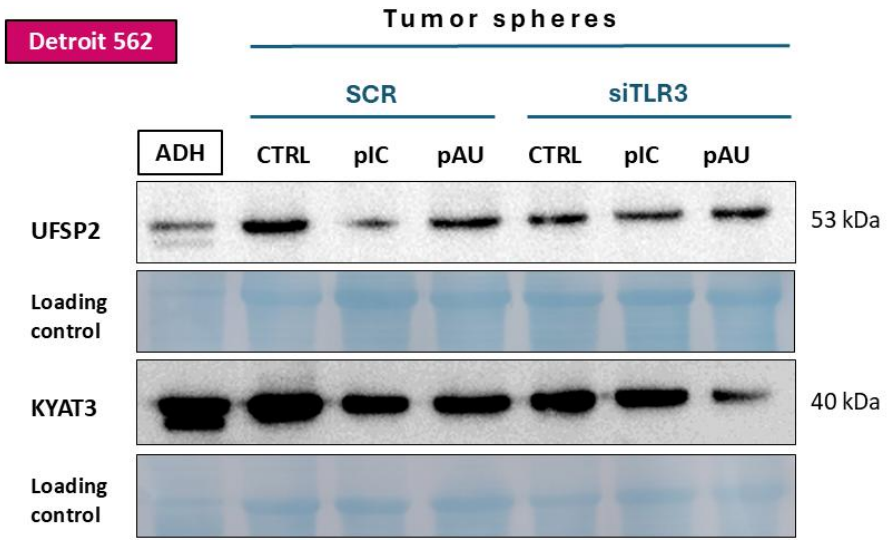

Figure 4.26. The Western blot of UFSP2 and KYAT3 in Detroit 562 cells transfected with control siRNA (SCR) or TLR3 siRNA, treated with poly(I:C) or poly(A:U). ADH = adherent untreated cells, CTRL = untreated tumor spheres, and pIC/pAU = poly(I:C)/poly(A:U), which were used in a concentration of 10 µg/mL. The loading controls were membranes stained with naphthol blue.

4.4.5. The effect of TLR3 silencing on tumor sphere morphology and UFSP2/KYAT3 expression in FaDu and SQ20B cells

Using another method to verify whether TLR3 is involved in the observed changes in UFSP2 and KYAT3 protein expression, FaDu and SQ20B cell lines that are stably transfected with a plasmid pTRIPZ carrying shRNA targeting TLR3 in an inducible manner were used based on doxycycline-inducible silencing of TLR3 expression.

FaDu shCTRL and FaDu shTLR3 tumor spheres had similar morphology (Figure 4.27). However, SQ20B shTLR3 tumor spheres showed changed morphology compared to the SQ20B (shCTRL). Tumor spheres were smaller in size, and spheres were more dissociated (Figure 4.28). This indicates that TLR3 expression is necessary for the sphere formation in SQ20B cells, and that with the loss of TLR3, these cells lose their ability to form spheres and eventually die. Morphology was changed when TLR3 is silenced, and tumor spheres are dissociated in all three conditions (Figure 4.28).

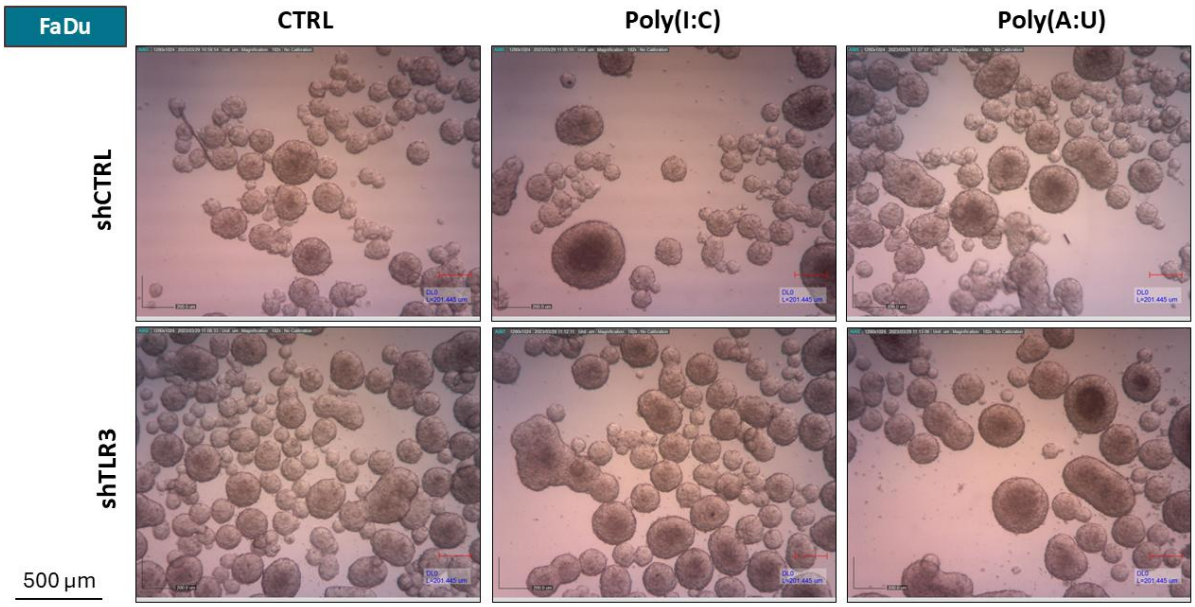

Figure 4.27. Photomicrographs of tumor spheres derived from FaDu cells. Tumor spheres were produced from FaDu cells stably transfected with plasmid pTRIPZ carrying shRNA targeting TLR3 (shTLR3) or FaDu cells stably transfected with the control plasmid (shCTRL), treated with 10 µg/mL poly(I:C) or poly(A:U), and doxycycline. CTRL = untreated tumor spheres. Magnification 2.5X times 72,5 for a digital camera objective.

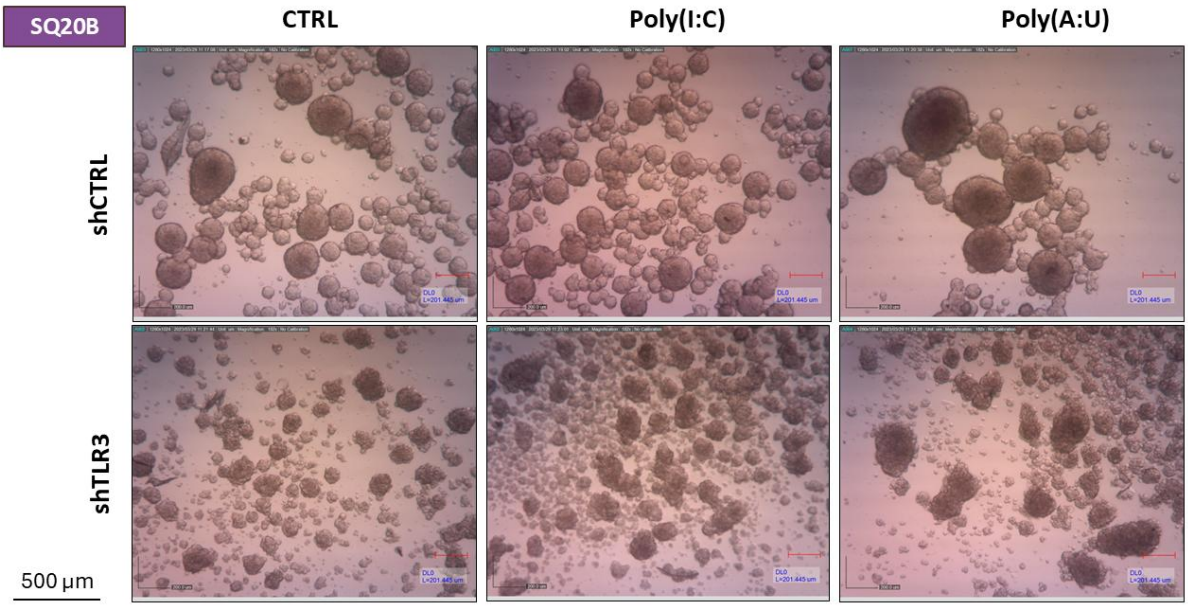

Figure 4.28. Photomicrographs of tumor spheres derived from SQ20B cells. Tumor spheres were produced from FaDu cells stably transfected with plasmid pTRIPZ carrying shRNA targeting TLR3 (shTLR3) or FaDu cells stably transfected with the control plasmid (shCTRL), treated with 10 µg/mL poly(I:C) or poly(A:U), and doxycycline. CTRL = untreated tumor spheres. Magnification 2.5X times 72,5 for a digital camera objective.

The role of TLR3 was confirmed in FaDu cells by demonstrating UFSP2 expression similar to that in Detroit 562 cells. The expression of UFSP2 was reduced after the stimulation of TLR3 with poly(A:U) in tumor spheres in cells transfected with the shCTRL plasmid. On the other hand, when TLR3 was silenced, there was no difference in UFSP2 expression between unstimulated and TLR3-induced cells, so the decrease in expression was abrogated. In SQ20B cells, UFSP2 expression remained the same across tumor spheres in cells transfected with the shCTRL plasmid. In spheres transfected with shTLR3 plasmid, UFSP2 expression was reduced after the treatment with poly(I:C) and poly(A:U) when compared to untreated tumor spheres (Figure 4.29).

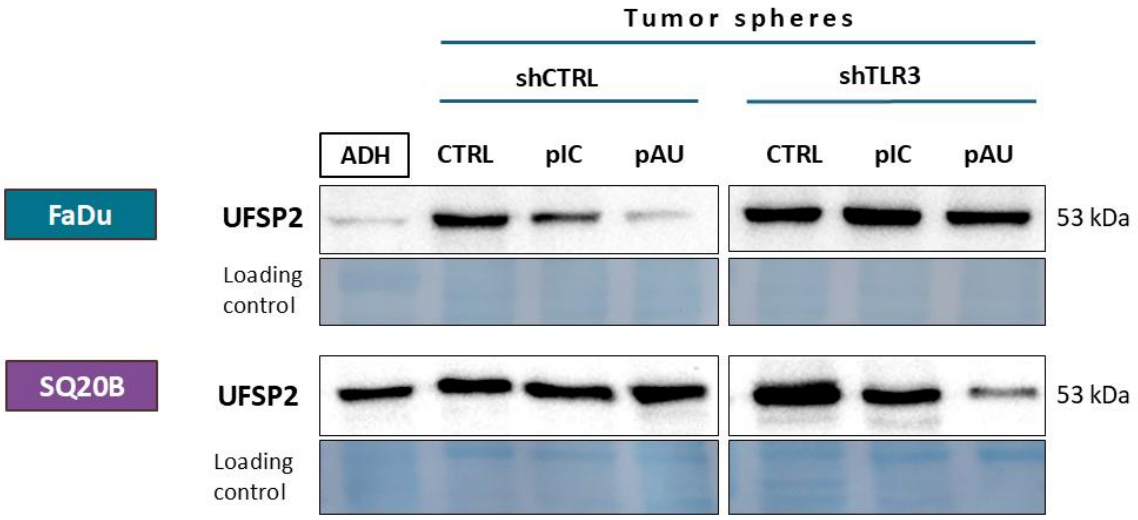

Figure 4.29. Expression of the UFSP2 protein in FaDu (shCTRL and shTLR3) and SQ20B (shCTRL and shTLR3) cells. shCTRL- cells transfected with a control plasmid, shTLR3- cells transfected with a plasmid containing shTLR3, leading to inducible silencing of TLR3 with the addition of doxycycline. ADH = adherent untreated cells, CTRL = untreated tumor spheres, pIC/pAU = poly(I:C)/poly(A:U), which were used in a concentration of 10 µg/mL. The loading controls were membranes stained with naphthol blue.

The role of TLR3 was also confirmed in FaDu cells by demonstrating KYAT3 expression similar to that in Detroit 562 cells. The expression of KYAT3 was reduced after the stimulation of TLR3 with poly(A:U) in tumor spheres in cells transfected with the shCTRL plasmid. On the other hand, when TLR3 is silenced, there is a minimal difference in KYAT3 expression between unstimulated and TLR3-induced cells, so the decrease in expression following poly(I:C)/poly(A:U) treatment is abrogated. In SQ20B cells, KYAT3 expression was reduced in shCTRL control tumor spheres and shCTRL tumor spheres treated with poly(I:C), but its expression increased in tumor spheres transfected with shCTRL plasmid treated with poly(A:U). In spheres transfected with the shTLR3 plasmid, KYAT3 expression remained the same in all samples (Figure 4.30).

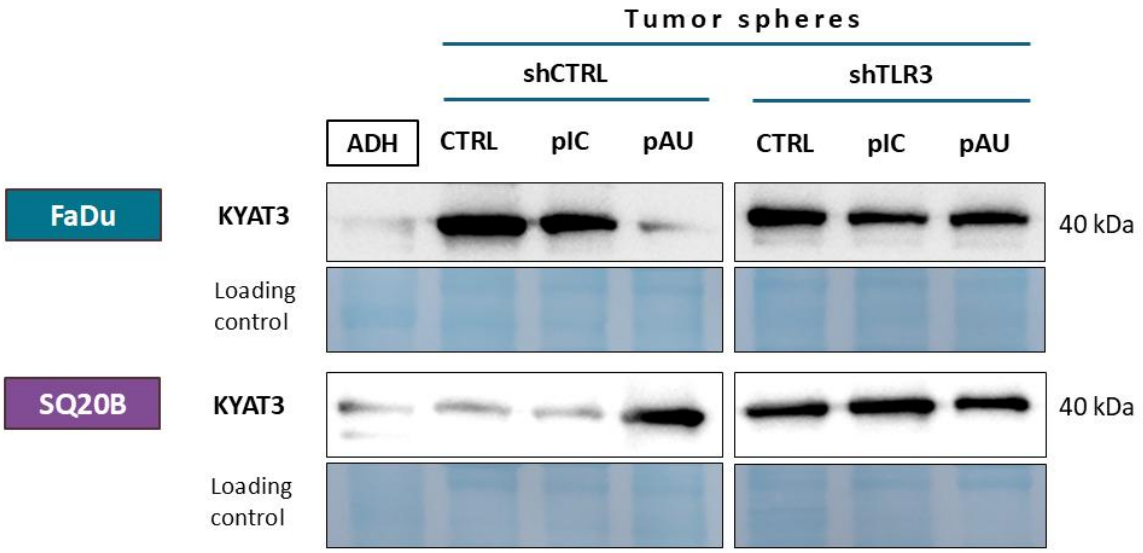

Figure 4.30. Expression of the KYAT3 protein in FaDu (shControl and shTLR3) and SQ20B (shCTRL and shTLR3) cells. shCTRL- cells transfected with a control plasmid, shTLR3- cells transfected with a plasmid containing shTLR3, leading to inducible silencing of TLR3 with the addition of doxycycline. ADH = adherent untreated cells, CTRL = untreated tumor spheres, pIC/pAU = poly(I:C)/poly(A:U), which were used in a concentration of 10 µg/mL. The loading controls were membranes stained with naphthol blue.

5. DISCUSSION

Here we investigated the role of TLR3 in promoting and maintaining CSC characteristics in HNSCC *in vitro*. Our initial aim was to determine whether TLR3 contributes to CSC maintenance, as previously demonstrated in breast cancer (Jia et al., 2015). Our results reveal that in HNSCC cell lines Detroit 562, FaDu, and SQ20B, TLR3 stimulation enhances tumor sphere formation and increases the size of tumor spheres. TLR3 activation affected their size, with particularly notable effects observed in the Detroit 562 cell line. The observed ability of HNSCC tumor cells to form tumor spheres is consistent with previous findings that indicate TLR3 activation promotes CSC formation in breast cancer. Specifically, Jia et al. (2015) demonstrated in breast cancer that the simultaneous activation of the NF-κB and β-catenin signaling pathways is necessary in acquiring the CSC phenotype. However, our study is the only study focusing on the role of TLR3 in HNSCC cancer stem cells, which indicates the novelty of this research. Our findings suggest that Detroit 562 cells under optimized culture conditions can robustly form tumor spheres even without the TLR3 activation, emphasizing their inherent CSC-like potential. The fact that TLR3 stimulation enhances the CSC phenotype supports the hypothesis on the role of TLR3 signaling in the promotion of head and neck cancers. This finding aligns with earlier research by Pries et al. (2008), who demonstrated that TLR3 activation contributes to the proliferation of HNSCC by activating the NF-κB and c-Myc proto-oncogene. The authors have also found that TLR3 is expressed only in cancer cells but not in the adjacent normal tissue. Our results demonstrated enhanced stemness properties, as evidenced by the increased number and size of tumor spheres, as well as the expression of HNSCC CSC stemness markers, including CD133 and ALDH1A1. These markers are associated with enhanced invasiveness, high tumorigenicity, and metastasis in HNSCC (Chiou et al., 2008; Chen et al., 2009). According to Rydberg et al. (2009), TLR3 activation with poly(I:C) in Detroit 562 leads to the activation of the NF-κB pathway, which can increase the expression of pro-inflammatory cytokines, such as Interleukins IL-1β, IL-6, IL-8, and Intercellular adhesion molecule 1 (ICAM-1). This enhances the ability of tumor cells to migrate while paradoxically reducing overall cell viability. Matijevic et al. (2009) further demonstrated that while TLR3 is expressed in several HNSCC primary and metastatic cell lines, it is only functional in Detroit 562, as IL-6 is secreted following treatment with poly(I:C). Salaun et al. (2006) showed that poly(I:C)-mediated TLR3 activation induces apoptosis in cancer cells. These data suggest a dual function of the TLR3 agonists in HNSCCs – acting as both, immune

stimulators and tumor promoters, but also as apoptosis inducers. We conclude here, based on the available literature and our first results, that the Detroit 562 cell line is a suitable model for investigating the role of TLR3 in HNSCC, with special emphasis on CSCs. For this reason, the Detroit 562 cell line was selected as the primary research model for investigating role of TLR3 in HNSCC, and the validation of FaDu and SQ20B cell lines was done only to confirm results in certain experiments.

We also hypothesized that tumor cells undergoing necrotic death due to hypoxia, chemotherapy, or irradiation therapy could release endogenous ligands (DAMPs) into the TME, which could activate TLR3. These DAMPs could support the formation and maintenance of CSCs or even boost their stemness properties. Previous studies have shown that TLR3 can be activated by DAMPs, such as variants of cellular mRNA originating from necrotic cells (Karikó et al., 2004). Once released, DAMPs could bind to various receptors and trigger signaling pathways that lead to cancer progression and metastasis. However, we also wanted to establish whether TLR3 activation alone can also induce the formation of DAMPs. We have shown here that TLR3 activation induced strong expression of DAMPs in tumor spheres and adherent cells. Among the DAMPs identified, S100 calcium-binding protein A9 (S100A9), high-mobility group box 1 (HMGB1), heat shock protein 70 (HSP70), and their receptor for advanced glycation end products (RAGE) were upregulated following TLR3 activation in tumor spheres. S100A9 is frequently overexpressed in many cancers, including breast cancer, prostate cancer, colon cancer, and melanoma. Its elevated expression is associated with poor prognosis and is implicated in the promotion of immune evasion and metastasis (Bresnick et al., 2015). In the context of HNSCC, S100A9 inhibition suppresses the growth and invasive behavior of cancer cells by blocking the signaling of NF-κB (Wu et al., 2017). HMGB1 and RAGE are closely linked to tumorigenesis and metastasis. HMGB1 suppresses the anti-tumor immune response, promotes invasion, and plays a role in resistance to anti-cancer therapy (Zapletal et al., 2023). RAGE is a receptor for several endogenous ligands released from damaged tissues, including HMGB1, and its activation is associated with inflammation and cancer progression (Cross et al., 2024). HSP70, a stress-inducible chaperone, has various roles in cancer; it can promote angiogenesis, suppress apoptosis, and enhance metastasis (Albakova et al., 2020). Interestingly, a study by Tavassol et al. (2011) reported that the lower HSP70 expression in patients with oral cancer correlated with poorer survival rates. A study from 2016 by Liu et al. demonstrated that tumor exosomal RNAs originating from primary lung cancer support the creation of the pre-metastatic microenvironment. These RNAs can activate TLR3 in lung epithelial cells and induce chemokine release and neutrophil activation, which predicts poor prognosis. Similarly,

our previous study (Vasiljevic et al., 2023) also reported that TLR3 can be activated without external stimuli such as viral RNA, but with only endogenous cellular RNAs, indicating that the TME is sufficient. TLR3 endogenous ligands were found in necrotic tumor fluids from both mice and patients, but also in HNSCC cell line supernatants after exposing cells to different stressors, including hypoxia, serum starvation, irradiation, and oxidative stress. Additionally, exosomes isolated from HNSCC supernatants of irradiated cells contained endogenous ligands for TLR3. Supernatants and necrotic fluids were used to treat HEKBlue-TLR3 reporter cells to determine TLR3 activation. This suggests that endogenous agonists of TLR3, composed of dsRNA fragments, may already be present in HNSCC necrotic fluids. These endogenous ligands may bind to TLR3 and potentially promote tumor progression.

Since TLR activation causes DAMP release, we explore here the potential of DAMP inhibitors as therapeutic agents in cancer treatment. Regulating DAMP release can reduce inflammation and regulate tumor metastasis (Jang et al., 2020). Our extensive literature search revealed certain drugs that can act as DAMP inhibitors. They are already being used as pharmacological agents in treating other diseases or as dietary supplements. Our main premise was to use old drugs that could be repurposed to treat cancer, especially for the effective targeting of CSCs. The advantage of these pharmacological agents is that they have already gone through preclinical and clinical studies and are approved for use in patient treatment. Therapeutic use of DAMP inhibitors can potentially decrease cancer cell survival, stemness, and chemoresistance. DAMP inhibitors we have explored here include kahweol (HSP70 inhibitor) (Choi et al., 2015), metformin (RAGE inhibitor) (Ishibashi et al., 2012), paquinimod (S100A8/A9 inhibitor) (Miura et al., 2024), and aspirin (acetylsalicylic acid) as an HMGB1 inhibitor (Huang et al., 2015). In our study, migration and viability of tumor spheres were inhibited when aspirin or metformin were combined with TLR3 ligand poly(I:C). The results on adherent cells indicate that treatment with aspirin and metformin alone can inhibit the growth of Detroit 562 tumor cells, which is further reduced with the addition of poly(I:C). Additionally, the survival of tumor cells was reduced by more than 50% when DAMP inhibitors were combined with poly(I:C). The strongest overall effect was observed in treatment with poly(I:C) combined with aspirin in both adherent cells and tumor spheres. In HNSCC, TLR3 activation may trigger cell death or contribute to tumor progression. Previous work by Matijevic & Pavelic (2011) showed that stimulation of TLR3 induces cell migration of the Detroit 562 cells. Based on that, we investigated whether CSC-derived DAMPs may increase tumor cell motility. Our data show that the stimulation of the TLR3 receptor with poly(I:C) in tumor spheres and subsequent treatment of adherent cells with this conditioned medium promotes tumor cell

migration, suggesting that poly(I:C) treatment of tumor spheres induces the secretion of factors that induce cell motility. Moreover, even untreated tumor spheres released some factors into the supernatant that increased cell migration. The migration of tumor cells was inhibited when aspirin or metformin was applied to tumor spheres. These findings imply that DAMPs released from CSCs play a role in promoting HNSCC tumor cell migration, suggesting their potential involvement in cancer progression. We propose that TLR3 stimulation in CSC induces DAMP release, such as S100A9, HMGB1, HSP70, or others, which have not been explored here. They further interact with receptors like TLR2, TLR4, or RAGE on neighboring cells, setting off paracrine signals that promote the migration of surrounding tumor cells. Therefore, targeting DAMPs may provide a strategy to suppress the migration of cancer cells in HNSCC. In the context of invasion, the inhibition of DAMPs did not significantly impact the invasive capacity of tumor cells. This indicates that while DAMPs may be important for the migration of tumor cells, invasion may be induced by other mechanisms. While migration requires cell movement, invasion also involves ECM degradation. It is usually managed by the matrix metalloproteinases (MMPs) and other proteases (Friedl & Alexander, 2011). Those pathways may not be influenced by DAMPs, and further research is necessary to elucidate this. Overall, the treatment with aspirin consistently demonstrated the most pronounced effects, not only in reducing the viability of tumor spheres, but also in inhibiting migration and downregulation of stemness and drug resistance markers (*OCT4* and *ABCG2)*. These results suggest that aspirin, especially in combination with poly(I:C), which activates TLR3 and is a known apoptosis inducer, holds promise as a potential cancer therapy targeting CSCs. Moreover, given its low cost and proven safety profile, it really could be a good strategy for targeting HNSCC CSCs. Future research should be conducted to investigate *in vivo* effects.

One of the main characteristics of CSCs is resistance to therapy. It contributes to treatment failure and consequently tumor relapse. Radiation therapy, often coupled with surgery and/or chemotherapy, represents a primary approach in cancer treatment. Conventional treatments like γ-rays and X-rays lack precision, and tumor cells (including CSCs) may acquire radio resistance. In this study, we investigated a new potential anticancer therapy by combining TLR3 activation with irradiation and treatment with DAMP inhibitors, aiming to exploit TLR3 pro-apoptotic properties while inhibiting its tumor-promoting properties (DAMPs). For that reason, we explored the potential of novel HNSCC therapy using two types of radiation, γ-rays and proton beam, combined with pharmacological inhibitors of DAMPs and poly(I:C). Our data demonstrated that combined treatment with γ-irradiation targets adherent Detroit 562 tumor cells effectively. The most efficient results were obtained with the treatment including the lower

dose of aspirin (100 μM) or metformin, which completely abolished the survival of adherent tumor cells. These results suggest a radiosensitizing effect on adherent tumor cells and confirm the potential of this combined treatment as a prospective therapy for HNSCC. However, γ-irradiation of tumor spheres was not effective, which was further confirmed by the lack of reduction in expression of *OCT4* and *ABCG2*, where γ-radiation did not further diminish gene expression in comparison to aspirin and aspirin combined with poly(I:C). We have observed only a slight reduction in tumor sphere viability and limited morphology changes of tumor spheres treated with aspirin in combination with poly(I:C) with γ-irradiation. These findings suggest that tumor spheres may have activated intrinsic mechanisms to induce radioresistance through the activation of DNA repair (Schulz et al., 2019) or anti-apoptotic pathways induction. Overall, this combined treatment with γ-rays may be appropriate therapy for adherent tumor cells, but not tumor spheres, i.e., CSCs. Proton irradiation, however, in combination with poly(I:C) and aspirin, significantly reduced the survival of HNSCC CSCs. Not only was tumor sphere viability decreased, but also stemness and drug resistance genes were downregulated. Moreover, extensive PARP cleavage confirms apoptosis as the mechanism of cell death. The combination of aspirin and proton irradiation successfully eliminated cancer stem cells. Consequently, this irradiation method demonstrates a better potential treatment option compared to γ-irradiation, since a lower dose is necessary to obtain more effective treatment. Proton therapy generally offers more benefits due to the unique physical properties of the Bragg peak. This means protons can precisely target the tumor, depositing most of their energy directly within the cancerous tissue and sparing surrounding healthy tissue (Bragg & Kleeman, 1904). While research on proton therapy in HNSCC treatment is expanding, this is the first study where the combined treatment of TLR3 activation and DAMP inhibitors with proton irradiation was applied.

The role of aspirin in cancer treatment has been investigated for a few decades now. Long-term research has demonstrated that consistent aspirin intake can lower the risk of cancer development, metastasis and can improve overall survival, particularly in colorectal cancer. Additionally, aspirin is being investigated for its potential to suppress tumor proliferation, inflammation, and metastasis in various cancer types. Its anti-tumorigenic properties are based on COX-2 inhibition, but it can also inhibit pro-survival pathways β-catenin/TCF, NF-κB, Wnt, and IL-6/STAT3 (Laila et al., 2025). Aspirin's anti-tumorigenic properties are highly supported by recent research. Besides colorectal cancer, aspirin has tumor suppressive effects in breast cancer, where aspirin intake was associated with better prognosis, decreased metastasis (Holmes et al., 2010), but also with inhibitory effects on tumor angiogenesis, invasion, and

migration through reverting of EMT (Rezania et al., 2022). In breast cancer, aspirin enhances TRAIL-induced cell death and reduces survivin (Lu et al., 2008). Meta-analysis shows that the use of aspirin may have a positive effect on hepatocellular carcinoma outcomes over the years (Memel et al., 2021). Zou et al. (2021) demonstrated in esophageal cancer that aspirin improves the therapeutic effects of chemotherapy through targeting CSCs. Zhang et al. (2024) suggested a potential role of aspirin in pancreatic cancer via CSC markers inhibition. In addition to that, Deng et al. (2013) showed that celecoxib, a selective COX-2 NSAID, inhibits CD133 expression in CSCs through targeting and downregulating the Wnt signaling cascade in colon cancer. Aspirin inhibits HMGB1, which was shown to trigger epithelial-mesenchymal transition (Chen et al., 2016), a key process in CSC formation and maintenance. The inhibition of HMGB1 could abolish this process. Some research suggests that HMGB1 inhibition leads to elevated apoptosis of breast cancer (Ni et al., 2015), bladder urothelial carcinoma (Huang et al., 2015), renal cell carcinoma (Wu et al., 2018), and multiple myeloma (Guo et al., 2018)(Guo et al., 2018) cells. Wen et al. (2023) showed that the inhibition of HMGB1 in HNSCC suppresses cancer cell proliferation, invasion, and migration. Another study showed that HMGB1 can promote radioresistance in breast (Jiao et al., 2007) and in esophageal cancer (Ma et al., 2019); therefore, its inhibition could increase irradiation response. This combined approach might improve HNSCC therapy by targeting CSCs more effectively, resulting in better patient outcomes by reducing tumor recurrence. This approach for targeting CSC directly addresses the main treatment difficulties: radioresistance, chemoresistance, and immune evasion. Future studies should investigate the exact mechanisms of this combined treatment to discover the exact pathways that are involved.

In the last part of this thesis, we aimed to identify potential novel biomarkers for HNSCC by proteomic analysis of Detroit 562 tumor spheres. Proteomic analysis revealed different proteins that exhibited significantly altered expression in tumor spheres compared to adherent cells, but also in TLR3-activated tumor spheres compared to the untreated tumor spheres (Derfi et al., 2024). Upon TLR3 activation, several potential novel biomarkers were uncovered that might play an important role in HNSCC CSCs. Among them was STARD10, whose elevated expression is associated with increased malignancy and poor prognosis in alcohol-induced breast cancer (Floris et al., 2019). Another protein was gasdermin, known for its dual role; it is involved in pyroptosis but also plays a role in chronic inflammation, leading to tumor progression (Gao et al., 2024). The upregulation of these proteins may play a role in pro-tumorigenic properties in HNSCC. Downregulated after TLR3 stimulation were the following proteins: NUP62, which plays a role in the growth and progression of squamous cell carcinomas

(Hazawa et al., 2018), GSTT1, involved in tumor metastasis and dissemination, but is not necessary for primary tumor development (Ferrer et al., 2024). GRWD1, whose overexpression in some cancers is linked with poor prognosis (Zhou et al., 2021), and in HNSCC, it demonstrated altered expression compared to healthy tissues, indicating its potential role as a diagnostic biomarker (Gill et al., 2024). Next, UCHL5, which regulates apoptosis and cell proliferation in cancer, and it plays a role in the proliferation and survival of HNSCC (Morgan et al., 2023); and Syntenin, which facilitates the invasion and progression of HNSCC (Cui et al., 2016). The above-mentioned proteins need to be further evaluated in order to determine whether they have a role in CSCs.

Among the detected proteins, UFSP2 and KYAT3 were overexpressed in tumor spheres compared to the adherent cells. The expression of UFSP2 and KYAT3 was reduced after TLR3 activation in Detroit 562 spheres. The results were confirmed in HNSCC Detroit 562 cells following transient transfection with TLR3 siRNA and in FaDu cells containing a plasmid with inducible shTLR3, but not in SQ20B containing a plasmid with inducible shTLR3. However, for SQ20B cell line we observed that the TLR3 expression in necessary for tumor spheres formation, and that with the loss of TLR3, these cells lose their ability to form spheres and eventually die. We selected UFSP2 for further investigation due to its central role in the UFMylation process, a post-translational modification similar to ubiquitination. In the UFMylation process, UFSP2, together with UFSP1, plays a dual role. It is critical for the activation process of the UFM1 protein (by cleaving its precursor form), which performs a similar function to ubiquitin by binding to target proteins. It can also detach UFM1 from the target substrate. The UFMylation pathway remains poorly understood, despite it being discovered 20 years ago, and this is particularly true in tumors, where there are only a few studies. UFMylation remains largely unexplored in CSC, with our study being the only one published on this topic (Derfi et al., 2024). Therefore, our research focused on revealing the significance of these preliminary findings and exploring the role of UFSP2 in HNSCC CSC. This work was not included in this thesis, but will be discussed here as it was recently published by this group.

In our recent publication (Derfi et al., 2024), we investigated the role of UFMylation in HNSCC CSCs. The results from proteomic analysis showed different expressions of DDRGK1 and UFSP2 proteins, involved in UFMylation. These results were confirmed with western blot analysis, which showed us that the expression of these proteins is increased in tumor spheres compared to the adherent cells. Bioinformatic analysis from GEPIA, an online platform that extracts data from The Cancer Genome Atlas and from the GTEx repository of normal tissue,

showed overexpression of UFM1 in head and neck cancer when compared to normal tissue, which was confirmed with immunocytochemistry. UFM1 overexpression was linked to poor disease prognosis. UFM1 silencing resulted in a lower number of tumor spheres and reduced stemness, indicating its possible role in maintaining CSC characteristics. Bioinformatic analysis also showed that increased UMF1 expression correlates with increased expression of EMT genes TWIST1, ZEB1, and FN1, which are associated with unfavorable prognosis in patients. Bioinformatic analysis also showed Sp1 as the main transcription factor that controls UFMylation pathway protein expression. The inhibition of CSC could be accomplished by introducing Mithramycin, which targets Sp1. The effect of Mithramycin was confirmed in Detroit 562, Cal27, and FaDu HNSCC cell lines, where it reduced the survival of tumor spheres. Besides the reduced expression of key UFMylation genes, it also reduced the expression of stemness genes *ABCG2*, *OCT4*, and *CD133*. Mithramycin also reduced the expression of *RPL26*, a known UFMylation substrate. PARP cleavage after mithramycin treatment indicated that the cells died of apoptosis. This inhibition can reduce stemness, the survival of tumor spheres, and trigger apoptosis, but also reduce the UFMylation process.

Supporting this, Wang et al. (2023) have demonstrated that UFMylation is present in pancreatic adenocarcinoma, both in pancreatic cancer cell lines and patient' tumor samples. Liu et al. (2020) showed that p53 is a UFMylation target and that its UFMylation stabilizes it by antagonizing its ubiquination and degradation. UFMylation proteins DDRGK1 and UFL1 are downregulated in renal cancer, which correlates with low stability of p53 and increased tumor progression and tumor formation. This demonstrates that the role of UFMylation in cancer depends on the context and type of cancer, and it needs to be further studied in order to be clarified. In pancreatic adenocarcinoma, the UFMylation effect is stronger in tumors compared to the surrounding tissue (Wang et al., 2023). This leads to upregulated proliferation of tumor cells. In the same study, they showed that UFSP2 overexpression disrupts the UFMylation of ribosomal protein L10 (RPL10), a substrate of UFMylation. This leads to suppressed cell proliferation and decreased clonogenic potential, but it also results in reduced size of tumor spheres and decreased expression of stemness-associated markers. While Lin et al. (2022) showed that reduced expression of UFM1 and CDK5RAP3 (CDK5 regulatory subunit-associated protein 3) is linked with poor prognosis in patients with gastric cancer, Hu et al. (2021) showed that in gastric cancer, UFM1-binding protein 1 (UFBP1, also known as DDRGK1) enhances the responsiveness of tumor cells to cisplatin through the facilitation of the proteasomal degradation of Nrf2, a key transcription factor that is involved in the oxidative stress response. Kumari et al. (2022) showed that the overexpression of the UBA5 enzyme in

HeLa cells has the same effect as UBA5 deletion. The precise control of UFMylation is essential for healthy cells, as dysregulation can lead directly to disease.

In our study, TLR3 activation enhanced the formation of tumor spheres with increased CSC properties, while UFSP2 expression was downregulated after TLR3 activation. Based on its role in UFMylation, the downregulation of UFSP2 can lead to reduced UFMylation due to its role in the maturation of UFM1, or it can cause a cellular buildup of the UFMylated proteins, potentially causing disrupted homeostasis due to protein dysfunction, cellular stress, and ultimately leading to various pathological conditions.

Zhou et al. (2023) showed that programmed cell death ligand 1 (PD-L1) binds to UFM1 and interacts with UFSP2 and with other proteins within the UFMylation system. They also observed that UFSP2 can remove the UFM1 from PD-L1 and act as the de-UFMylating PD-L1 enzyme. This further supports the importance of UFSP2 in the immunity regulation.

In the same study, they found that compound-8, a covalent inhibitor of UFSP2, could play a role in UFMylation of the PD-L1, which destabilizes the protein and results in downregulated PD-L1 and tumor suppression. This indicates that UFSP2 inhibitors could be a promising option for cancer treatment. In our study, the activation of TLR3 did exactly that; we demonstrated reduced expression of UFSP2 in tumor spheres. To our knowledge, this is the first research demonstrating reduced UFSP2 in CSC following TLR3 activation in HNSCC. However, more research needs to be conducted to draw more specific conclusions.

Another protein of interest that we studied in several HNSCC cell lines is KYAT3. In literature, KYAT3 can also be found as KAT3, glutamine transaminase L (GTL), or cysteine conjugate beta-lyase 2 (CCBL2) (Yang et al., 2016). We chose KYAT3 due to its involvement in the tryptophan metabolism from kynurenine to kynurenic acid, and in recent studies, tryptophan metabolism has been identified as a potential target for cancer treatment. There is no knowledge about the role of KYAT3 in CSCs. However, the role of KYAT3 in different cancers has been investigated, but they are limited. Its expression in breast cancer was found to be downregulated and indicating an overall poor prognosis (Meng et al., 2022). In HNSCC, a study from 2020 (Riess et al.) showed that Dinaciclib, a cyclin-dependent kinase inhibitor, can downregulate the kynurenine pathway, but the effect on survival has not been studied. It has been shown in other studies that dinaciclib exhibits a cytotoxic effect in different cancers, including cholangiocarcinoma (Saqub et al., 2020; Ablinger et al., 2024) and oral squamous cell carcinoma (Oner et al., 2025).

In recent studies, targeting tryptophan metabolism has been proposed as a potential new strategy for cancer treatment (Platten et al., 2019; Yan et al., 2024). A study from Tankiewicz et al.

(2006) showed an increase in tryptophan metabolites in oral squamous cell carcinoma. Alterations in the kynurenine pathway have been associated with poor outcomes in some cancers, which might contribute to immune system evasion (Hornigold et al., 2020). Increased indolamine 2,3-dioxygenase (IDO), which is activated through the transforming growth factor–beta–Smad 3 (TGF-β-Smad-3) signaling pathway, is one of the key enzymes of the tryptophan/kynurenine pathway, causing a drop in tryptophan levels and a buildup of kynurenine within the tumor microenvironment. This leads to immunosuppressive settings where T cells are unresponsive, and their differentiation is inhibited; therefore, kynurenine could potentially promote tumor growth (León-Letelier et al., 2023; Schlichtner et al., 2023). Schlichtner et al. (2023) also demonstrated that L-kynurenine suppresses the function of T cells, thereby facilitating immune evasion. In primary breast cancer, L-Kynurenine level was normal, but in metastatic breast cancer, it was significantly elevated. One of the DAMPs that Schlichtner et al. (2023) studied was HMGB1. They demonstrated a positive correlation between HMGB1 secretion and upregulation of L-Kynurenine levels and, consequently, suppression of cytotoxic T lymphocytes. Taken together, since aspirin inhibits HMGB1, the immunosuppressive role of L-Kynurenine in metastatic cancers may potentially be inhibited with aspirin, but this should be further verified. Recognizing promising new CSC biomarkers is essential; it not only advances our knowledge of cancer stem cells but also guides the quest for innovative therapies.

6. CONCLUSION

Since in HNSCC the development of distant metastasis, therapy resistance, and late diagnosis is often observed, there is a high demand for the development of new treatments and new therapeutic approaches.

- In this study, we demonstrated that TLR3 activation supports tumor sphere formation and maintenance. TLR3 activation induced the formation of increased number of larger tumor spheres.
- TLR3 stimulation induced the expression of DAMPs (S100A9, HMBG1, and HSP70) in Detroit 562 tumor spheres.
- Release of DAMPs into the microenvironment by CSC promotes the migration of surrounding tumor cells. This pro-tumorigenic effect can be mitigated using specific DAMP inhibitors, especially aspirin and metformin.
- The combined treatment approach with irradiation, DAMP inhibitors, and poly(I:C) might improve HNSCC therapy. Adherent tumor cells were responsive to treatment with aspirin and potentially metformin combined with poly(I:C) and γ-irradiation. Tumor spheres were responsive to treatment with aspirin combined with poly(I:C), and proton irradiation.
- Using proteomic analysis, we identified UFSP2 and KYAT3 as potential novel biomarkers for CSCs. The identification of potential novel CSC biomarkers contributes to a deeper understanding of CSC, with potential for the development of novel therapy targeting specifically CSCs and eradicating the CSC populations.

7. BIBLIOGRAPHY

Ablinger, C., Neureiter, D., Mähr, T., Mayr, C., Kiesslich, T., Maeding, N., Valenta, I., Ardelt, M., Wilhelm, F., Neureiter, E., Ritter, M., Pachmayr, J. & Huber-Cantonati, P. (2024) The Cdk inhibitor dinaciclib as a promising anti-tumorigenic agent in biliary tract cancer. *Cancer Biology & Therapy*, 25 (1).

Agrawal, N., Dasaradhi, P.V.N., Mohmmed, A., Malhotra, P., Bhatnagar, R.K. & Mukherjee, S.K. (2003) RNA Interference: Biology, Mechanism, and Applications. *Microbiology and Molecular Biology Reviews*, 67 (4), pp.657–685.

Albakova, Z., Armeev, G.A., Kanevskiy, L.M., Kovalenko, E.I. & Sapozhnikov, A.M. (2020) HSP70 Multi-Functionality in Cancer. *Cells*, 9 (3), p.587.

Alexopoulou, L., Holt, A.C., Medzhitov, R. & Flavell, R.A. (2001) Recognition of double-stranded RNA and activation of NF-κB by Toll-like receptor 3. *Nature*, 413, pp.732–738.

Alshaer, W., Zureigat, H., Al Karaki, A., Al-Kadash, A., Gharaibeh, L., Hatmal, M.M., Aljabali, A.A.A. & Awidi, A. (2021) siRNA: Mechanism of action, challenges, and therapeutic approaches. *European Journal of Pharmacology*, 905, p.174178.

Ang, H.L., Mohan, C.D., Shanmugam, M.K., Leong, H.C., Makvandi, P., Rangappa, K.S., Bishayee, A., Kumar, A.P. & Sethi, G. (2023) Mechanism of epithelial-mesenchymal transition in cancer and its regulation by natural compounds. *Medicinal Research Reviews*, 43 (4), pp.1141–1200.

Ang, K.K., Harris, J., Wheeler, R., Weber, R., Rosenthal, D.I., Nguyen-Tân, P.F., Westra, W.H., Chung, C.H., Jordan, R.C., Lu, C., Kim, H., Axelrod, R., Silverman, C.C., Redmond, K.P. & Gillison, M.L. (2010) Human Papillomavirus and Survival of Patients with Oropharyngeal Cancer. *New England Journal of Medicine*, 363 (1), pp.24–35.

Argiris, A., Karamouzis, M. V, Raben, D. & Ferris, R.L. (2008) Head and neck cancer. *The Lancet*, 371 (9625), pp.1695–1709.

Badawy, A.A.-B. (2017) Kynurenine Pathway of Tryptophan Metabolism: Regulatory and Functional Aspects. *International journal of tryptophan research : IJTR*, 10, p.1178646917691938.

Barton, G.M. & Medzhitov, R. (2002) Toll-Like Receptors and Their Ligands. In: pp.81–92.

Batlle, E. & Clevers, H. (2017) Cancer stem cells revisited. *Nature Medicine*, 23 (10), pp.1124–1134.

Bell, J.K., Mullen, G.E.D., Leifer, C.A., Mazzoni, A., Davies, D.R. & Segal, D.M. (2003) Leucine-rich repeats and pathogen recognition in Toll-like receptors. *Trends in Immunology*, 24 (10), pp.528–533.

Bengtsson, A.A., Sturfelt, G., Lood, C., Rönnblom, L., van Vollenhoven, R.F., Axelsson, B., Sparre, B., Tuvesson, H., Öhman, M.W. & Leanderson, T. (2012) Pharmacokinetics, tolerability, and preliminary efficacy of paquinimod (ABR-215757), a new quinoline-3-carboxamide derivative: Studies in lupus-prone mice and a multicenter, randomized, double-blind, placebo-controlled, repeat-dose, dose-ranging study in patients with systemic lupus erythematosus. *Arthritis & Rheumatism*, 64 (5), pp.1579–1588.

Bonnet, D. & Dick, J.E. (1997) Human acute myeloid leukemia is organized as a hierarchy that originates from a primitive hematopoietic cell. *Nature Medicine*, 3 (7), pp.730–737.

Botos, I., Segal, D.M. & Davies, D.R. (2011) The Structural Biology of Toll-like Receptors. *Structure*, 19 (4), pp.447–459.

Bragg, W.H. & Kleeman, R. (1904) On the ionization curves of radium. *The London, Edinburgh, and Dublin Philosophical Magazine and Journal of Science*, 8 (48), pp.726–738.
Bresnick, A.R., Weber, D.J. & Zimmer, D.B. (2015) S100 proteins in cancer. *Nature Reviews Cancer*, 15 (2), pp.96–109.
Brinkmann, M.M., Spooner, E., Hoebe, K., Beutler, B., Ploegh, H.L. & Kim, Y.-M. (2007) The interaction between the ER membrane protein UNC93B and TLR3, 7, and 9 is crucial for TLR signaling. *The Journal of Cell Biology*, 177 (2), pp.265–275.
Brinston, R.M. & Norton, J.L. (1994) Cobalt-60: the heart of gamma-radiation sterilization. *Medical device technology*, 5, pp.14–16.
Brown, J., Wang, H., Hajishengallis, G.N. & Martin, M. (2011) TLR-signaling Networks. *Journal of Dental Research*, 90 (4), pp.417–427.
Bugge, M., Bergstrom, B., Eide, O.K., Solli, H., Kjønstad, I.F., Stenvik, J., Espevik, T. & Nilsen, N.J. (2017) Surface Toll-like receptor 3 expression in metastatic intestinal epithelial cells induces inflammatory cytokine production and promotes invasiveness. *Journal of Biological Chemistry*, 292 (37), pp.15408–15425.
Burusapat, C., Jarungroongruangchai, W. & Charoenpitakchai, M. (2015) Prognostic factors of cervical node status in head and neck squamous cell carcinoma. *World Journal of Surgical Oncology*, 13 (1), p.51.
Carballo, G.B., Honorato, J.R., de Lopes, G.P.F. & Spohr, T.C.L. de S. e (2018) A highlight on Sonic hedgehog pathway. *Cell Communication and Signaling*, 16 (1), p.11.
de Caro, A., Bellard, E., Kolosnjaj-Tabi, J., Golzio, M. & Rols, M.-P. (2023) Gene Electrotransfer Efficiency in 2D and 3D Cancer Cell Models Using Different Electroporation Protocols: A Comparative Study. *Pharmaceutics*, 15 (3), p.1004.
Cavassani, K.A., Ishii, M., Wen, H., Schaller, M.A., Lincoln, P.M., Lukacs, N.W., Hogaboam, C.M. & Kunkel, S.L. (2008) TLR3 is an endogenous sensor of tissue necrosis during acute inflammatory events. *The Journal of Experimental Medicine*, 205 (11), pp.2609–2621.
Chaffer, C.L., Marjanovic, N.D., Lee, T., Bell, G., Kleer, C.G., Reinhardt, F., D'Alessio, A.C., Young, R.A. & Weinberg, R.A. (2013) Poised Chromatin at the ZEB1 Promoter Enables Breast Cancer Cell Plasticity and Enhances Tumorigenicity. *Cell*, 154 (1), pp.61–74.
Chattopadhyay, S. & Sen, G.C. (2014) dsRNA-Activation of TLR3 and RLR Signaling: Gene Induction-Dependent and Independent Effects. *Journal of Interferon & Cytokine Research*, 34 (6), pp.427–436.
Chaturvedi, A. & Pierce, S.K. (2009) How location governs toll-like receptor signaling. *Traffic*, 10, pp.621–628.
Chen, D. & Wang, C.-Y. (2019) Targeting cancer stem cells in squamous cell carcinoma. *Precision Clinical Medicine*, 2 (3), pp.152–165.
Chen, W., Dong, J., Haiech, J., Kilhoffer, M.-C. & Zeniou, M. (2016) Cancer Stem Cell Quiescence and Plasticity as Major Challenges in Cancer Therapy. *Stem Cells International*, 2016 (1).
Chen, Y.-C., Chen, Y.-W., Hsu, H.-S., Tseng, L.-M., Huang, P.-I., Lu, K.-H., Chen, D.-T., Tai, L.-K., Yung, M.-C., Chang, S.-C., Ku, H.-H., Chiou, S.-H. & Lo, W.-L. (2009) Aldehyde dehydrogenase 1 is a putative marker for cancer stem cells in head and neck squamous cancer. *Biochemical and Biophysical Research Communications*, 385 (3), pp.307–313.
Chen, Y.-C., Statt, S., Wu, R., Chang, H.-T., Liao, J.-W., Wang, C.-N., Shyu, W.-C. & Lee, C.-C. (2016) High mobility group box 1-induced epithelial mesenchymal transition in human airway epithelial cells. *Scientific Reports*, 6 (1), p.18815.

Chen, Y.-S., Wu, M.-J., Huang, C.-Y., Lin, S.-C., Chuang, T.-H., Yu, C.-C. & Lo, J.-F. (2011) CD133/Src Axis Mediates Tumor Initiating Property and Epithelial-Mesenchymal Transition of Head and Neck Cancer. *PLoS ONE*, 6 (11), p.e28053.
Chien, M.-L., Lai, J.-H., Lin, T.-F., Yang, W.-S. & Juang, Y.-L. (2020) NUP62 is required for the maintenance of the spindle assembly checkpoint and chromosomal stability. *The International Journal of Biochemistry & Cell Biology*, 128, p.105843.
Chikamatsu, K., Ishii, H., Takahashi, G., Okamoto, A., Moriyama, M., Sakakura, K. & Masuyama, K. (2012) Resistance to apoptosis-inducing stimuli in CD44+ head and neck squamous cell carcinoma cells. *Head & Neck*, 34 (3), pp.336–343.
Chinn, S.B., Darr, O.A., Peters, R.D. & Prince, M.E. (2012) The role of head and neck squamous cell carcinoma cancer stem cells in tumorigenesis, metastasis, and treatment failure. *Frontiers in Endocrinology*, 3.
Chiou, S.-H., Yu, C.-C., Huang, C.-Y., Lin, S.-C., Liu, C.-J., Tsai, T.-H., Chou, S.-H., Chien, C.-S., Ku, H.-H. & Lo, J.-F. (2008) Positive Correlations of Oct-4 and Nanog in Oral Cancer Stem-Like Cells and High-Grade Oral Squamous Cell Carcinoma. *Clinical Cancer Research*, 14 (13), pp.4085–4095.
Choi, D.W., Lim, M.S., Lee, J.W., Chun, W., Lee, S.H., Nam, Y.H., Park, J.M., Choi, D.H., Kang, C.D., Lee, S.J. & Park, S.C. (2015) The Cytotoxicity of Kahweol in HT-29 Human Colorectal Cancer Cells Is Mediated by Apoptosis and Suppression of Heat Shock Protein 70 Expression. *Biomolecules & Therapeutics*, 23 (2), pp.128–133.
Chong, Z.X., Yeap, S.K. & Ho, W.Y. (2021) Transfection types, methods and strategies: a technical review. *PeerJ*, 9, p.e11165.
Chu, X., Tian, W., Ning, J., Xiao, G., Zhou, Y., Wang, Z., Zhai, Z., Tanzhu, G., Yang, J. & Zhou, R. (2024) Cancer stem cells: advances in knowledge and implications for cancer therapy. *Signal Transduction and Targeted Therapy*, 9.
Creighton, C.J., Li, X., Landis, M., Dixon, J.M., Neumeister, V.M., Sjolund, A., Rimm, D.L., Wong, H., Rodriguez, A., Herschkowitz, J.I., Fan, C., Zhang, X., He, X., Pavlick, A., Gutierrez, M.C., Renshaw, L., Larionov, A.A., Faratian, D., Hilsenbeck, S.G., Perou, C.M., Lewis, M.T., Rosen, J.M. & Chang, J.C. (2009) Residual breast cancers after conventional therapy display mesenchymal as well as tumor-initiating features. *Proceedings of the National Academy of Sciences*, 106 (33), pp.13820–13825.
Cross, K., Vetter, S.W., Alam, Y., Hasan, Md.Z., Nath, A.D. & Leclerc, E. (2024) Role of the Receptor for Advanced Glycation End Products (RAGE) and Its Ligands in Inflammatory Responses. *Biomolecules*, 14 (12), p.1550.
Cui, L., Cheng, S., Liu, X., Messadi, D., Yang, Y. & Hu, S. (2016) Syntenin-1 is a promoter and prognostic marker of head and neck squamous cell carcinoma invasion and metastasis. *Oncotarget*, 7 (50), pp.82634–82647.
Daffu, G., Del Pozo, C., O'Shea, K., Ananthakrishnan, R., Ramasamy, R. & Schmidt, A. (2013) Radical Roles for RAGE in the Pathogenesis of Oxidative Stress in Cardiovascular Diseases and Beyond. *International Journal of Molecular Sciences*, 14 (10), pp.19891–19910.
Dean, M., Fojo, T. & Bates, S. (2005) Tumour stem cells and drug resistance. *Nature Reviews Cancer*, 5 (4), pp.275–284.
Deng, Y., Su, Q., Mo, J., Fu, X., Zhang, Y. & Lin, E.H. (2013) Celecoxib Downregulates CD133 Expression Through Inhibition of the Wnt Signaling Pathway in Colon Cancer Cells. *Cancer Investigation*, 31 (2), pp.97–102.
Deol, K.K., Crowe, S.O., Du, J., Bisbee, H.A., Guenette, R.G. & Strieter, E.R. (2020) Proteasome-Bound UCH37/UCHL5 Debranches Ubiquitin Chains to Promote Degradation. *Molecular Cell*, 80 (5), pp.796-809.e9.

Derfi, K.V., Vasiljevic, T., Dragicevic, T. & Glavan, T.M. (2024) Mithramycin targets head and neck cancer stem cells by inhibiting Sp1 and UFMylation. *Cancer Cell International*, 24 (1), p.412.
Donato, R., R. Cannon, B., Sorci, G., Riuzzi, F., Hsu, K., J. Weber, D. & L. Geczy, C. (2012) Functions of S100 Proteins. *Current Molecular Medicine*, 13, pp.24–57.
Dubey, P., Gupta, R., Mishra, A., Kumar, V., Bhadauria, S. & Bhatt, M.L.B. (2022) Evaluation of correlation between CD44, radiotherapy response, and survival rate in patients with advanced stage of head and neck squamous cell carcinoma (HNSCC). *Cancer Medicine*, 11 (9), pp.1937–1947.
El-Ashmawy, N.E., Al-Ashmawy, G.M., Hamada, O.B. & Khedr, N.F. (2025) The role of ABCG2 in health and disease: Linking cancer therapy resistance and other disorders. *Life Sciences*, 360, p.123245.
Estornes, Y., Toscano, F., Virard, F., Jacquemin, G., Pierrot, A., Vanbervliet, B., Bonnin, M., Lalaoui, N., Mercier-Gouy, P., Pachéco, Y., Salaun, B., Renno, T., Micheau, O. & Lebecque, S. (2012) dsRNA induces apoptosis through an atypical death complex associating TLR3 to caspase-8. *Cell Death & Differentiation*, 19 (9), pp.1482–1494.
Faraji, F., Ramirez, S.I., Anguiano Quiroz, P.Y., Mendez-Molina, A.N. & Gutkind, J.S. (2022) Genomic Hippo Pathway Alterations and Persistent YAP/TAZ Activation: New Hallmarks in Head and Neck Cancer. *Cells*, 11 (8), p.1370.
Fares, J., Fares, M.Y., Khachfe, H.H., Salhab, H.A. & Fares, Y. (2020) Molecular principles of metastasis: a hallmark of cancer revisited. *Signal Transduction and Targeted Therapy*, 5 (1), p.28.
Ferrer, C.M., Cho, H.M., Boon, R., Bernasocchi, T., Wong, L.P., Cetinbas, M., Haggerty, E.R., Mitsiades, I., Wojtkiewicz, G.R., McLoughlin, D.E., Aboushousha, R., Abdelhamid, H., Kugel, S., Rheinbay, E., Sadreyev, R., Juric, D., Janssen-Heininger, Y.M.W. & Mostoslavsky, R. (2024) The glutathione S-transferase Gstt1 drives survival and dissemination in metastases. *Nature Cell Biology*, 26 (6), pp.975–990.
Floris, A., Luo, J., Frank, J., Zhou, J., Orrù, S., Biancolella, M., Pucci, S., Orlandi, A., Campagna, P., Balzano, A., Ramani, K. & Tomasi, M.L. (2019) Star-related lipid transfer protein 10 (STARD10): a novel key player in alcohol-induced breast cancer progression. *Journal of Experimental & Clinical Cancer Research*, 38 (1), p.4.
Friedl, P. & Alexander, S. (2011) Cancer Invasion and the Microenvironment: Plasticity and Reciprocity. *Cell*, 147 (5), pp.992–1009.
Fritz, G. (2011) RAGE: a single receptor fits multiple ligands. *Trends in Biochemical Sciences*, 36 (12), pp.625–632.
Fu, M., Hu, Y., Lan, T., Guan, K.-L., Luo, T. & Luo, M. (2024) Correction: The Hippo signalling pathway and its implications in human health and diseases. *Signal Transduction and Targeted Therapy*, 9 (1), p.5.
Fukata, M., Breglio, K., Chen, A., Vamadevan, A.S., Goo, T., Hsu, D., Conduah, D., Xu, R. & Abreu, M.T. (2008) The Myeloid Differentiation Factor 88 (MyD88) Is Required for CD4+ T Cell Effector Function in a Murine Model of Inflammatory Bowel Disease. *The Journal of Immunology*, 180 (3), pp.1886–1894.
Funami, K. (2004) The cytoplasmic 'linker region' in Toll-like receptor 3 controls receptor localization and signaling. *International Immunology*, 16 (8), pp.1143–1154.
Furth, J., Kahn, M.C. & Breedis, C. (1937) The transmission of leukemia of mice with a single cell. *American Journal of Cancer*, 31, pp.276–282.
Gao, H., Li, W., Xu, S., Xu, Z., Hu, W., Pan, L., Luo, K., Xie, T., Yu, Y., Sun, H., Huang, L., Chen, Peishan, Wu, J., Yang, D., Li, L., Luan, S., Cao, M. & Chen, Pengfei (2024) Gasdermin D promotes development of intestinal tumors through regulating IL-1β

release and gut microbiota composition. *Cell Communication and Signaling*, 22 (1), p.511.
Gilazieva, Z., Ponomarev, A., Rutland, C., Rizvanov, A. & Solovyeva, V. (2020) Promising Applications of Tumor Spheroids and Organoids for Personalized Medicine. *Cancers*, 12 (10), p.2727.
Gill, J.S., Bansal, B., Poojary, R., Singh, H., Huang, F., Weis, J., Herman, K., Schultz, B., Coban, E., Guo, K. & Mathur, R. (2024) Immunological Signatures for Early Detection of Human Head and Neck Squamous Cell Carcinoma through RNA Transcriptome Analysis of Blood Platelets. *Cancers*, 16 (13), p.2399.
Glorieux, M., Dok, R. & Nuyts, S. (2020) The influence of PI3K inhibition on the radiotherapy response of head and neck cancer cells. *Scientific Reports*, 10 (1), p.16208.
Goto, Y., Arigami, T., Kitago, M., Nguyen, S.L., Narita, N., Ferrone, S., Morton, D.L., Irie, R.F. & Hoon, D.S.B. (2008) Activation of toll-like receptors 2, 3, and 4 on human melanoma cells induces inflammatory factors. *Molecular Cancer Therapeutics*, 7 (11), pp.3642–3653.
Grada, A., Otero-Vinas, M., Prieto-Castrillo, F., Obagi, Z. & Falanga, V. (2017) Research Techniques Made Simple: Analysis of Collective Cell Migration Using the Wound Healing Assay. *Journal of Investigative Dermatology*, 137 (2), pp.e11–e16.
Greaves, M. & Maley, C.C. (2012) Clonal evolution in cancer. *Nature*, 481 (7381), pp.306–313.
Gudkov, A. V. & Komarova, E.A. (2016) p53 and the Carcinogenicity of Chronic Inflammation. *Cold Spring Harbor Perspectives in Medicine*, 6 (11), p.a026161.
Gunti, S., Hoke, A.T.K., Vu, K.P. & London, N.R. (2021) Organoid and Spheroid Tumor Models: Techniques and Applications. *Cancers*, 13 (4), p.874.
Guo, X., He, D., Zhang, E., Chen, J., Chen, Q., Li, Y., Yang, L., Yang, Y., Zhao, Y., Wang, G., He, J. & Cai, Z. (2018) HMGB1 knockdown increases MM cell vulnerability by regulating autophagy and DNA damage repair. *Journal of Experimental & Clinical Cancer Research*, 37 (1), p.205.
Häcker, H., Redecke, V., Blagoev, B., Kratchmarova, I., Hsu, L.-C., Wang, G.G., Kamps, M.P., Raz, E., Wagner, H., Häcker, G., Mann, M. & Karin, M. (2006) Specificity in Toll-like receptor signalling through distinct effector functions of TRAF3 and TRAF6. *Nature*, 439 (7073), pp.204–207.
Hamilton, G. & Rath, B. (2019) Role of circulating tumor cell spheroids in drug resistance. *Cancer Drug Resistance*.
Han, J., Fujisawa, T., Husain, S.R. & Puri, R.K. (2014) Identification and characterization of cancer stem cells in human head and neck squamous cell carcinoma. *BMC Cancer*, 14 (1), p.173.
Hanahan, D. & Coussens, L.M. (2012) Accessories to the Crime: Functions of Cells Recruited to the Tumor Microenvironment. *Cancer Cell*, 21 (3), pp.309–322.
Hanke, M.L. & Kielian, T. (2011) Toll-like receptors in health and disease in the brain: mechanisms and therapeutic potential. *Clinical Science*, 121 (9), pp.367–387.
Hashimoto, C., Hudson, K.L. & Anderson, K. V. (1988) The Toll gene of drosophila, required for dorsal-ventral embryonic polarity, appears to encode a transmembrane protein. *Cell*, 52, pp.269–279.
Hassn Mesrati, M., Syafruddin, S.E., Mohtar, M.A. & Syahir, A. (2021) CD44: A Multifunctional Mediator of Cancer Progression. *Biomolecules*, 11 (12), p.1850.
Hazawa, M., Lin, D., Kobayashi, A., Jiang, Y., Xu, L., Dewi, F.R.P., Mohamed, M.S., Hartono, Nakada, M., Meguro-Horike, M., Horike, S., Koeffler, H.P. & Wong, R.W. (2018) ROCK-dependent phosphorylation of NUP62 regulates p63 nuclear transport and squamous cell carcinoma proliferation. *EMBO reports*, 19 (1), pp.73–88.

Helmy, M., Gohda, J., Inoue, J., Tomita, M., Tsuchiya, M. & Selvarajoo, K. (2009) Predicting Novel Features of Toll-Like Receptor 3 Signaling in Macrophages. *PLoS ONE*, 4 (3), p.e4661.
Henne, W.M., Buchkovich, N.J. & Emr, S.D. (2011) The ESCRT Pathway. *Developmental Cell*, 21 (1), pp.77–91.
Holmes, M.D., Chen, W.Y., Li, L., Hertzmark, E., Spiegelman, D. & Hankinson, S.E. (2010) Aspirin Intake and Survival After Breast Cancer. *Journal of Clinical Oncology*, 28 (9), pp.1467–1472.
Hornigold, N., Dunn, K.R., Craven, R.A., Zougman, A., Trainor, S., Shreeve, R., Brown, J., Sewell, H., Shires, M., Knowles, M., Fukuwatari, T., Maher, E.R., Burns, J., Bhattarai, S., Menon, M., Brazma, A., Scelo, G., Feulner, L., Riazalhosseini, Y., Lathrop, M., Harris, A., Selby, P.J., Banks, R.E. & Vasudev, N.S. (2020) Dysregulation at multiple points of the kynurenine pathway is a ubiquitous feature of renal cancer: implications for tumour immune evasion. *British Journal of Cancer*, 123 (1), pp.137–147.
Hsieh, K., Hotca, A.E., Dickstein, D.R., Lehrer, E.J., Hsieh, C., Gupta, V., Sindhu, K.K., Liu, J.T., Reed, S.H., Chhabra, A., Misiukiewicz, K., Roof, S., Kahn, M.N., Kirke, D., Urken, M., Posner, M., Genden, E. & Bakst, R.L. (2024) Adjuvant Reirradiation With Proton Therapy in Head and Neck Squamous Cell Carcinoma. *Advances in Radiation Oncology*, 9 (4), p.101418.
Hu, X., li, J., Fu, M., Zhao, X. & Wang, W. (2021) The JAK/STAT signaling pathway: from bench to clinic. *Signal Transduction and Targeted Therapy*, 6 (1), p.402.
Hu, Z., Wang, X., Li, D., Cao, L., Cui, H. & Xu, G. (2021) UFBP1, a key component in ufmylation, enhances drug sensitivity by promoting proteasomal degradation of oxidative stress-response transcription factor Nrf2. *Oncogene*, 40 (3), pp.647–662.
Huang, J., Xie, Y., Sun, X., Zeh, H.J., Kang, R., Lotze, M.T. & Tang, D. (2015) DAMPs, ageing, and cancer: The 'DAMP Hypothesis'. *Ageing Research Reviews*, 24, pp.3–16.
Huang, Y.-L., Huang, M.-T., Sung, P.-S., Chou, T.-Y., Yang, R.-B., Yang, A.-S., Yu, C.-M., Hsu, Y.-W., Chang, W.-C. & Hsieh, S.-L. (2021) Endosomal TLR3 co-receptor CLEC18A enhances host immune response to viral infection. *Communications Biology*, 4 (1), p.229.
Hughes, C.S., Postovit, L.M. & Lajoie, G.A. (2010) Matrigel: A complex protein mixture required for optimal growth of cell culture. *PROTEOMICS*, 10 (9), pp.1886–1890.
Human Protein Atlas (2024) KYAT3 protein expression summary [Internet].
Ishibashi, Y., Matsui, T., Takeuchi, M. & Yamagishi, S. (2012) Metformin Inhibits Advanced Glycation End Products (AGEs)-induced Renal Tubular Cell Injury by Suppressing Reactive Oxygen Species Generation via Reducing Receptor for AGEs (RAGE) Expression. *Hormone and Metabolic Research*, 44 (12), pp.891–895.
Jakšić, M., Provatas, G., Mihalić, I.B., Crnjac, A., Cosic, D., Dunatov, T., Romanenko, O. & Siketić, Z. (2023) The dual ion beam microprobe. *Nuclear Instruments and Methods in Physics Research Section B: Beam Interactions with Materials and Atoms*, 539, pp.120–126.
Jang, G.-Y., Lee, J. won, Kim, Y.S., Lee, S.E., Han, H.D., Hong, K.-J., Kang, T.H. & Park, Y.-M. (2020) Interactions between tumor-derived proteins and Toll-like receptors. *Experimental & Molecular Medicine*, 52 (12), pp.1926–1935.
Jia, D., Yang, W., Li, L., Liu, H., Tan, Y., Ooi, S., Chi, L., Filion, L.G., Figeys, D. & Wang, L. (2015) β-Catenin and NF-κB co-activation triggered by TLR3 stimulation facilitates stem cell-like phenotypes in breast cancer. *Cell Death & Differentiation*, 22 (2), pp.298–310.
Jiao, Y., Wang, H. & Fan, S. (2007) Growth suppression and radiosensitivity increase by HMGB1 in breast cancer. *Acta Pharmacologica Sinica*, 28 (12), pp.1957–1967.

Jing, Y., Mao, Z. & Chen, F. (2022) UFMylation System: An Emerging Player in Tumorigenesis. *Cancers*, 14 (14), p.3501.
Johnson, D.E., Burtness, B., Leemans, C.R., Lui, V.W.Y., Bauman, J.E. & Grandis, J.R. (2020) Head and neck squamous cell carcinoma. *Nature Reviews Disease Primers*, 6 (1), p.92.
Justus, C.R., Marie, M.A., Sanderlin, E.J. & Yang, L. V. (2023) Transwell In Vitro Cell Migration and Invasion Assays. In: pp.349–359.
Kang, S.H., Kim, G.R., Seong, M., Baek, S.H., Seol, J.H., Bang, O.S., Ovaa, H., Tatsumi, K., Komatsu, M., Tanaka, K. & Chung, C.H. (2007) Two Novel Ubiquitin-fold Modifier 1 (Ufm1)-specific Proteases, UfSP1 and UfSP2. *Journal of Biological Chemistry*, 282 (8), pp.5256–5262.
Kao, T.-W., Bai, G.-H., Wang, T.-L., Shih, I.-M., Chuang, C.-M., Lo, C.-L., Tsai, M.-C., Chiu, L.-Y., Lin, C.-C. & Shen, Y.-A. (2023) Novel cancer treatment paradigm targeting hypoxia-induced factor in conjunction with current therapies to overcome resistance. *Journal of Experimental & Clinical Cancer Research*, 42 (1), p.171.
Karikó, K., Ni, H., Capodici, J., Lamphier, M. & Weissman, D. (2004) mRNA Is an Endogenous Ligand for Toll-like Receptor 3. *Journal of Biological Chemistry*, 279 (13), pp.12542–12550.
Kawai, T. & Akira, S. (2006) TLR signaling. *Cell Death & Differentiation*, 13 (5), pp.816–825.
Kawasaki, T. & Kawai, T. (2014) Toll-Like Receptor Signaling Pathways. *Frontiers in Immunology*, 5.
Kayama, K., Watanabe, S., Takafuji, T., Tsuji, T., Hironaka, K., Matsumoto, M., Nakayama, K.I., Enari, M., Kohno, T., Shiraishi, K., Kiyono, T., Yoshida, K., Sugimoto, N. & Fujita, M. (2017) GRWD1 negatively regulates p53 via the RPL11-MDM2 pathway and promotes tumorigenesis. *EMBO reports*, 18 (1), pp.123–137.
Kim, Y.-M., Brinkmann, M.M., Paquet, M.-E. & Ploegh, H.L. (2008) UNC93B1 delivers nucleotide-sensing toll-like receptors to endolysosomes. *Nature*, 452 (7184), pp.234–238.
Komatsu, M., Chiba, T., Tatsumi, K., Lemura, S.I., Tanida, I., Okazaki, N., Ueno, T., Konminani, E., Natsume, T. & Tanaka, K. (2004) A novel protein-conjugating system for Ufm1, a ubiquitin-fold modifier. *EMBO Journal*, 23, pp.1977–1986.
Krishnamurthy, S., Dong, Z., Vodopyanov, D., Imai, A., Helman, J.I., Prince, M.E., Wicha, M.S. & Nör, J.E. (2010) Endothelial Cell-Initiated Signaling Promotes the Survival and Self-Renewal of Cancer Stem Cells. *Cancer Research*, 70 (23), pp.9969–9978.
Krishnamurthy, S. & Nör, J.E. (2012) Head and Neck Cancer Stem Cells. *Journal of Dental Research*, 91 (4), pp.334–340.
Krishnan, J., Selvarajoo, K., Tsuchiya, M., Lee, G. & Choi, S. (2007) Toll-like receptor signal transduction. *Experimental & Molecular Medicine*, 39 (4), pp.421–438.
Kumar, H., Koyama, S., Ishii, K.J., Kawai, T. & Akira, S. (2008) Cutting Edge: Cooperation of IPS-1- and TRIF-Dependent Pathways in Poly IC-Enhanced Antibody Production and Cytotoxic T Cell Responses. *The Journal of Immunology*, 180 (2), pp.683–687.
Kumari, S., Banerjee, S., Kumar, M., Hayashi, A., Solaimuthu, B., Cohen-Kfir, E., Shaul, Y.D., Rouvinski, A. & Wiener, R. (2022) Overexpression of UBA5 in Cells Mimics the Phenotype of Cells Lacking UBA5. *International Journal of Molecular Sciences*, 23 (13), p.7445.
Kwon, Y.J., Kwon, H.H., Leem, J. & Jang, Y.Y. (2024) Kahweol Inhibits Pro-Inflammatory Cytokines and Chemokines in Tumor Necrosis Factor-α/Interferon-γ-Stimulated Human Keratinocyte HaCaT Cells. *Current Issues in Molecular Biology*, 46 (4), pp.3470–3483.

Laila, U.E., Zhao, Z.L., Lui, H. & Xu, Z.-X. (2025) Aspirin in Cancer Therapy: Pharmacology and Nanotechnology Advances. *International Journal of Nanomedicine*, Volume 20, pp.2327–2365.
Lee, C.-H., Yu, C.-C., Wang, B.-Y. & Chang, W.-W. (2016) Tumorsphere as an effective in vitro platform for screening anti-cancer stem cell drugs. *Oncotarget*, 7 (2), pp.1215–1226.
Lemaitre, B., Nicolas, E., Michaut, L., Reichhart, J.M. & Hoffmann, J.A. (1996) The dorsoventral regulatory gene cassette spatzle/Toll/Cactus controls the potent antifungal response in Drosophila adults. *Cell*, 86, pp.973–983.
León-Letelier, R.A., Dou, R., Vykoukal, J., Sater, A.H.A., Ostrin, E., Hanash, S. & Fahrmann, J.F. (2023) The kynurenine pathway presents multi-faceted metabolic vulnerabilities in cancer. *Frontiers in Oncology*, 13.
Li, L., Li, Chao, Wang, S., Wang, Z., Jiang, J., Wang, W., Li, X., Chen, J., Liu, K., Li, Chunhua & Zhu, G. (2016) Exosomes Derived from Hypoxic Oral Squamous Cell Carcinoma Cells Deliver miR-21 to Normoxic Cells to Elicit a Prometastatic Phenotype. *Cancer Research*, 76 (7), pp.1770–1780.
Li, Q., Tie, Y., Alu, A., Ma, X. & Shi, H. (2023) Targeted therapy for head and neck cancer: signaling pathways and clinical studies. *Signal Transduction and Targeted Therapy*, 8 (1), p.31.
Li, X., Jiang, S. & Tapping, R.I. (2010) Toll-like receptor signaling in cell proliferation and survival. *Cytokine*, 49 (1), pp.1–9.
Li, Z. (2013) CD133: a stem cell biomarker and beyond. *Experimental Hematology & Oncology*, 2 (1), p.17.
Li, Z., Duan, Y., Cheng, S., Chen, Y., Hu, Y., Zhang, L., He, J., Liao, Q., Yang, L. & Sun, L.-Q. (2015) EBV-encoded RNA via TLR3 induces inflammation in nasopharyngeal carcinoma. *Oncotarget*, 6 (27), pp.24291–24303.
Lim, C.S., Jang, Y.H., Lee, G.Y., Han, G.M., Jeong, H.J., Kim, J.W. & Lee, J.-O. (2022) TLR3 forms a highly organized cluster when bound to a poly(I:C) RNA ligand. *Nature Communications*, 13 (1), p.6876.
Lin, M., Lian, N.-Z., Cao, L.-L., Huang, C.-M., Zheng, C.-H., Li, P., Xie, J.-W., Wang, J.-B., Lu, J., Chen, Q.-Y., Li, Y.-H., Peng, Z.-H., Zhang, X.-Y., Mei, Y.-X. & Lin, J.-X. (2022) Down-regulated expression of CDK5RAP3 and UFM1 suggests a poor prognosis in gastric cancer patients. *Frontiers in oncology*, 12, p.927751.
Liu, J., Guan, D., Dong, M., Yang, J., Wei, H., Liang, Q., Song, L., Xu, L., Bai, J., Liu, C., Mao, J., Zhang, Q., Zhou, J., Wu, X., Wang, M. & Cong, Y.-S. (2020) UFMylation maintains tumour suppressor p53 stability by antagonizing its ubiquitination. *Nature Cell Biology*, 22 (9), pp.1056–1063.
Liu, J., Xiao, Q., Xiao, J., Niu, C., Li, Y., Zhang, X., Zhou, Z., Shu, G. & Yin, G. (2022) Wnt/β-catenin signalling: function, biological mechanisms, and therapeutic opportunities. *Signal Transduction and Targeted Therapy*, 7 (1), p.3.
Liu, S.-Y., Sanchez, D.J., Aliyari, R., Lu, S. & Cheng, G. (2012) Systematic identification of type I and type II interferon-induced antiviral factors. *Proceedings of the National Academy of Sciences*, 109 (11), pp.4239–4244.
Liu, Y., Gu, Y., Han, Y., Zhang, Q., Jiang, Z., Zhang, X., Huang, B., Xu, X., Zheng, J. & Cao, X. (2016) Tumor Exosomal RNAs Promote Lung Pre-metastatic Niche Formation by Activating Alveolar Epithelial TLR3 to Recruit Neutrophils. *Cancer Cell*, 30 (2), pp.243–256.
Lu, B.-C., Li, J., Yu, W.-F., Zhang, G.-Z., Wang, H.-M. & Ma, H.-M. (2016) Elevated expression of Nrf2 mediates multidrug resistance in CD133+ head and neck squamous cell carcinoma stem cells. *Oncology letters*, 12, pp.4333–4338.

Lu, M., Strohecker, A., Chen, F., Kwan, T., Bosman, J., Jordan, V.C. & Cryns, V.L. (2008) Aspirin Sensitizes Cancer Cells to TRAIL–Induced Apoptosis by Reducing Survivin Levels. *Clinical Cancer Research*, 14 (10), pp.3168–3176.
Ma, H., Zheng, S., Zhang, X., Gong, T., Lv, X., Fu, S., Zhang, S., Yin, X., Hao, J., Shan, C. & Huang, S. (2019) High mobility group box 1 promotes radioresistance in esophageal squamous cell carcinoma cell lines by modulating autophagy. *Cell Death & Disease*, 10 (2), p.136.
Manavalan, B., Basith, S. & Choi, S. (2011) Similar Structures but Different Roles – An Updated Perspective on TLR Structures. *Frontiers in Physiology*, 2.
Masciale, V., Grisendi, G., Banchelli, F., D'Amico, R., Maiorana, A., Sighinolfi, P., Stefani, A., Morandi, U., Dominici, M. & Aramini, B. (2019) Isolation and Identification of Cancer Stem-Like Cells in Adenocarcinoma and Squamous Cell Carcinoma of the Lung: A Pilot Study. *Frontiers in Oncology*, 9.
Matijevic Glavan, T., Cipak Gasparovic, A., Vérillaud, B., Busson, P. & Pavelic, J. (2017) Toll-like receptor 3 stimulation triggers metabolic reprogramming in pharyngeal cancer cell line through Myc, MAPK, and HIF. *Molecular Carcinogenesis*, 56 (4), pp.1214–1226.
Matijevic, T., Marjanovic, M. & Pavelic, J. (2009) Functionally Active Toll-Like Receptor 3 on Human Primary and Metastatic Cancer Cells. *Scandinavian Journal of Immunology*, 70 (1), pp.18–24.
Matijevic, T. & Pavelic, J. (2011) The dual role of TLR3 in metastatic cell line. *Clinical & Experimental Metastasis*, 28 (7), pp.701–712.
Matsumoto, M., Kikkawa, S., Kohase, M., Miyake, K. & Seya, T. (2002) Establishment of a monoclonal antibody against human Toll-like receptor 3 that blocks double-stranded RNA-mediated signaling. *Biochemical and Biophysical Research Communications*, 293 (5), pp.1364–1369.
Mazari, A.M.A., Zhang, L., Ye, Z.-W., Zhang, J., Tew, K.D. & Townsend, D.M. (2023) The Multifaceted Role of Glutathione S-Transferases in Health and Disease. *Biomolecules*, 13 (4), p.688.
McDermott, S.C., Rodriguez-Ramirez, C., McDermott, S.P., Wicha, M.S. & Nör, J.E. (2018) FGFR signaling regulates resistance of head and neck cancer stem cells to cisplatin. *Oncotarget*, 9, pp.25148–25165.
Medzhitov, R., Preston-Hurlburt, P. & Janeway, C.A. (1997) A human homologue of the Drosophila Toll protein signals activation of adaptive immunity. *Nature*, 388 (6640), pp.394–397.
Memel, Z.N., Arvind, A., Moninuola, O., Philpotts, L., Chung, R.T., Corey, K.E. & Simon, T.G. (2021) Aspirin Use Is Associated with a Reduced Incidence of Hepatocellular Carcinoma: A Systematic Review and Meta-analysis. *Hepatology Communications*, 5 (1), pp.133–143.
Meng, X., Wang, L., He, M., Yang, Z., Jiao, Y., Hu, Y. & Wang, K. (2022) Cysteine conjugate beta-lyase 2 (CCBL2) expression as a prognostic marker of survival in breast cancer patients. *PLOS ONE*, 17 (6), p.e0269998.
Mikulandra, M., Kobescak, A., Verillaud, B., Busson, P. & Matijevic Glavan, T. (2019) Radio-sensitization of head and neck cancer cells by a combination of poly(I:C) and cisplatin through downregulation of survivin and c-IAP2. *Cellular Oncology*, 42 (1), pp.29–40.
Millrine, D., Peter, J.J. & Kulathu, Y. (2023) A guide to UFMylation, an emerging posttranslational modification. *FEBS Journal*, 290, pp.5040–5056.
Miura, S., Iwamoto, H., Namba, M., Yamaguchi, K., Sakamoto, S., Horimasu, Y., Masuda, T., Miyamoto, S., Nakashima, T., Ohshimo, S., Fujitaka, K., Hamada, H. & Hattori, N.

(2024) High S100A9 level predicts poor survival, and the S100A9 inhibitor paquinimod is a candidate for treating idiopathic pulmonary fibrosis. *BMJ Open Respiratory Research*, 11 (1), p.e001803.
Morgan, E.L., Toni, T., Viswanathan, R., Robbins, Y., Yang, X., Cheng, H., Gunti, S., Huynh, A., Sowers, A.L., Mitchell, J.B., Allen, C.T., Chen, Z. & Van Waes, C. (2023) Inhibition of USP14 promotes TNFα-induced cell death in head and neck squamous cell carcinoma (HNSCC). *Cell Death & Differentiation*, 30 (5), pp.1382–1396.
Mukherjee, S., Kong, J. & Brat, D.J. (2015) Cancer Stem Cell Division: When the Rules of Asymmetry Are Broken. *Stem Cells and Development*, 24 (4), pp.405–416.
Mumaw, D.A., Hazy, A.J., Vayntraub, A., Quinn, T.J., Salari, K., Chang, J.H., Kalman, N., Katz, S., Urbanic, J., Press, R.H., Thukral, A.D., Tsai, H., Laramore, G.E., Molitoris, J., Vargas, C., Patel, S.H., Stevens, C. & Deraniyagala, R.L. (2024) Low contralateral failure rate with unilateral proton beam radiotherapy for oropharyngeal squamous cell carcinoma: A multi-institutional prospective study from the proton collaborative group. *Radiotherapy and Oncology*, 190, p.109977.
Muresan, X.M., Bouchal, J., Culig, Z. & Souček, K. (2020) Toll-Like Receptor 3 in Solid Cancer and Therapy Resistance. *Cancers*, 12 (11), p.3227.
Nathansen, J., Lukiyanchuk, V., Hein, L., Stolte, M.-I., Borgmann, K., Löck, S., Kurth, I., Baumann, M., Krause, M., Linge, A. & Dubrovska, A. (2021) Oct4 confers stemness and radioresistance to head and neck squamous cell carcinoma by regulating the homologous recombination factors PSMC3IP and RAD54L. *Oncogene*, 40 (24), pp.4214–4228.
Ni, P., Zhang, Y., Liu, Y., Lin, X., Su, X., Lu, H., Shen, H., Xu, W., Xu, H. & Su, Z. (2015) HMGB1 silence could promote MCF-7 cell apoptosis and inhibit invasion and metastasis. *International Journal of Clinical and Experimental Pathology*, 8, pp.15940–15946.
Nishiya, T., Kajita, E., Miwa, S. & DeFranco, A.L. (2005) TLR3 and TLR7 Are Targeted to the Same Intracellular Compartments by Distinct Regulatory Elements. *Journal of Biological Chemistry*, 280 (44), pp.37107–37117.
Nomi, N., Kodama, S. & Suzuki, M. (2010) Toll-like receptor 3 signaling induces apoptosis in human head and neck cancer via survivin associated pathway. *Oncology Reports*, 24, pp.225–231.
Nuyts, S., Bollen, H., Ng, S.P., Corry, J., Eisbruch, A., Mendenhall, W.M., Smee, R., Strojan, P., Ng, W.T. & Ferlito, A. (2022) Proton Therapy for Squamous Cell Carcinoma of the Head and Neck: Early Clinical Experience and Current Challenges. *Cancers*, 14 (11), p.2587.
Olayioye, M.A., Vehring, S., Müller, P., Herrmann, A., Schiller, J., Thiele, C., Lindeman, G.J., Visvader, J.E. & Pomorski, T. (2005) StarD10, a START Domain Protein Overexpressed in Breast Cancer, Functions as a Phospholipid Transfer Protein. *Journal of Biological Chemistry*, 280 (29), pp.27436–27442.
O'Neill, L.A.J. & Bowie, A.G. (2007) The family of five: TIR-domain-containing adaptors in Toll-like receptor signalling. *Nature Reviews Immunology*, 7 (5), pp.353–364.
Oner, M., Cheng, Y.-C., Soong, S.-W., Cheng, P.-T., Wang, Y.-H., Yang, S.-F., Tsai, S.C.-S. & Lin, H. (2025) Dinaciclib Interrupts Cell Cycle and Induces Apoptosis in Oral Squamous Cell Carcinoma: Mechanistic Insights and Therapeutic Potential. *International Journal of Molecular Sciences*, 26 (5), p.2197.
Pal, A., Barrett, T.F., Paolini, R., Parikh, A. & Puram, S. V. (2021) Partial EMT in head and neck cancer biology: a spectrum instead of a switch. *Oncogene*, 40 (32), pp.5049–5065.
Paone, A., Galli, R., Gabellini, C., Lukashev, D., Starace, D., Gorlach, A., De Cesaris, P., Ziparo, E., Del Bufalo, D., Sitkovsky, M. V., Filippini, A. & Riccioli, A. (2010) Toll-like

Receptor 3 Regulates Angiogenesis and Apoptosis in Prostate Cancer Cell Lines through Hypoxia-Inducible Factor 1α. *Neoplasia*, 12 (7), pp.539–549.
Pastrana, E., Silva-Vargas, V. & Doetsch, F. (2011) Eyes Wide Open: A Critical Review of Sphere-Formation as an Assay for Stem Cells. *Cell Stem Cell*, 8 (5), pp.486–498.
Peitzsch, C., Kurth, I., Kunz-Schughart, L., Baumann, M. & Dubrovska, A. (2013) Discovery of the cancer stem cell related determinants of radioresistance. *Radiotherapy and Oncology*, 108 (3), pp.378–387.
Perrot, I., Deauvieau, F., Massacrier, C., Hughes, N., Garrone, P., Durand, I., Demaria, O., Viaud, N., Gauthier, L., Blery, M., Bonnefoy-Berard, N., Morel, Y., Tschopp, J., Alexopoulou, L., Trinchieri, G., Paturel, C. & Caux, C. (2010) TLR3 and Rig-Like Receptor on Myeloid Dendritic Cells and Rig-Like Receptor on Human NK Cells Are Both Mandatory for Production of IFN-γ in Response to Double-Stranded RNA. *The Journal of Immunology*, 185 (4), pp.2080–2088.
Petrić, T. & Sabol, M. (2023) Let's Go 3D! New Generation of Models for Evaluating Drug Response and Resistance in Prostate Cancer. *International Journal of Molecular Sciences*, 24 (6), p.5293.
Phi, L.T.H., Sari, I.N., Yang, Y.-G., Lee, S.-H., Jun, N., Kim, K.S., Lee, Y.K. & Kwon, H.Y. (2018) Cancer Stem Cells (CSCs) in Drug Resistance and their Therapeutic Implications in Cancer Treatment. *Stem Cells International*, 2018, pp.1–16.
Piccinini, A.M. & Midwood, K.S. (2010) DAMPening Inflammation by Modulating TLR Signalling. *Mediators of Inflammation*, 2010, pp.1–21.
Platten, M., Nollen, E.A.A., Röhrig, U.F., Fallarino, F. & Opitz, C.A. (2019) Tryptophan metabolism as a common therapeutic target in cancer, neurodegeneration and beyond. *Nature Reviews Drug Discovery*, 18 (5), pp.379–401.
Pohar, J., Pirher, N., Benčina, M., Manček-Keber, M. & Jerala, R. (2013) The Role of UNC93B1 Protein in Surface Localization of TLR3 Receptor and in Cell Priming to Nucleic Acid Agonists. *Journal of Biological Chemistry*, 288 (1), pp.442–454.
Prickett, T.D., Ninomiya-Tsuji, J., Broglie, P., Muratore-Schroeder, T.L., Shabanowitz, J., Hunt, D.F. & Brautigan, D.L. (2008) TAB4 Stimulates TAK1-TAB1 Phosphorylation and Binds Polyubiquitin to Direct Signaling to NF-κB. *Journal of Biological Chemistry*, 283 (28), pp.19245–19254.
Pries, R., Hogrefe, L., Xie, L., Frenzel, H., Brocks, C., Ditz, C. & Wollenberg, B. (2008) Induction of c-Myc-dependent cell proliferation through toll-like receptor 3 in head and neck cancer. *International Journal of Molecular Medicine*, 21, pp.209–215.
Prince, M.E., Sivanandan, R., Kaczorowski, A., Wolf, G.T., Kaplan, M.J., Dalerba, P., Weissman, I.L., Clarke, M.F. & Ailles, L.E. (2007) Identification of a subpopulation of cells with cancer stem cell properties in head and neck squamous cell carcinoma. *Proceedings of the National Academy of Sciences*, 104 (3), pp.973–978.
Rezania, M.A., Eghtedari, A., Taha, M.F., Ardekani, A.M. & Javeri, A. (2022) A novel role for aspirin in enhancing the reprogramming function of miR-302/367 cluster and breast tumor suppression. *Journal of Cellular Biochemistry*, 123 (6), pp.1077–1090.
Rich, J.N. (2016) Cancer stem cells: Understanding tumor hierarchy and heterogeneity. *Medicine (United States)*, 95, pp.S2–S7.
Riehl, A., Németh, J., Angel, P. & Hess, J. (2009) The receptor RAGE: Bridging inflammation and cancer. *Cell Communication and Signaling*, 7 (1), p.12.
Riess, C., Schneider, B., Kehnscherper, H., Gesche, J., Irmscher, N., Shokraie, F., Classen, C.F., Wirthgen, E., Domanska, G., Zimpfer, A., Strüder, D., Junghanss, C. & Maletzki, C. (2020) Activation of the Kynurenine Pathway in Human Malignancies Can Be Suppressed by the Cyclin-Dependent Kinase Inhibitor Dinaciclib. *Frontiers in Immunology*, 11.

Rock, F.L., Hardiman, G., Timans, J.C., Kastelein, R.A. & Bazan, J.F. (1998) A family of human receptors structurally related to *Drosophila* Toll. *Proceedings of the National Academy of Sciences*, 95 (2), pp.588–593.
Romesser, P.B., Cahlon, O., Scher, E.D., Hug, E.B., Sine, K., DeSelm, C., Fox, J.L., Mah, D., Garg, M.K., Han-Chih Chang, J. & Lee, N.Y. (2016) Proton Beam Reirradiation for Recurrent Head and Neck Cancer: Multi-institutional Report on Feasibility and Early Outcomes. *International Journal of Radiation Oncology*Biology*Physics*, 95 (1), pp.386–395.
Rydberg, C., Månsson, A., Uddman, R., Riesbeck, K. & Cardell, L. (2009) Toll-like receptor agonists induce inflammation and cell death in a model of head and neck squamous cell carcinomas. *Immunology*, 128 (1pt2).
Salaun, B., Coste, I., Rissoan, M.-C., Lebecque, S.J. & Renno, T. (2006) TLR3 Can Directly Trigger Apoptosis in Human Cancer Cells. *The Journal of Immunology*, 176 (8), pp.4894–4901.
dos Santos, L. V., Abrahão, C.M. & William, W.N. (2021) Overcoming Resistance to Immune Checkpoint Inhibitors in Head and Neck Squamous Cell Carcinomas. *Frontiers in Oncology*, 11.
Saqub, H., Proetsch-Gugerbauer, H., Bezrookove, V., Nosrati, M., Vaquero, E.M., de Semir, D., Ice, R.J., McAllister, S., Soroceanu, L., Kashani-Sabet, M., Osorio, R. & Dar, A.A. (2020) Dinaciclib, a cyclin-dependent kinase inhibitor, suppresses cholangiocarcinoma growth by targeting CDK2/5/9. *Scientific Reports*, 10 (1), p.18489.
Schindelin, J., Arganda-Carreras, I., Frise, E., Kaynig, V., Longair, M., Pietzsch, T., Preibisch, S., Rueden, C., Saalfeld, S., Schmid, B., Tinevez, J.-Y., White, D.J., Hartenstein, V., Eliceiri, K., Tomancak, P. & Cardona, A. (2012) Fiji: an open-source platform for biological-image analysis. *Nature Methods*, 9 (7), pp.676–682.
Schlichtner, S., Yasinska, I.M., Klenova, E., Abooali, M., Lall, G.S., Berger, S.M., Ruggiero, S., Cholewa, D., Milošević, M., Gibbs, B.F., Fasler-Kan, E. & Sumbayev, V. V. (2023) L-Kynurenine participates in cancer immune evasion by downregulating hypoxic signaling in T lymphocytes. *OncoImmunology*, 12 (1).
Schulz, A., Meyer, F., Dubrovska, A. & Borgmann, K. (2019) Cancer Stem Cells and Radioresistance: DNA Repair and Beyond. *Cancers*, 11 (6), p.862.
Sen, G. & Sarkar, S. (2005) Transcriptional signaling by double-stranded RNA: role of TLR3. *Cytokine & Growth Factor Reviews*, 16 (1), pp.1–14.
Shi, G. & Jin, Y. (2010) Role of Oct4 in maintaining and regaining stem cell pluripotency. *Stem Cell Research & Therapy*, 1 (5), p.39.
Shortall, K., Djeghader, A., Magner, E. & Soulimane, T. (2021) Insights into Aldehyde Dehydrogenase Enzymes: A Structural Perspective. *Frontiers in Molecular Biosciences*, 8.
Singh, M.K., Shin, Y., Ju, S., Han, S., Choe, W., Yoon, K.-S., Kim, S.S. & Kang, I. (2024) Heat Shock Response and Heat Shock Proteins: Current Understanding and Future Opportunities in Human Diseases. *International Journal of Molecular Sciences*, 25 (8), p.4209.
Springer (2004) Radiation Types and Sources. In: *Handbook on Radiation Probing, Gauging, Imaging and Analysis*. Dordrecht, Kluwer Academic Publishers, pp.19–62.
Tak, P.P. & Firestein, G.S. (2001) NF-κB: a key role in inflammatory diseases. *Journal of Clinical Investigation*, 107 (1), pp.7–11.
Tankiewicz, A., Dziemiańczyk, D., Buczko, P., Szarmach, I.J., Grabowska, S.Z. & Pawlak, D. (2006) Tryptophan and its metabolites in patients with oral squamous cell carcinoma: preliminary study. *Advances in medical sciences*, 51 Suppl 1, pp.221–224.

Tavassol, F., Starke, O.F., Kokemüller, H., Wegener, G., Müller-Tavassol, C.C., Gellrich, N.-C. & Eckardt, A. (2011) Prognostic significance of heat shock protein 70 (HSP70) in patients with oral cancer. *Head & Neck Oncology*, 3 (1), p.10.
Toussi, D. & Massari, P. (2014) Immune Adjuvant Effect of Molecularly-defined Toll-Like Receptor Ligands. *Vaccines*, 2 (2), pp.323–353.
Tsai, W.-C., Tsai, S.-T., Jin, Y.-T. & Wu, L.-W. (2006) Cyclooxygenase-2 Is Involved in S100A2-Mediated Tumor Suppression in Squamous Cell Carcinoma. *Molecular Cancer Research*, 4 (8), pp.539–547.
Uematsu, S. & Akira, S. (2007) Toll-like Receptors and Type I Interferons. *Journal of Biological Chemistry*, 282 (21), pp.15319–15323.
Vane, J.R. & Botting, R.M. (2003) The mechanism of action of aspirin. *Thrombosis Research*, 110 (5–6), pp.255–258.
Vasiljevic, T., Tarle, M., Hat, K., Luksic, I., Mikulandra, M., Busson, P. & Matijevic Glavan, T. (2023) Necrotic Cells from Head and Neck Carcinomas Release Biomolecules That Are Activating Toll-like Receptor 3. *International Journal of Molecular Sciences*, 24 (20), p.15269.
Vijay, K. (2018) Toll-like receptors in immunity and inflammatory diseases: Past, present, and future. *International Immunopharmacology*, 59, pp.391–412.
Vukovic Đerfi, K., Vasiljevic, T. & Matijevic Glavan, T. (2023) Recent Advances in the Targeting of Head and Neck Cancer Stem Cells. *Applied Sciences*, 13 (24), p.13293.
Walczak, K., Wnorowski, A., Turski, W.A. & Plech, T. (2020) Kynurenic acid and cancer: facts and controversies. *Cellular and Molecular Life Sciences*, 77 (8), pp.1531–1550.
Wang, C., Deng, L., Hong, M., Akkaraju, G.R., Inoue, J. & Chen, Z.J. (2001) TAK1 is a ubiquitin-dependent kinase of MKK and IKK. *Nature*, 412 (6844), pp.346–351.
Wang, K., Chen, S., Wu, Y., Wang, Y., Lu, Y., Sun, Y. & Chen, Y. (2023) The ufmylation modification of ribosomal protein L10 in the development of pancreatic adenocarcinoma. *Cell Death & Disease*, 14 (6), p.350.
Wang, S.J., Wong, G., de Heer, A., Xia, W. & Bourguignon, L.Y.W. (2009) CD44 variant isoforms in head and neck squamous cell carcinoma progression. *The Laryngoscope*, 119 (8), pp.1518–1530.
Warburg, O. (1956) On the Origin of Cancer Cells. *Science*, 123 (3191), pp.309–314.
Wen, J., Yin, P., Su, Y., Gao, F., Wu, Y., Zhang, W., Chi, P., Chen, J. & Zhang, X. (2023) Knockdown of HMGB1 inhibits the crosstalk between oral squamous cell carcinoma cells and tumor-associated macrophages. *International Immunopharmacology*, 119, p.110259.
Wicks, E.E. & Semenza, G.L. (2022) Hypoxia-inducible factors: cancer progression and clinical translation. *Journal of Clinical Investigation*, 132 (11).
Willert, K. & Jones, K.A. (2006) Wnt signaling: is the party in the nucleus? *Genes & Development*, 20 (11), pp.1394–1404.
Wilson, R.R. (1946) Radiological Use of Fast Protons. *Radiology*, 47 (5), pp.487–491.
Wu, C.-Z., Zheng, J.-J., Bai, Y.-H., Xia, P., Zhang, H.-C. & Guo, Y. (2018) HMGB1/RAGE axis mediates the apoptosis, invasion, autophagy, and angiogenesis of the renal cell carcinoma. *OncoTargets and therapy*, 11, pp.4501–4510.
Wu, P., Quan, H., Kang, J., He, J., Luo, S., Xie, C., Xu, J., Tang, Y. & Zhao, S. (2017) Downregulation of Calcium-Binding Protein S100A9 Inhibits Hypopharyngeal Cancer Cell Proliferation and Invasion Ability Through Inactivation of NF-κB Signaling. *Oncology Research Featuring Preclinical and Clinical Cancer Therapeutics*, 25 (9), pp.1479–1488.
Wu, Y. & Wu, P.Y. (2009) CD133 as a Marker for Cancer Stem Cells: Progresses and Concerns. *Stem Cells and Development*, 18 (8), pp.1127–1134.

Yamamoto, M., Sato, S., Hemmi, H., Hoshino, K., Kaisho, T., Sanjo, H., Takeuchi, O., Sugiyama, M., Okabe, M., Takeda, K. & Akira, S. (2003) Role of Adaptor TRIF in the MyD88-Independent Toll-Like Receptor Signaling Pathway. *Science*, 301 (5633), pp.640–643.

Yan, J., Chen, D., Ye, Z., Zhu, X., Li, X., Jiao, H., Duan, M., Zhang, C., Cheng, J., Xu, L., Li, H. & Yan, D. (2024) Molecular mechanisms and therapeutic significance of Tryptophan Metabolism and signaling in cancer. *Molecular Cancer*, 23 (1), p.241.

Yang, C., Zhang, L., Han, Q., Liao, C., Lan, J., Ding, H., Zhou, H., Diao, X. & Li, J. (2016) Kynurenine aminotransferase 3/glutamine transaminase L/cysteine conjugate beta-lyase 2 is a major glutamine transaminase in the mouse kidney. *Biochemistry and Biophysics Reports*, 8, pp.234–241.

Yang, H., Pellegrini, L., Napolitano, A., Giorgi, C., Jube, S., Preti, A., Jennings, C.J., De Marchis, F., Flores, E.G., Larson, D., Pagano, I., Tanji, M., Powers, A., Kanodia, S., Gaudino, G., Pastorino, S., Pass, H.I., Pinton, P., Bianchi, M.E. & Carbone, M. (2015) Aspirin delays mesothelioma growth by inhibiting HMGB1-mediated tumor progression. *Cell Death & Disease*, 6 (6), pp.e1786–e1786.

Yang, Y., Wang, X.-L., Yue, Y.-X., Chen, G. & Xia, H.-F. (2025) TSG101 overexpression enhances metastasis in oral squamous cell carcinoma through cell cycle regulation. *Cellular Signalling*, 125, p.111519.

Yeh, S.-A. (2010) Radiotherapy for Head and Neck Cancer. *Seminars in Plastic Surgery*, 24 (02), pp.127–136.

Yu, Z., Pestell, T.G., Lisanti, M.P. & Pestell, R.G. (2012) Cancer stem cells. *The International Journal of Biochemistry & Cell Biology*, 44 (12), pp.2144–2151.

Yuan, P., Jiang, S., Wang, Q., Wu, Y., Jiang, Y., Xu, H., Jiang, L. & Luo, X. (2024) Prognostic and chemotherapeutic implications of a novel four-gene pyroptosis model in head and neck squamous cell carcinoma. *PeerJ*, 12, p.e17296.

Zapletal, E., Vasiljevic, T., Busson, P. & Matijevic Glavan, T. (2023) Dialog beyond the Grave: Necrosis in the Tumor Microenvironment and Its Contribution to Tumor Growth. *International Journal of Molecular Sciences*, 24 (6), p.5278.

Zhang, J., Lou, X., Jin, L., Zhou, R., Liu, S., Xu, N. & Liao, D.J. (2014) Necrosis, and then stress induced necrosis-like cell death, but not apoptosis, should be the preferred cell death mode for chemotherapy: clearance of a few misconceptions. *Oncoscience*, 1 (6), pp.407–422.

Zhang, X., Lin, S.H., Fang, B., Gillin, M., Mohan, R. & Chang, J.Y. (2013) Therapy-Resistant Cancer Stem Cells Have Differing Sensitivity to Photon versus Proton Beam Radiation. *Journal of Thoracic Oncology*, 8 (12), pp.1484–1491.

Zhang, Y., Liu, L., Fan, P., Bauer, N., Gladkich, J., Ryschich, E., Bazhin, A. V., Giese, N.A., Strobel, O., Hackert, T., Hinz, U., Gross, W., Fortunato, F. & Herr, I. (2024) Correction: Aspirin counteracts cancer stem cell features, desmoplasia and gemcitabine resistance in pancreatic cancer. *Oncotarget*, 15 (1), pp.504–506.

Zhao, W., Li, Y. & Zhang, X. (2017) Stemness-related markers in cancer. *Cancer Translational Medicine*, 3 (3), p.87.

Zhou, B., Lin, W., Long, Y., Yang, Y., Zhang, H., Wu, K. & Chu, Q. (2022) Notch signaling pathway: architecture, disease, and therapeutics. *Signal Transduction and Targeted Therapy*, 7 (1), p.95.

Zhou, J., Ma, X., He, X., Chen, B., Yuan, J., Jin, Z., Li, L., Wang, Z., Xiao, Q., Cai, Y. & Zou, Y. (2023) Dysregulation of PD-L1 by UFMylation imparts tumor immune evasion and identified as a potential therapeutic target. *Proceedings of the National Academy of Sciences of the United States of America*, 120.

Zhou, M., McFarland-Mancini, M.M., Funk, H.M., Husseinzadeh, N., Mounajjed, T. & Drew, A.F. (2009) Toll-like receptor expression in normal ovary and ovarian tumors. *Cancer Immunology, Immunotherapy*, 58 (9), pp.1375–1385.

Zhou, X., Shang, J., Liu, X., Zhuang, J.-F., Yang, Y.-F., Zhang, Y.-Y. & Guan, G.-X. (2021) Clinical Significance and Oncogenic Activity of GRWD1 Overexpression in the Development of Colon Carcinoma. *OncoTargets and Therapy*, Volume 14, pp.1565–1580.

Zimmermann, P., Tomatis, D., Rosas, M., Grootjans, J., Leenaerts, I., Degeest, G., Reekmans, G., Coomans, C. & David, G. (2001) Characterization of Syntenin, a Syndecan-binding PDZ Protein, as a Component of Cell Adhesion Sites and Microfilaments. *Molecular Biology of the Cell*, 12 (2), pp.339–350.

Zou, Z., Zheng, W., Fan, H., Deng, G., Lu, S.-H., Jiang, W. & Yu, X. (2021) Aspirin enhances the therapeutic efficacy of cisplatin in oesophageal squamous cell carcinoma by inhibition of putative cancer stem cells. *British Journal of Cancer*, 125 (6), pp.826–838.

8. BIOGRAPHY

Tea Vasiljević was born in 1993 in Split, Croatia. She began her academic career by earning a master's degree in biomedical sciences at the University of Applied Sciences in Bonn, Germany, in 2019. As part of the Erasmus+ program, she spent a research period at the Institute of Biomedicine in Valencia, Spain, where she conducted the research for her master's thesis, which was later published as an original scientific article. In 2021, she began working at the Ruđer Bošković Institute (RBI) in the Laboratory for Personalized Medicine under the supervision of Tanja Matijević Glavan, PhD, where she completed her doctoral thesis. The same year, she enrolled in the Postgraduate Doctoral Study of Biology at the University of Zagreb. During her PhD, she published three original scientific papers, serving as the first author on two of them. Additionally, she co-authored two review papers. She presented her work at nine conferences with international participation. She attended five workshops and was actively involved in science popularization. Besides serving as vice president of the "Udruga Penkala", she was a speaker at the "Znanost u prolazu" 2024 event and represented RBI at MUZZA 2024 Week of Science. She also represented the assistants of the Division of Molecular Medicine in the Assistants' Council of the Institute and the Disciplinary Council (biomedicine). She was the head of the Young Research Section, which is a part of the Croatian Natural Science Society. She is one of two national representatives of Croatia in Eurodoc, the European Council for Doctoral Candidates and Junior Researchers. In 2024, she received funding from RBI's call for "Education and strengthening the potential of young scientists" and organized a workshop on scientific writing. Additionally, she was a member of the organizing committee for the PhD symposium 2024 at PMF. In 2024, together with her mentor, she received the Rudjer Boskovic Institute's annual award for publication from 2023. During her PhD, she was awarded three travel grants: one for the EMBO workshop in Split, Croatia; another one for the workshop in computational biology in Mainz, Germany; and the third to present her work at a conference in Lodz, Poland. Within the framework of the HrZZ project, she undertook two study visits. She speaks several languages besides her native Croatian: English (C1), Spanish (B1), and German (A2).

List of publications:

Vasiljevic, T., Zapletal, E., Tarle, M., Bozicevic Mihalic, I., Gouasmia, S., Provatas, G., Vukovic Djerfi, K., Müller, D., Hat, K., Luksic, I., & Matijevic Glavan, T. (2025). Targeting DAMPs by Aspirin Inhibits Head and Neck Cancer Stem Cells and Stimulates Radio-Sensitization to Proton Therapy. Cancers, 17(13), 2157. https://doi.org/10.3390/cancers17132157

Derfi, K. V., **Vasiljevic, T.**, Dragicevic, T., & Glavan, T. M. (2024). Mithramycin targets head and neck cancer stem cells by inhibiting Sp1 and UFMylation. Cancer Cell International, 24(1), 412. https://doi.org/10.1186/s12935-024-03609-6

Vukovic Đerfi, K., **Vasiljevic, T.**, & Matijevic Glavan, T. (2023). Recent Advances in the Targeting of Head and Neck Cancer Stem Cells. Applied Sciences, 13(24), 13293. https://doi.org/10.3390/app132413293

Vasiljevic, T., Tarle, M., Hat, K., Luksic, I., Mikulandra, M., Busson, P., & Matijevic Glavan, T. (2023). Necrotic Cells from Head and Neck Carcinomas Release Biomolecules That Are Activating Toll-like Receptor 3. International Journal of Molecular Sciences, 24(20), 15269. https://doi.org/10.3390/ijms242015269

Zapletal, E., **Vasiljevic, T.**, Busson, P., & Matijevic Glavan, T. (2023). Dialog beyond the Grave: Necrosis in the Tumor Microenvironment and Its Contribution to Tumor Growth. International Journal of Molecular Sciences, 24(6), 5278. https://doi.org/10.3390/ijms24065278

Vasiljević, T., & Proft, M. (2021). Regulation of the pleiotropic drug resistance transcription factors Pdr1 and Pdr3 in yeast. St Open, 2, 1–17. https://doi.org/10.48188/so.2.7

List of conferences with active participation:

Vasiljevic, Tea; Matijevic Glavan, Tanja; DAMPs Released from Cancer Stem Cells enhance Head and Neck Tumor Cell Migration // BIOOPEN Book of Abstracts – 10th International Doctoral Students' Conference in Life Sciences, University of Łódź, Lodz, **Poland**, (**2025)**. pg. 50-50

Vasiljevic, Tea; Matijević Glavan, Tanja; The identification of novel cancer stem cell biomarkers in head and neck squamous cell carcinoma // 9th Faculty of Science PhD Student Symposium: Book of Abstracts, Zagreb: Faculty of Science, University of Zagreb, Zagreb, **Croatia**, (**2025)**. pg. 95-95

Vasiljevic, Tea; Bozicevic Mihalic, Iva; Gouasmia, Sabrina; Provatas, Georgios; Matijevic Glavan, Tanja; Combining Proton Therapy and TLR3 Activation to Target Head and Neck Cancer Stem Cells // HDIR-7: Advances in Cancer Research and Treatment: Book of Abstracts /Zagreb: **Croatia**, (**2024)**. pg. 57-57

Dragičević, Tea; **Vasiljević, Tea**; Matijević Glavan, Tanja; Comparison of the Expression of Protein UFSP2 in Human Adherent Head and Neck Cancer Cells and Cancer Stem Cells After

the Activation of TLR3 // HDIR-7: Advances in Cancer Research and Treatment: Book of Abstracts /Zagreb, **Croatia**, (**2024)**. pg. 38-38

Vasiljević, Tea; Tarle, Marko; Vuković Đerfi, Kristina; Zapletal, Emilija; Müller, Danko; Matijevic Glavan, Tanja; The role of Toll-like receptor 3 and damage-associated molecular patterns in head and neck cancer stem cells // Molecular oncology, 18, Suppl. 1. Rotterdam, **The Netherlands**, (**2024)**. pg. 104-104

Vasiljević, Tea; Matijević Glavan, Tanja; Optimization of the siRNA transfection in tumor spheres // 8th Faculty of Science PhD Student Symposium: Book of Abstracts, Zagreb: Faculty of Science, University of Zagreb, Zagreb, **Croatia**, (**2024)**. pg. 80-80

Vasiljević, Tea; Zapletal, Emilija; Matijevic Glavan, Tanja; TLR3 stimulation induces the expression of damage-associated molecular patterns in head and neck cancer cell line // "HDIR-6: Targeting Cancer" - Book of Abstracts. Zagreb, **Croatia** (**2022)**. pg. 51

Vasiljevic, Tea; Tarle, Marko; Hat, Koraljka; Busson, Pierre; Matijevic Glavan, Tanja; The activation of Toll-like receptor 3 by endogenous ligands released from necrotic cancer cells // Book of Abstract - Cancer metabolism; Bilbao, **Spain** (**2022)**. pg. 93, 1.

Vasiljević, Tea; Matijević Glavan, Tanja; Isolation and characterization of exosomes isolated from tumor cells // Book of Abstracts - Science and Us: 1st Biomedicine and Health PhD Students Congress with International Participation. Rijeka, **Croatia** (**2022)**. pg. 78-78

Study visits:

- Gustave Roussy Institute, Villejuif, Paris, **France** (**2022**)
- CEITEC Institute, Masaryk University, Brno, **Czech Republic** (**2021**)

Workshops:

- Workshop in computational biology, Mainz, **Germany** (**2025**)
- Workshop: How to publish a scientific paper in a high-IF journal, RBI, **Croatia (2024)**
- EMBO workshop (Fellowship and Communication research), Split**, Croatia (2024)**
- 1st Workshop on Mass Spectrometry in Life Sciences**,** Zagreb**, Croatia (2022)**
- EMBO workshop on research integrity**,** Zagreb**, Croatia (2022)**
- EACR early career researchers**, online (2022)**

Memberships:

- European Association for Cancer Research (**EACR**)
- Croatian Society for Cancer Research (**HDIR**)
- European Council for Doctoral Candidates and Junior Researchers **(EURODOC)**

Awards:

Rudjer Boskovic Institute's annual award for publication **Vasiljevic et al. (2023)**

APPENDIX A

List of abbreviations

ABCG2 - ATP binding cassette subfamily G member 2
ADAM – a disintegrin and metalloprotease
ADH - adherent
AFMID - arylformamidase
AGEs - advanced glycation end products
Ago2 – Argonaute 2
ALDH - aldehyde dehydrogenase
AML - acute myeloid leukemia
AMPK - AMP-activated protein kinase pathway
AP-1- activator protein-1
APC - adenomatous polyposis coli
ASA - acetylsalicylic acid, aspirin
ATM- ataxia-telangiectasia mutated
ATP - adenosine triphosphate
BME - β-Mercaptoethanol
Bmi - MI1 - B-cell specific Moloney murine leukemia virus integration site 1
BSA - bovine serum albumin
CCBL2 - cysteine conjugate beta-lyase 2
CD283 - cluster of differentiation 283
CDK5RAP3 - CDK5 regulatory subunit-associated protein 3
cDNA - complementary DNA
CHK1/CHK2 - checkpoint kinase 1 and 2
CK1- casein kinase 1
CLEC18A - human C-type lectin member 18A
COX - cyclooxygenase enzymes COX-1 and COX-2
COX-2 - cyclooxygenase-2
CSCs - cancer stem cells
CSL - CBF-1, Suppressor of hairless, Lag-1
CTRL - control
DAMPs - damage-associated molecular patterns
DDRGK1- DDRGK domain-containing protein 1
DLL1, DLL3, DLL4- delta-like canonical Notch ligand 1, 3, 4
DMEM - Dulbecco's Modified Eagle Medium
DMSO - dimethyl sulfoxide
dsRNA - double-stranded RNA
EBV - Epstein–Barr virus
ECM – extracellular matrix
EDTA - ethylenediaminetetraacetic acid

EGF - fibroblast growth factor
EGFR - epidermal growth factor receptor
EMT - epithelial-mesenchymal transition
ER – endoplasmic reticulum
ERK 1/ 2 – extracellular signal-regulated kinase 1 and 2
ESCRT - endosomal sorting complexes required for transport
FACS - fluorescence-activated cell sorting
FC1 - ubiquitin-fold modifier conjugating enzyme 1
FGF - fibroblast growth factor
FGFR - fibroblast growth factor receptor
FITC - fluorescein isothiocyanate
FN1 - fibronectin 1
GRWD1 - rich WD repeat-containing 1
GSK3 - glycogen synthase kinase 3
GSTT1 - glutathione S-transferase theta 1
GSMD - Gasdermin
GTL - glutamine transaminase L
Gy - grey
HAAO - 3-hydroxyanthranilate 3,4-dioxygenase
HIF-1α - hypoxia inducible factor 1 subunit alpha
HMGB1 - high mobility group box 1
HNSCC - head and neck squamous cell carcinoma
HPV - human papillomavirus
HRP – horseradish peroxidase
HSP70 - heat shock protein 70
ICAM-1 - intercellular adhesion molecule 1
IDO - indolamine 2,3-dioxygenase
IFN - interferon
IKK - IkappaB kinase
IL - interleukin
IRFs - interferon regulatory factors
JAG1 and JAG2 - the jagged protein family
JAK-STAT – Janus kinases – signal transducer and activator of transcription proteins
JNK- c-Jun N-terminal kinase
KMO - kynurenine 3-monooxygenase
KW - kahweol
KYAT3, KAT - kynurenine aminotransferase 3
Kyn - kynurenine
KYNU - kynureninase
LATS1/2 - large tumor suppressor kinase ½
LLR - leucine-rich repeats
LPS - lipopolysaccharides
LRP - low-density lipoprotein receptor
MAP4K - mitogen-activated protein 4 kinase

MAPK - mitogen-activated protein kinase
MDA5 - melanoma differentiation-associated protein 5
MEBM - Mammary Epithelium Basal Medium
MF - metformin
miRNA - microRNA
MMP - matrix metalloproteinase
MST1/2 - mammalian STE20-like kinase
MTT - 3-(4,5-dimethylthiazol-2-yl)-2,5-diphenyltetrazolium bromide
MyD88 - myeloid differentiation primary response 88
NAD(P)+ - nicotinamide adenine dinucleotide phosphate
NEMO - NF-kappa-B essential modulator
NF-κB - nuclear factor-kappa B
NICD - notch intracellular domain
NLRs - NOD1-like receptors
NO – nitric oxide
NOTCH 1/4 - notch receptors in humans
Nrf2 - Nuclear factor erythroid 2-related factor
NSAID - non-steroidal anti-inflammatory drug
NUP62 - nucleoporin 62
OCT4 - octamer-binding transcription factor 4
OSCC - oral squamous cell carcinoma
PAMPs - pathogen-associated molecular patterns
PAQ - paquinimod
PARP - poly (ADP-ribose) polymerase
PBS - phosphate-buffered saline
PCR - polymerase chain reaction
PD-L1 - programmed death ligand 1
poly(A:U) - polyadenylic:polyuridylic acid
poly(I:C) - polyinosinic:polycytidylic acid
PPRs - pattern recognition receptors
PTCH – patched
qPCR - quantitative polymerase chain reaction
QPRT - quinolinate phosphoribosyltransferase
RAGE - receptor for advanced glycation end products
RIG-I - retinoic acid-inducible gene I
RIP1 - receptor-interacting protein kinase 1
RISC – RNA-induced silencing complex
RLR – RIG-I-like receptor
RNAi – RNA interference
ROS - reactive oxygen species
RPL10 - ribosomal protein L10
RT-PCR – real-time polymerase chain reaction
rtTA3 – reverse tetracycline transactivator 3
S100A9 – S100 calcium-binding protein A9

Sav1 - Salvador homolog 1
SDS-PAGE - Sodium Dodecyl Sulfate Polyacrylamide Gel Electrophoresis
SH2 - src homology 2
SHH - Sonic-Hedgehog
shRNA – small hairpin RNA
siRNA- small interfering RNA
SMO - smoothened
Sox2 - transcription factor belonging to the SRY-box (SOX) family
StarD10- StAR-related lipid transfer domain containing 10
STAT3 - signal transducer and activator of transcription 3
Syntenin - syndecan-binding protein
TAB2/3 - TAK1-binding protein 2 & 3
TAK1- TGFβ-activated kinase
TBK1- TANK-binding kinase 1
TCF/LEF - T-cell factor/lymphoid enhancer-binding factor
TD - transmembrane domain
TDO - tryptophan 2,3-dioxygenase
TEAD - TEA domain transcription factor
TFs - transcription factors
TGF-β-Smad-3 - transforming growth factor–beta–Smad 3
TIR - toll/interleukin-1 receptor
TLR - toll-like receptor
TLR 3 - toll-like receptor 3
TME - tumor microenvironment
TNFα - tumor necrosis factor alpha
TRAF3, TRAF6 -TNF receptor-associated factor 3, 6
TRE – tetracycline response element
TRIF - TIR-domain-containing adapter-inducing interferon-β
Trp - tryptophan
TS - tumor sphere
TSG101 - tumor susceptibility gene 101
UBA5 - ubiquitin-like modifier activating enzyme 5
UCHL5 - ubiquitin C-terminal hydrolase L5
UFBP1 - Ufm1 binding protein
UFL1 – UFM1-specific ligase 1
UFM1 – ubiquitin-fold modifier-1
UFSP1/UFSP2 - UFM1 Specific Peptidase 1/2
UNC93B1 - unc-93 homolog B1
VEGF - vascular endothelial growth factor
YAP/TAZ - yes-associated protein 1/tafazzin
ZEB1 - zinc finger E-box-binding homeobox 1